NASA/CR–2010-216384

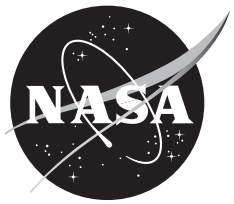

Technology Assessment for Large Vertical-Lift Transport Tiltrotors

Peter J. Germanowski, Brandon L. Stille, and Michael P. Strauss
Sikorsky Aircraft Corporation
Stratford, Connecticut

May 2010

The NASA STI Program Office . . . in Profile

Since its founding, NASA has been dedicated to the advancement of aeronautics and space science. The NASA Scientific and Technical Information (STI) Program Office plays a key part in helping NASA maintain this important role.

The NASA STI Program Office is operated by Langley Research Center, the Lead Center for NASA's scientific and technical information. The NASA STI Program Office provides access to the NASA STI Database, the largest collection of aeronautical and space science STI in the world. The Program Office is also NASA's institutional mechanism for disseminating the results of its research and development activities. These results are published by NASA in the NASA STI Report Series, which includes the following report types:

- TECHNICAL PUBLICATION. Reports of completed research or a major significant phase of research that present the results of NASA programs and include extensive data or theoretical analysis. Includes compilations of significant scientific and technical data and information deemed to be of continuing reference value. NASA's counterpart of peer-reviewed formal professional papers but has less stringent limitations on manuscript length and extent of graphic presentations.

- TECHNICAL MEMORANDUM. Scientific and technical findings that are preliminary or of specialized interest, e.g., quick release reports, working papers, and bibliographies that contain minimal annotation. Does not contain extensive analysis.

- CONTRACTOR REPORT. Scientific and technical findings by NASA-sponsored contractors and grantees.

- CONFERENCE PUBLICATION. Collected papers from scientific and technical conferences, symposia, seminars, or other meetings sponsored or cosponsored by NASA.

- SPECIAL PUBLICATION. Scientific, technical, or historical information from NASA programs, projects, and missions, often concerned with subjects having substantial public interest.

- TECHNICAL TRANSLATION. English-language translations of foreign scientific and technical material pertinent to NASA's mission.

Specialized services that complement the STI Program Office's diverse offerings include creating custom thesauri, building customized databases, organizing and publishing research results . . . even providing videos.

For more information about the NASA STI Program Office, see the following:

- Access the NASA STI Program Home Page at *http://www.sti.nasa.gov*

- E-mail your question via the Internet to help@sti.nasa.gov

- Fax your question to the NASA Access Help Desk at (301) 621-0134

- Telephone the NASA Access Help Desk at (301) 621-0390

- Write to:
  NASA Access Help Desk
  NASA Center for AeroSpace Information
  7115 Standard Drive
  Hanover, MD 21076-1320

NASA/CR–2010-216384

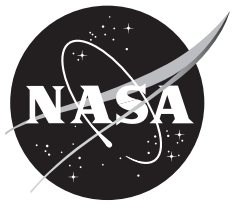

Technology Assessment for Large Vertical-Lift Transport Tiltrotors

Peter J. Germanowski, Brandon L. Stille, and Michael P. Strauss
Sikorsky Aircraft Corporation
Stratford, Connecticut

National Aeronautics and
Space Administration

Ames Research Center
Moffett Field, California 94035-1000

May 2010

Acknowledgments

This report was written and compiled by the following authors:

Peter Germanowski	Technical Lead
Brandon Stille	Lead Designer
Michael Strauss	Attributes Manager

With technical contributions from:

Steve Behnfeldt	Program Manager	Jinlu Wang	Dynamics
Andre Lewis	Systems Engineer	Cody Fegely	Handling Qualities
S. Jon Davis	Aerodynamics	Melvin Garelick	Handling Qualities
Robert Moffitt	Aerodynamics	Erez Eller	Loads & Criteria
Stephen Gatto	Affordability Analysis	Sean Ison	Mass Properties
Gary Heiden	Affordability Analysis	Robert Sartorelli	Propulsion
Greg Kiviat	Affordability Analysis	Joan Pham	Reliability Analysis
Bryan Baskin	Rotors & Blade Design	Akif Ersahin	Structures
Ryan Craft	Rotors & Blade Design	William Townsend	Structures
Todd Walker	Rotors & Blade Design	Bryan Holasek	System Engineering
Kris Hayden	Rotors & Blade Design	Thomas Sbabo	Transmission Design
Mikel Brigley	Dynamics	Todd Garcia	Transmission Design
Bryan Mayrides	Dynamics	Bruce Plasse	Transmission Design

Available from:

NASA Center for AeroSpace Information
7115 Standard Drive
Hanover, MD 21076-1320
(301) 621-0390

National Technical Information Service
5285 Port Royal Road
Springfield, VA 22161
(703) 487-4650

Table of Contents

List of Figures

List of Figures (cont.)

List of Tables

Nomenclature

2-D	two-dimensional
ANSYS	Finite Element Analysis Software
ARC	active rotor control
ARL	Army Research Lab
BVI	blade–vortex interaction
C	risk consequence
CAMRAD	Comprehensive Analytical Model of Rotorcraft Aerodynamics & Dynamics
CATIA	Computer Aided Three-Dimensional Interactive Application
CCHAP	Circulation Coupled Hover Analysis Program
CF	centrifugal force
cg	center of gravity
CFD	computational fluid dynamics
CDI	Continuum Dynamics Incorporated
CHARM	Comprehensive Hierarchical Aeromechanics Rotorcraft Model
CTD	Critical Technology Demonstrator
CTR	conventional tiltrotor
DARPA	Defense Advanced Research Projects Agency
DOD	Department of Defense
EHPIC	Evaluation of Hover Performance using Influence Coefficients
FAA	Federal Aviation Administration
FBW	fly-by-wire
FCS	flight-control system
FDTR	fixed-diameter tiltrotor
FEM	finite element method
FM	figure of merit
FTR	future transport rotorcraft
FWV	Fixed-Wing Variant
GDATS	General Dynamics Advanced Technology Systems, Inc.
GenHel	General Helicopter Flight Dynamics Simulation program
GVT	Ground Vibration Test
GW	gross weight
HERO	Helicopter Rotor Optimization
HOGE	hover out of ground effect
IPS	inlet particle separator
IR	infrared
ISA	International Standard Atmosphere
L	risk likelihood
L/D	lift/drag ratio
LOS	line of sight
LSAF	Lifting Surface Aerodynamics & Performance Analysis of Rotors in Axial Flight
LVLT	large vertical-lift transport
MCP	maximum continuous power

Nomenclature (cont.)

MEA	multielement rotors
MGB	main-rotor gearbox
MRP	Maximum Rated Power
MSES	Multi-element Airfoil Design/Analysis Software
MTOW	maximum takeoff gross weight
NASA	National Aeronautics and Space Administration
NASTRAN	NASA Structural Analysis Program
OEI	one engine inoperative
PASTA	Proprotor Aeroelastic STability Analysis
psf	pounds per square foot
QFD	Quality Function Deployment
RDM	Rotorcraft Design Model
RCAS	Rotorcraft Comprehensive Analysis System
RDS-21	Rotorcraft Drive System for the 21st Century
REVCON	Revolutionary Concepts in Aeronautics
ROA	radius of action
rpm	revolutions per minute
SAC	Sikorsky Aircraft Corporation
SDD	system design and development
SDGW	structural design gross weight
SFC	engine-specific fuel consumption
SHCT	Short Haul Civil Tiltrotor
SL	sea level
SLS	sea-level standard
STO	short takeoff
STOL	Short Takeoff and Landing
t/c	thickness/chord
TDT	Transonic Dynamics Tunnel
TOC	total operating cost
UMARC	University of Maryland Advanced Rotorcraft Code
USAF	United States Air Force
UTC	United Technologies Corporation
VBG	Value-Based Gage
VDIVE	dive speed
VDTR	variable-diameter tiltrotor
VDTR-S	shipboard-suitable VDTR
VGART	Variable-Geometry Advanced-Rotor Technology
V_H	maximum level cruise speed
VMS	Vertical Motion Simulator
VROC	vertical rate of climb
VSTR	variable-speed tiltrotor
VTOL	vertical takeoff and landing

Nomenclature (cont.)

WAT	weight-altitude-temperature
WE	Weight Empty
WRATS	Wing and Rotor Aeroelastic Test System
XMSN	Transmission
°F	degrees Fahrenheit
C_D	drag coefficient
C_f	skin-friction coefficient
C_L	lift coefficient
C_T	thrust coefficient
N_R	percent rotor rotational speed
V_{BE}	velocity for best endurance
V_{BR}	velocity for 99% best specific range
V_{MCP}	velocity for engine maximum continuous power or transmission torque
η_P	rotor propulsive efficiency factor
σ	rotor solidity (blade area over disk area)

Abstract

The technical community has identified rotor efficiency as a critical enabling technology for large vertical-lift transport (LVLT) rotorcraft. The size and performance of LVLT aircraft will be far beyond current aircraft capabilities, enabling a transformational change in cargo transport effectiveness. Two candidate approaches for achieving high efficiency were considered for LVLT applications: a variable-diameter tiltrotor (VDTR) and a variable-speed tiltrotor (VSTR); the former utilizes variable-rotor geometry and the latter utilizes variable-rotor speed. Conceptual aircraft designs were synthesized for the VDTR and VSTR and compared to a conventional tiltrotor (CTR). The aircraft were optimized to a common objective function and bounded by a set of physical- and requirements-driven constraints. The resulting aircraft were compared for weight, size, performance, handling qualities, and other attributes. These comparisons established a measure of the relative merits of the variable-diameter and -speed rotor systems as enabling technologies for LVLT capability.

1 Executive Summary

A system-level analysis of three tiltrotor aircraft configurations was conducted to compare the relative merits of the aircraft for a common set of large-vertical-lift transport LVLT mission requirements. The goal of this comparison was to quantify the relative value of various system-level technologies, including variable geometries and advanced drive systems. The analysis included a conventional tiltrotor (CTR) as the baseline and two alternate configurations examined as a means of increasing hover and cruise efficiency: a variable-diameter tiltrotor (VDTR) and variable-speed tiltrotor (VSTR). The VDTR employed the ability to reduce its rotor diameter by 23% during airplane mode, and the VSTR employed a two-speed transmission allowing its rotor to operate between 100% and 60% rotor rotational speed (N_R) during airplane mode. Upon completion of the synthesis for each aircraft, the attributes of the aircraft, including size, weight, and performance, were compared. The relative strengths and weaknesses of the designs were quantified as an indication of the merits of the underlying technology for each concept.

Sikorsky was selected to conduct this analysis in large part because of the company's previous VDTR development efforts, spanning approximately 10 years during the 1990s. These efforts included preliminary and detailed design of both the aircraft and rotor-system components as well as proof-of-concept testing of the system-level benefits and risk-reduction testing of critical subsystem components. Significant milestones included wind tunnel tests of the VDTR rotor aerodynamics, dynamics, and acoustics; full-scale ground tests of the blade retention and retraction mechanism; and simulations of the VDTR one engine inoperative (OEI) takeoff and landing capability using the NASA Vertical Motion Simulator (VMS). This historical background formed the foundation for the current design and analysis of the VDTR and provided lessons learned, which influenced the design of multiple sub-systems and the overall aircraft integration.

Aircraft Synthesis: Aircraft synthesis was performed using the Sikorsky Aircraft synthesis tool, the Rotorcraft Design Model (RDM), embedded within the Phoenix Integration ModelCenter® design environment. The aircraft were synthesized as "clean-sheet" designs, optimized to a common objective function by perturbation of common design variables and subjected to a set of physical- and requirements-driven constraints.

Design Description: The aircraft were designed to offer high cruise efficiency while maintaining significant hover capability. The tiltrotors utilize nongimbaled, flexbeam-style proprotors mounted on pivoting nacelles. The engine layout includes four engines, configured with two engines mounted in each nacelle. The engines remain horizontal in all modes of flight; only the transmissions and rotors rotate. The aircraft include wingtips that extend beyond the engine nacelles. The wingtips rotate independently of the nacelles to minimize vertical drag in hover and parasite drag during transition and level flight, increasing the overall wing-span efficiency. VDTR rotor geometry is controlled by a hydraulic reel mechanism embedded in the blade feathering axis. VSTR rotor revolutions-per-minute (rpm) variation is enabled by the addition of a shifting gearbox to the face-gear transmission-system layout common to all three aircraft. The composite fuselage is pressurized and has an integral rear ramp for rapid loading and unloading without interference from engine exhaust. The landing-gear configuration comprises three two-wheel main-gear bogeys on each side and a two-wheel truck for the nose gear.

Rotor Aerodynamics: Rotor aerodynamic design and performance estimation was performed using the Evaluation of Hover Performance using Influence Coefficients (EHPIC) tool. Validation of EHPIC was performed by correlating with V-22 experimental data. Figure-of-merit (FM) rotor propulsive efficiency factor (FM-η_P) boundaries for all three aircraft were defined that progress from an ideal hover twist to an ideal propeller twist. The unique boundaries for each configuration were used to select the optimum blade-twist distributions that balanced hover and cruise efficiency. EHPIC was then used to generate comprehensive rotor performance data, which were then incorporated into the aircraft synthesis tool RDM. Sikorsky rotor performance estimates compared very favorably against existing data and other codes, such as Comprehensive Hierarchical Aeromechanics Rotorcraft Model (CHARM) and Lifting Surface Aerodynamics & Performance Analysis of Rotors in Axial Flight (LSAF). A Circulation Coupled Hover Analysis Program (CCHAP) model, correlated to V-22 data, was used to derive the vertical drag of the three aircraft.

Aeroelastic Stability Analysis: Aeroelastic stability analysis was performed using the aeroelastic tool, Rotorcraft Comprehensive Analysis System (RCAS). Validation of RCAS for whirl-flutter stability was performed by correlating with V-22 test data from the Wing and Rotor Aeroelastic Test System (WRATS) test rig at the NASA Langley Transonic Dynamics Tunnel. RCAS was then used to perform stability analysis of the tiltrotor configurations. Initially, a gimbal-style hub was selected and analyzed; however, whirl-flutter stability analysis indicated a stiffer hub to be more desirable, leading to the design of a flexbeam-style rotor with greatly improved whirl-flutter stability. The final designs for all three aircraft were predicted to be stable throughout the required operating range.

Handling Qualities: The handling-qualities analysis was performed using the Sikorsky General Helicopter Flight Dynamics Simulation (GenHel) program. A correlated XV-15 tiltrotor aircraft GenHel simulation was created and used to build a generic GenHel tiltrotor simulation, including variable diameter rotor and variable incidence outboard wing tips. The generic simulation was used for handling qualities and performance analysis of the three tiltrotor aircraft designs. Trim characteristics of the three configurations were calculated and used to derive schedules of mast angle, flap position, and wing-tip incidence in helicopter, transition, and airplane modes at airspeeds from hover to greater than 300 knots. Helicopter-mode hover flight dynamics and airplane-mode longitudinal static stability and longitudinal flight dynamics were examined to evaluate handling qualities and verify operation of the simulations.

Mass Properties: The weight-prediction methodology employed for the tiltrotors was based on a combination of statistical, semianalytical, and analytical methods. These methods were mathematically modeled in RDM to permit weight trending as a function of the primary aircraft design parameters. Parametric weight estimates were generally correlated to V-22 weight data, with technology or requirements factors applied where appropriate. Requirements factors were applied to the VDTR rotor system and the VSTR drive system to account for their unique design features.

Rotor and Blade Design: A trade study focusing on weight minimization and whirl-flutter stability margin determined a gimbaled rotor solution to be unviable for the LVLT tiltrotor application. As a result, a nongimbaled, flexbeam-style rotor was adopted for all three tiltrotors. The flexbeam hub was mated to a blade pitch bearing couple, allowing blade pitch independent of flexbeam motion. The four light-weight, stiff rotor blades were designed using a mix of high-modulus and

high-strength composites to provide blades that met the dynamics requirements while still enabling operation in the austere environment of military aircraft. The VDTR blades include a telescoping spar section mated with a hydraulically actuated strap-and-reel retraction mechanism embedded in the feathering axis of the blade. The placement of the retraction mechanism in the feathering axis reduces the adverse reliability issues associated with past VDTR retraction-mechanism concepts and offers improved strap life. The strap design assumed a current state-of-the-art technology fiber mix as a conservative estimate and includes ample margin for wear and aging.

Transmissions Design: A state-of-the-art split-torque-style transmission design was found to be too heavy for the tiltrotor application, so a face-gear-style transmission was designed that yielded significant weight savings. The design was matured using knowledge gained from the Rotorcraft Drive System for the 21st Century (RDS-21) program and incorporating several technology enhancements currently in development. Additional effort was invested for designing a separate gearbox module based on an existing Sikorsky patent for the VSTR configuration.

Wing Design: A supercritical airfoil section was designed for the wings of the aircraft to balance the requirements of wing stiffness for dynamics and minimal drag for cruise efficiency. A NASA 18%-thick supercritical airfoil section was scaled to the required thickness and then modified using the Multi-element Airfoil Design/Analysis Software (MSES) analysis code to optimize the airfoil-section performance at the LVLT design conditions. The airfoil modification was done by using the MSES inverse-airfoil design method to eliminate local supersonic flow on the airfoil upper surface. The resulting airfoil-section aerodynamic characteristics were used to calculate wing aerodynamic characteristics for the GenHel simulations and for implementation into RDM for aircraft synthesis. The wing planform and twist geometry of each concept was optimized for operation in the unique rotor-wash environment of the three rotor types. Fuel is carried in the composite wings, and the wings offer fuel volume in excess of the volume dictated by the mission requirements.

Affordability Analysis: Parametric cost estimates were prepared for the three aircraft using the commercially available PRICE-H/HL suite and total-operating-cost (TOC) models from PRICE Systems LLC, calibrated to actual cost data. Unit-flyaway-price, system-design-and-development (SDD), and critical-technology-demonstrator (CTD) costs were estimated.

Alternate Aircraft Analysis: In addition to the three "clean-sheet" tiltrotor aircraft, two alternate configuration aircraft were synthesized as further points of comparison: a shipboard-suitable VDTR concept, arranged in a canard configuration with shortened fuselage and tandem cockpit; and a fixed-wing variant.

The remainder of this report discusses, in detail, the design synthesis and analysis process used to develop the three tiltrotor platforms considered for this comparison. Furthermore, the resulting aircraft attributes and performance capabilities are also compared in order to quantify the relative merits of the variable-diameter and -speed technologies compared to the baseline CTR. Additionally, a more detailed description of the preceding development work conducted by Sikorsky is presented, as well as a general description of the anticipated performance improvements attributable to the variable-diameter rotor technology. Finally, the two alternate configurations are also presented.

2 VDTR Historical Summary

The VDTR configuration balances hover performance with cruise efficiency. Power loading is directly determined by the hover requirement that sets the engine power, transmission ratings, and rotor diameter. The engine and engine-performance characteristics are configuration-independent. While the power and drive system are determined by hover, the cruise efficiency is a function of wing geometry, fuselage drag, and propeller efficiency. The fuselage geometry and subsequent drag are essentially configuration-independent. The wing geometry of the VDTR is unique in that it can be tailored for the cruise rotor diameter, allowing for a slightly smaller wingspan and optimization of the wingtip extensions. The ability to tailor the wing geometry for the VDTR combined with the overall improvement in propeller efficiency afforded by the increased blade loadings for the VDTR in cruise improve the overall fuel efficiency of the aircraft.

The variable-diameter concept was first explored as an application for single-main-rotor helicopter platforms. As early as 1972, research and design activities were being conducted to explore the benefits of a retracting rotor system. For compound, single-main-rotor helicopters, variable-diameter rotors offer the potential to increase the aircraft speed capability by mitigating blade aeroelastic responses at high speed, minimizing the drag of the exposed blades and decreasing the stowed size of the rotor. For tiltrotor platforms, the variable-diameter rotor provides a more optimal solution for both the hover and cruise condition; increasing the rotor diameter in hover decreases the blade loading leading to improved efficiency, and retracting the rotor during cruise increases the blade loading, providing increased propeller efficiency and lift/drag ratio (L/D). The work of Fradenburgh, Scott, and Wang (refs. 1 through 8 provide detailed comparisons of VDTR and conventional tiltrotor aircraft).

The decreased blade loadings in hover and increased blade loadings in cruise afforded by the ability to vary the rotor geometry offer more optimal solutions for the tiltrotor concept because in each state the rotor better matches the operational requirements placed upon it. The hover condition requires that the rotor be capable of generating enough thrust to lift the gross weight of the vehicle. The cruise condition requires that the rotor generate significantly less thrust as the total thrust need only balance the drag of the aircraft in trim, level flight. The wing carries the aircraft weight during cruise operations. If the rotor is sized to meet the hover requirement, then it is likely to be significantly oversized for generating the required cruise thrust. Similarly a rotor sized for the cruise condition will not provide nearly enough thrust to meet the requirements of the hover condition. A compromised rotor with a fixed geometry will not be ideally suited for either condition; the rotor size and blade loadings will not be adequate for hover or cruise, leading to compromised efficiency in both spectrums.

The variable-diameter concept alleviates some of the need to compromise the rotor design in order to meet the thrust requirements of the hover and cruise condition. The rotor operates at its maximum diameter in hover, typically extending over the main body of the fuselage, to minimize the hover disk loading, and then contracts during the transition to cruise flight. This contraction increases the blade loading during cruise, primarily by decreasing the rotor tip speed and blade area, leading to an overall increase in rotor propulsive efficiency. This increase in efficiency is generated without the need to significantly reduce rotor rpm by either slowing the power turbine

speed or reducing the main gearbox ratio.The main power turbine can operate within the 80% to 100% N_R range, allowing engine-specific fuel consumption (SFC) to remain near its peak during cruise.

Typically, conventional tiltrotor aircraft operate with very high disk loadings in hover, where 18 to 24 pounds per square foot (psf) is normal. These disk loadings are twice the loadings seen for conventional, single-main-rotor helicopters. Disk loadings in the 18 to 24 psf range are accompanied by excessive downwash and outwash velocities as well as poor autorotative characteristics. The VDTR mitigates some of these concerns. All other design attributes being equal, a VDTR typically offers the designer the ability to include a larger rotor diameter in hover than could be accommodated by a conventional tiltrotor. This larger diameter contributes to reduced disk loadings, lower downwash velocities, and improved autorotative capability.

The VDTR offers benefits not only in hover operations, but also in cruise operations. Typically conventional tiltrotor rotors have a large diameter because of the requirements of the hover spectrum. These rotors then operate in cruise as well, and partly because of their large diameters, are susceptible to propeller whirl-flutter instability. In fact, this instability often limits the forward-flight speed for tiltrotor aircraft. The VDTR has the potential to offer higher forward-flight-speed capabilities because the reduced rotor diameter is less susceptible to the whirl-flutter instability.

The variable-diameter concept can potentially affect the tiltrotor component designs in several areas. If the rotor and drive system are sized in hover, then the ability to reduce the disk loading in hover for a given blade loading may be advantageous. Reducing the disk loading will likely reduce the required installed power, and thereby overall aircraft weight for the hover condition. However, the capability to reduce the disk loading is not freely available. The VDTR mechanism increases the overall weight and complexity of the rotor blades and hub. This increased weight may offset the savings yielded by the decreased disk loading in hover. The VDTR concept also affects the aircraft wing design in two ways. Since the rotor can expand and contract, the rotor blades can overlap the fuselage in hover. Then as the rotors transition to forward cruise the blades can retract to provide adequate fuselage clearance. Typically, the overall wingspan from the fuselage to the nacelles can be reduced for a VDTR design compared to a similar conventional tiltrotor aircraft. Furthermore, the VDTR concept potentially opens the design to higher cruise speeds than those seen for current tiltrotor platforms. The ability to increase the maximum airspeed capability, as well as the cruise-speed capability, influences the aircraft wing design by reducing the required wing incidence and wing area. Reduced incidence will likely benefit aircraft-induced drag, and reduced wing area will reduce the overall wing weight. Aircraft gross weight may trend lower as airspeed increases for a VDTR concept.

With regard to operational suitability, the VDTR has the advantage of a large, lightly loaded rotor for hover operations with the added ability to reduce the rotor size for cruise and ground operations. The variable-rotor geometry provides the capability to minimize the aircraft operational footprint during parking and taxi operations. Minimizing this footprint allows the aircraft to be parked and to taxi in confined areas.

While the benefits of a variable-diameter rotor for compound, single-main-rotor platforms should not be ignored, tiltrotor platforms experience a much greater potential benefit. During the late

1980s, 1990s, and the early part of the 21st century, Sikorsky Aircraft Corporation conducted significant research and development activities to mature the variable-diameter tiltrotor concept. These activities were conducted in partnership with the National Aeronautics and Space Administration (NASA), the United States Army, the United States Air Force (USAF), and the Defense Advanced Research Projects Agency (DARPA). The various activities included preliminary design, detailed design, model-scale experiments, and full-scale testing of the VDTR concept and its subcomponents. Each of the programs added to the fundamental understanding of the VDTR concept, and they progressively matured the design. Several of the more significant efforts are described in greater detail in the following sections.

2.1 Technology Needs for High-Speed Rotorcraft ('90–'91)

References 5 and 7 describe an analytical study conducted to identify rotorcraft concepts best capable of combining a cruise speed of 350 to 450 knots with helicopter-like low-speed attributes, and to define the technology advancements needed to make them viable for full-scale development by the year 2000. A systematic approach was used to compare the relative attributes and required gross weights for a wide range of concepts, resulting in a downselect to the most promising concept/mission pairs. For the transport missions, tiltwing and VDTR concepts were found to be superior. For a military scout/attack role, the VDTR was best, although a shrouded-rotor concept could provide a highly agile, low observable alternative if its weight-empty fraction could be reduced. A design speed of 375 to 425 knots was found to be the maximum desirable for transport missions, with higher speed producing rapidly diminishing benefits in productivity. The key technologies that required advancement to make the tiltwing and VDTR concepts viable were in the areas of wing and proprotor aerodynamics, efficient structural design, and flight controls. Specific attention was needed regarding proprotor-blade-geometry optimization, refinement of the geared flap-pitch control system, expansion of the speed/descent envelope, and the structural and aerodynamic trade-offs of wing thickness and forward sweep.

Of the 16 high-speed VTOL concepts studies, five of these concepts were deemed to have desirable high-speed vertical-takeoff-and-landing (VTOL) attributes. Preliminary design efforts were undertaken to explore the physical characteristics, performance, and sensitivity to technology assumptions for the most promising concepts. The study defined levels of new technology that were required to enable low-risk development and determined that weights, structural design, fly-by-wire, drag reduction, airfoil design, and propulsion-system design were critical to the success of these concepts.

2.2 Wind Tunnel Test of a VDTR Model ('94)

A wind tunnel test of a 1/6th scale VDTR was conducted as a joint effort between NASA Ames Research Center and Sikorsky Aircraft (ref. 9). The objective was to evaluate the aeroelastic and performance characteristics of the VDTR in conversion, hover, and cruise. The rotor diameter and nacelle angle of the model were remotely changed to represent tiltrotor operating conditions. Data were presented showing the propulsive force required in conversion, blade loads, angle-of-attack stability and simulated gust response, and hover and cruise performance. This test represented the first wind tunnel test of a variable-diameter rotor applied to a tiltrotor concept. The results

confirmed some of the potential advantages of the VDTR and established the variable-diameter rotor as a viable candidate for an advanced tiltrotor. Current predictions for the LVLT VDTR concept indicate that predictions for hover figure-of-merit and cruise efficiency correlate well with the data generated by this test effort.

This wind tunnel test successfully demonstrated the feasibility of the VTDR for tiltrotor aircraft. A wide range of test points were taken in hover, conversion, and cruise modes. The concept was shown to have numerous advantages over conventional tiltrotors, such as reduced hover downwash with lower disk loading and significantly reduced longitudinal gust response in cruise.

In the conversion regime, a high propulsive force was demonstrated for sustained flight with acceptable blade loads. The VDTR demonstrated excellent gust-response capabilities. The horizontal gust response correlated well with the predictions, revealing only half the response to turbulence relative to the conventional tiltrotor. Figure 1 shows the Sikorsky VDTR wind tunnel model.

Figure 1. Sikorsky VDTR wind tunnel model.

2.3 VMS Simulation of a Variable-Diameter Tiltrotor (’97)

A joint NASA/Sikorsky simulation was performed in the NASA-Ames Vertical Motion Simulator to evaluate the performance and handling qualities of a VDTR compared to a fixed-diameter tiltrotor (FDTR) during normal and emergency terminal-area operations (ref. 10). Pilots from the Federal Aviation Administration (FAA), NASA, academia, and industry evaluated both the VDTR and FDTR during OEI takeoffs and approaches and all-engine inoperative landings. The simulation math model was based on NASA’s preliminary-design version of the Generic Tiltrotor Simulation code. Both fixed- and variable-diameter rotor versions exhibited Level One handling qualities during normal maneuvers with both engines operating. In general, the VDTR had a greater power margin and performance in helicopter mode resulting from a lower disk loading requiring 20% to 25% less power at similar thrust levels. This power margin was an advantage during one- and all-engine inoperative procedures. This simulation study quantified the performance merits of the VDTR concept and demonstrated that the VDTR offers enhanced performance and terminal-area safety for future civil tiltrotor transports. The simulation was also beneficial in identifying areas for further investigation for the VDTR and basic civil tiltrotor concepts. Figure 2 shows the NASA VMS Simulator.

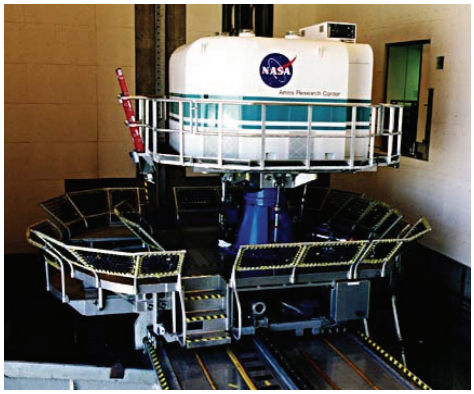

Figure 2. NASA Vertical Motion Simulator.

2.4 Variable-Diameter Retraction-Mechanism Risk Reduction and Trade Studies ('98–'99)

Mechanical trade studies and a risk-reduction plan were developed for the VDTR retraction mechanism. The viability of the VDTR had been demonstrated under NASA's Short Haul Civil Tiltrotor (SHCT) program through model scale tests and piloted simulation studies. These risk-reduction plans and trade studies addressed the next challenge for the VDTR development: determining the feasibility of VDTR applied to full-scale flight vehicles. This report clarified VDTR technical and mechanical issues and presented a risk-reduction plan for large-scale retraction mechanism testing and wind tunnel testing.

2.5 Variable-Diameter Tiltrotor Technology ('99–'00)

The Variable-Diameter Tiltrotor Technology program addressed the fundamental risk issues of the VDTR concept through a combination of large-scale component testing. This cooperative DARPA/Sikorsky program was established to explore several fundamental issues surrounding VDTR, including the feasibility of a large-scale retraction mechanism under conditions representative of a realistic flight environment, including a centrifugal force field and vibration and the aeroelastic stability of a VDTR in high-speed airplane-mode flight. Accelerated ground testing of the critical mechanisms of a large-scale VDTR retraction mechanism was performed under realistic environmental conditions. Development of a VDTR aeroelastic wind tunnel model was initiated that was aimed at validating the aeroelastic stability of a VDTR in the high-speed airplane mode. Congressional funding cuts forced termination of this program for convenience prior to completion of all planned risk-reduction activities.

2.6 Variable-Geometry Advanced Rotor Technology (VGART) Phase 1 ('99–'00)

The Variable-Geometry Advanced-Rotor Technology (VGART) Phase I study evaluated the application of active rotor control systems to both a helicopter and a VDTR, sized to meet the future-transport-rotorcraft (FTR) requirements. This study was performed by a consortium comprising Sikorsky Aircraft Corporation (SAC) and General Dynamics Advanced Technology Systems, Inc.

(GDATS). The study concluded that a trailing-edge flap driven by a hydraulic lapfit actuator provided the lightest weight, smallest, most affordable single-main-rotor helicopter solution for FTR. Similarly, a hydraulically powered individual-blade control system provided the smallest, lightest weight, most affordable VDTR solution for FTR. Both aircraft were sized for the same FTR missions and requirements, except, naturally, for speed. The VDTR solution had a maximum cruise speed of 295 knots, while that of the helicopter was 175 knots.

In arriving at recommended design solutions, a thorough life-cycle cost analysis was conducted, comparing numerous active control approaches and actuator concepts. The chosen concepts represented the solutions with the lowest life-cycle cost. The study also assessed technical, scaling, reliability, maintainability, manufacturing, produceability, and affordability issues. The results indicated that all major hardware scalability, produceability, accessibility, and implementation issues could be resolved though risk-reduction tests. [Examples of recommended risk-reduction tests included wind tunnel tests to verify flap effectiveness, actuator bench tests under load, hydraulic power-supply-development tests, and manufacturing-risk-reduction tests.

The project also addressed the existence of potential interactions between the aircraft flight control system and the active control system, and found these interactions to be negligible. Further investigation of this issue, using higher-fidelity simulations, was recommended in order to resolve any potential software implementation issues.

2.7 Revolutionary Concepts in Aeronautics (REVCON) Phase 1 (’00–’01)

The Revolutionary Concept Study “Development and Flight Test of a Variable Diameter Tilt Rotor Experimental Aircraft” was conducted in 2000–2001 as part of the REVCON Phase 1 Cooperative Agreement between NASA and Sikorsky Aircraft Corporation. The REVCON Phase 1 study evaluated the system benefits and flight feasibility for a VDTR experimental aircraft, and defined an appropriate REVCON flight-test program. Teamed with Sikorsky in this eight-month effort were NASA Dryden Flight Research Facility, NASA Ames Research Center, and NASA Langley Research Center, with NASA Glenn Research Center joining the team towards the end of Phase 1. A systems benefits analysis was performed utilizing the V-22 as the baseline configuration to help expedite the study because a significant database was available on the aircraft. In addition, a significant database already existed on VDTR technology, resident at NASA centers, as a result of some eight years of prior investigations on this concept as part of the Short Haul Civil Tilt Rotor Program. This team’s systems evaluation confirmed significant potential performance and safety benefits for VDTR compared to conventional tiltrotor designs.

VDTR safety benefits were quantified as a result of a joint NASA/Sikorsky piloted simulation study conducted in the Ames VMS facility (ref. 10). The system analysis also determined that the extra power margin inherent with the VDTR gave it a large advantage during emergency situations with one engine inoperative. The Category A-style takeoff procedures provided a framework to quantify this benefit. Overall, the VDTR had a power margin and performance capability such that the pilots were able to comfortably continue the takeoff if the engine failed after the takeoff decision point. Analyses of various other emergency scenarios indicate that the VDTR significantly reduced takeoff distances for VTOL takeoffs for rejected takeoffs compared to conventional

tiltrotors. Furthermore, VDTR improved safety during all-engines-out maneuvers because of decreased disk loadings and high rotor inertia compared to conventional tiltrotors.

2.8 Variable-Geometry Advanced Rotor Technology (VGART) Phase 2 (’00)

The VGART program was established to determine the feasibility of critical technologies and components required for high-risk rotor concepts needed to provide substantial improvements in the aerodynamic performance, external noise, and vibration characteristics of future rotorcraft. The tasks conducted under VGART Phase 2 developed and demonstrated technologies for active rotor control (ARC), high lift, multielement rotors (MEA), and VDTRs. ARC tasks included simulating a coupled active rotor-control–flight-control system to identify any unfavorable interactions, demonstrating wireless rotating to fixed-frame information transfer, studying the benefits of an on-blade active flap at model scale, and adapting and applying a closed-loop active controller as part of a cooperative study of an active twist rotor. MEA tasks included a full-scale, two-dimensional (2-D) aerodynamic evaluation, a design trade study of application of active and passive MEA concepts, and a wind tunnel experiment on a Mach-scale MEA model rotor. Aeroelastic stability of the VDTR in forward flight (propeller mode) was experimentally investigated to verify the predicted increase in the speed of the whirl-flutter boundary.

2.9 VDTR Measured Acoustic and Aerodynamic Data Compared with the V-22 (’02)

A wind tunnel test was conducted using the NASA Langley 14- by 22-Foot Subsonic Wind Tunnel to evaluate the acoustic and aerodynamic benefits of the Sikorsky Variable Diameter Tilt Rotor. This test is discussed in reference 8. The results were evaluated against a baseline current-technology V-22 rotor. The test evaluated four VDTR configurations, each representing a potential noise-reduction technology compared to conventional proprotors. In addition, baseline data were obtained for a V-22 rotor for comparison with the measured VDTR acoustic and aerodynamic results. The aim of the program was to demonstrate a 6-dBA reduction in blade–vortex interaction (BVI) source noise through design, relative to the current-technology V-22. This reduction was part of the total SHCT external-noise-reduction goal of 12 dBA. The noise-reduction goals were to assist in overcoming the primary obstacle to the ready acceptance of tiltrotors for commercial carrying service. Sikorsky’s VDTR succeeded in achieving the SHCT external-noise-source reduction goal.

3 Design and Synthesis

The LVLT aircraft were optimized and designed around a common set of requirements with the intent of exposing the nuances that differentiate the configurations. Where common designs could be applied to all of the configurations, a single design was applied to all three configurations. Where a specific design effort could differentiate between the configurations, these areas were the primary focus of effort.

The tiltrotors utilize nongimbaled flexbeam-style proprotors mounted on pivoting nacelles. The engine layout includes four engines, configured with two engines mounted in each nacelle, which remain horizontal in all modes of flight (only the transmissions and rotors rotate). The aircraft include wingtips that extend beyond the engine nacelles. The wingtips rotate independently of the nacelles to minimize vertical drag in hover and parasite drag during transition and level flight, increasing the overall wingspan efficiency. VDTR rotor geometry is controlled by a hydraulic reel mechanism embedded in the blade feathering axis. VSTR rotor rpm variation is enabled by the addition of a shifting gearbox to the common face-gear transmission-system layout. The composite fuselage is pressurized and has an integral rear ramp for rapid loading and unloading without interference from engine exhaust. The landing-gear configuration comprises three two-wheel main-gear bogeys on each side and a two-wheel truck for the nose gear. Figure 3 shows the general arrangements of the CTR, VDTR, and VSTR.

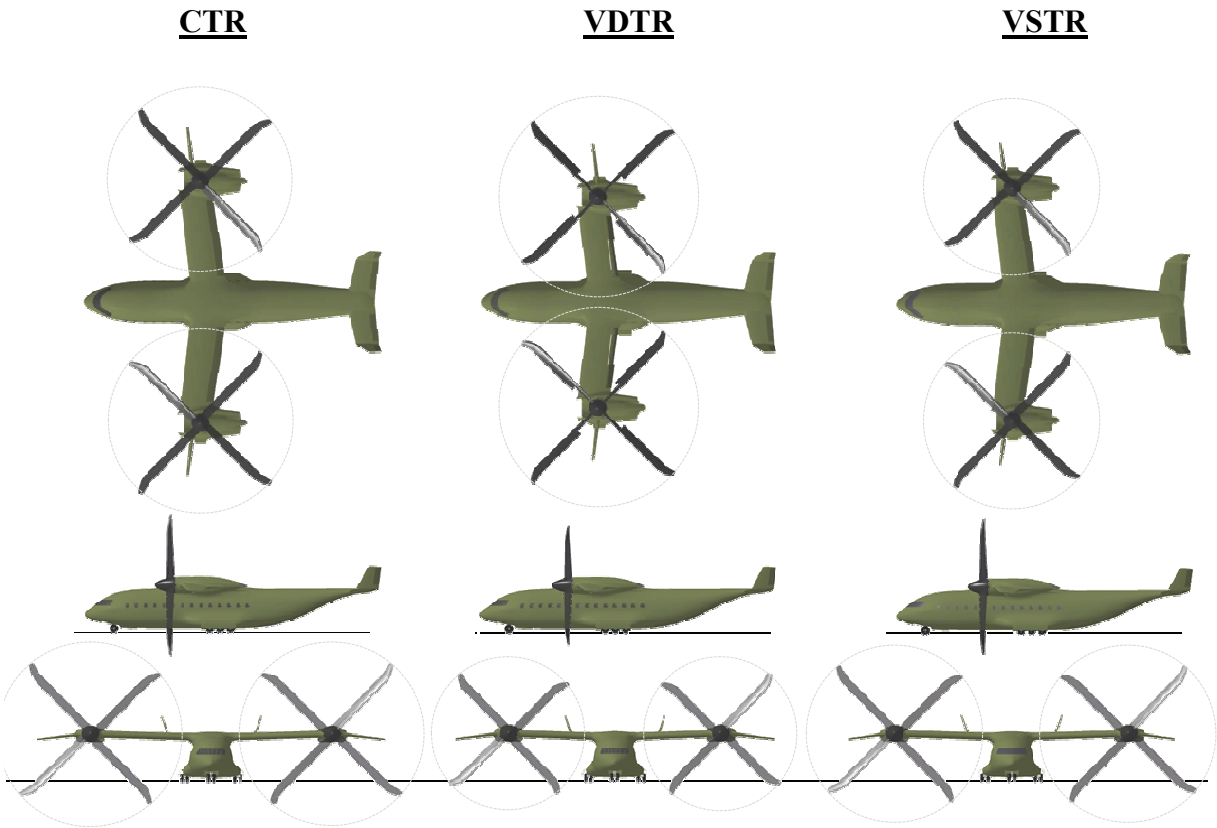

Figure 3. General arrangements of CTR, VDTR, and VSTR.

The aircraft were synthesized as "clean-sheet" designs, optimized to a common-objective function by perturbation of common design variables and subjected to a set of physical- and requirements-driven constraints. This approach provided a means of fairly comparing the emergent performance and attributes (physical size, weight, and geometry) of the aircraft necessary to meet the design requirements, based on the unique characteristics of each configuration.

3.1 Synthesis Approach

Aircraft sizing was performed using the Sikorsky aircraft synthesis tool, Rotorcraft Design Model (RDM). RDM is a comprehensive aircraft design and analysis code developed for new conceptual design, derivative design, and competitive analysis. RDM is a physics-based model coupled with empirical corrections derived from flight-test data and/or higher-fidelity analysis. Aircraft sizing and performance are based on a longitudinal force trim, parametric weight estimation correlated to existing aircraft, scalable engine power and fuel flow-lapse rates, and flexible mission definition. RDM is primarily executed in one of two modes: design/sizing mode and mission-analysis mode.

In design/sizing mode, RDM calculates the aircraft weights, geometry (rotor diameter, rotor solidity, wing area, wing chord, etc.), and propulsion-system attributes (installed engine power and SFC) required to perform a user-prescribed design mission profile. The design/sizing mode can be run in one of two fashions: for a given payload, the structural design gross weight is determined; or, for a given gross weight, the resulting payload is found. In mission-analysis mode a sized aircraft must be provided with fully defined weights, geometry, and propulsion-system characteristics. RDM segregates a mission profile into discrete elements at required altitudes, temperatures, speeds, and durations or distances. Forward-flight segments may be at specified speeds or coded to either provide speeds such as maximum range or maximum endurance or match a gearbox design rating or engine power setting. Fuel burn-off is then tracked per mission segment. Weight and drag changes can be applied per segment to account for payload unloading, ordinance expenditure, or external lift pickup.

LVLT synthesis was accomplished using Phoenix Integration's ModelCenter®. ModelCenter® enables multiple instances of RDM to be graphically integrated into a seamless, automated engineering process. A highly coupled design environment was constructed to design the optimal aircraft while balancing the requirements of each mission. This environment included one instance of RDM running a composite sizing mission in design/sizing mode and other instances, each running one of the LVLT mission profiles in mission-analysis mode. The synthesis process, illustrated in Figure **4**, was as follows:

1. Starting values were assumed for aircraft weights and the fuel capacity. RDM was executed in design/sizing mode using a defined structural design gross weight (SDGW). The empty weight was calculated from this SDGW based on a detailed set of parametric-weight correlations and fixed-weight allocations. Rotor diameter was determined based on a design disk loading at a given midmission gross weight and rotor solidity was determined based on a design C_T/σ (thrust coefficient/rotor solidity) at the same midmission gross weight and ambient conditions. Wing area was determined based on a design wing loading at SDGW, and wingspan was determined based on a design-wing aspect ratio.

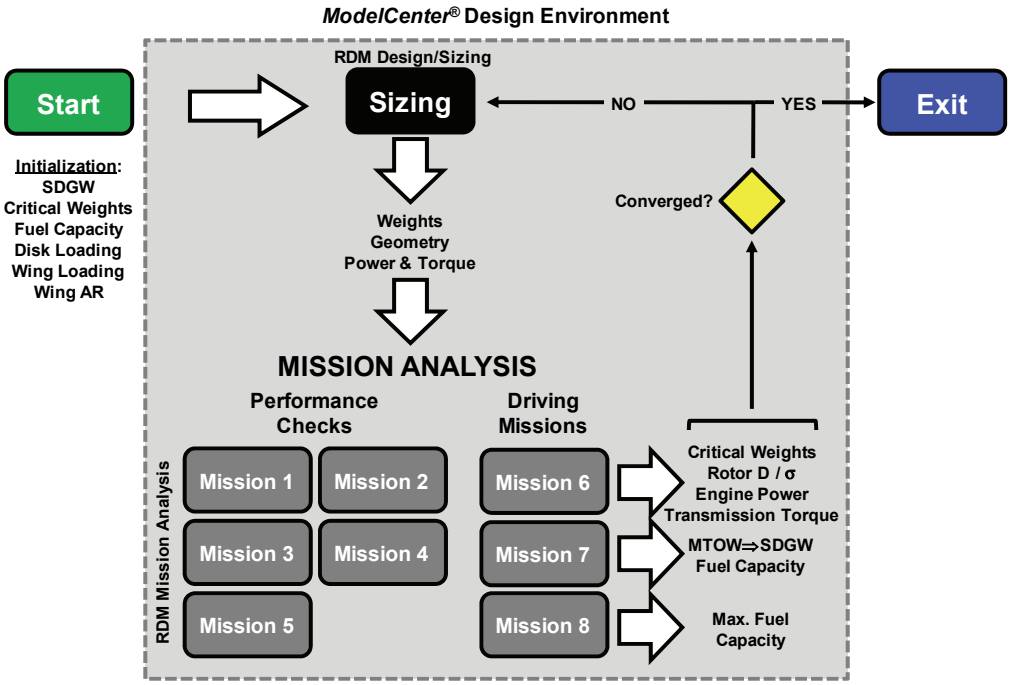

Figure 4. LVLT synthesis process.

2. All required missions were executed using RDM in mission-analysis mode using the weight, power, and geometry information generated by RDM in its first run in design/sizing mode. The baseline fuel required of each mission was compared with the maximum value extracted as the updated value of the fuel capacity. The takeoff gross weight of each mission was compared with the maximum value extracted as the updated value of SDGW. A critical midmission hover-out-of-ground-effect (HOGE) weight was also extracted.

3. RDM was executed in design/sizing mode again and the updated values of SDGW, midmission gross weight, and fuel capacity were used to determine a new aircraft empty weight, engine power required, transmission rating, rotor geometry, and wing geometry.

4. Steps 2 and 3 were repeated until the weights and fuel capacity were converged upon.

Two primary missions emerged as the aircraft sizing drivers. The first was a radius-of-action (ROA) mission with a midmission HOGE, which sets the minimum fuel capacity and whose mid-mission hover criterion dictates the main-rotor transmission rating and the installed engine power required. The HOGE takeoff criterion for this mission dictates the vertical takeoff weight of the aircraft. The second mission was a long-range transport mission that drove the maximum takeoff gross weight (MTOW) of the aircraft and in turn the structural design gross weight (SDGW).

3.2 Design Space Exploration and Optimization Strategy

The design space exploration and optimization approach was to present the best CTR, best VDTR, and best VSTR for the given LVLT requirements, optimizing each aircraft independent of the other two so that objective comparisons could be made on the merits of each configuration. The three configurations were sized to the same objective function and minimum aircraft empty weight (to minimize logistic footprint and cost), and subjected to performance and several physical, geometric, or operational constraints. Thus, all three aircraft emerged with comparable performance, but different attributes (physical size, weight, and geometry) necessary to meet the LVLT requirements indicative of each configuration.

A single performance-based constraint requiring a minimum threshold for cruise efficiency, derived from the LVLT requirements, coupled with the minimum empty-weight objective function, was chosen to yield the "fastest, lightest, cheapest" aircraft possible.

The independent design variables chosen for optimization were rotor disk loading, wing loading, and wing aspect ratio. These design variables are inextricably linked to the physical/geometric constraints present in the design space. These constraints include:

1. Minimum wing inboard aspect ratio: Minimum wing root chord is dictated by wing structural requirements. While higher wing aspect ratios are desirable because they decrease induced drag and result in reduced fuel consumption, high wing aspect ratios correspond to lower wing root chords for a given span. Therefore a balance between cruise efficiency and adequate structural stiffness was required.

2. Maximum rotor-blade aspect ratio/minimum rotor-blade chord: Maximum rotor-blade aspect ratio was dictated by structural requirements, dynamic requirements, and the physical constraints of the VDTR retraction mechanism. Lower rotor disk loadings were desirable for all configurations because installed engine power required is driven by the HOGE condition, and specifically for VDTR because the VDTR suffers a figure-of-merit penalty due to the elliptically shaped inboard section of the rotor. However, as disk loading decreases, for a given hover design C_T/σ, blade aspect ratio becomes higher. A maximum blade-aspect-ratio limit was imposed on the design to bound the disk-loading trade space. Further, the VDTR blade was constrained to have a minimum allowable geometric chord based on the packaging volume needed for the retraction mechanism.

3. Maximum rotor disk loading: A maximum rotor disk loading for the midmission hover condition was selected to maintain outwash velocities less than or equal to those currently accepted within the Department of Defense (DOD) inventory.

4. Maximum operating-wing lift coefficient (C_L): The wing loading was constrained to yield the maximum allowable operating-wing C_L. The C_L corresponding to the maximum lift/drag coefficient ($C_L/C_{D)}$ was extracted for each Mach number to derive the maximum wing C_L as a function of Mach number. For any given Mach number, the maximum C_L, with a margin of 20%, was selected as an upper bound to the capability of the wing section. Higher wing

loadings were desirable because they corresponded to less wing area for a given vehicle weight, directly reducing wing weight and overall vehicle empty weight. However, for a given span, higher wing loadings resulted in increasingly high operating-wing C_L.

A final imposed constraint was the relationship between hover rotor diameter and wingspan. While the wingspan, aspect ratio, and wing loading should be set to achieve the most efficient wing possible, the hover disk loading should be set to achieve the most efficient hovering rotor possible. Inboard (nacelle-to-nacelle) wingspan and rotor diameter are coupled by a physical constraint. For CTR and VSTR, that constraint is the fuselage width plus one foot of margin on either side; and for VDTR the constraint is that the two rotors are not permitted to intermesh (intermeshing rotors pose the concerns of asymmetrical dynamics and increased fuselage downloading as more of the rotor wake contraction is impeded by the fuselage).

3.3 Design Descriptions

Figure 5 through Figure 20 graphically compare the three NASA LVLT tiltrotor concepts. Key parameters and weights are shown, with the CTR considered the nominal 100% point and the values for the other aircraft shown as relative to the CTR. The VDTR rotor-retraction mechanism results in a 9% larger hover diameter (translating to 15% lower disk loading, 15% less rotor solidity required, and 3% greater overall hover efficiency) and a 16% lower cruise diameter relative to the CTR. The VDTR cruise tip speed is 13% less than the CTR and only 2% greater than the VSTR (a result of both reducing the rotor diameter and slowing the rotor N_R). These benefits come at the expense of 3% greater weight empty and 2% greater required fuel capacity relative to the CTR. Development cost is 11% greater than the CTR for the VDTR and 5% greater than the CTR for the VSTR, with the difference due primarily to the level of risk inherent in each configuration. Unit flyaway price trends similarly with risk, but more so with vehicle weight, with the VDTR being 9% greater than the CTR and the VSTR being 7% greater than the CTR. Recall that all three aircraft were optimized to equivalent cruise efficiency.

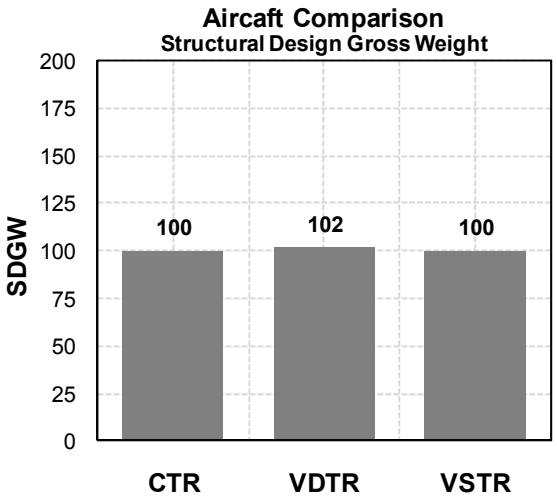

Figure 5. SDGW comparison.

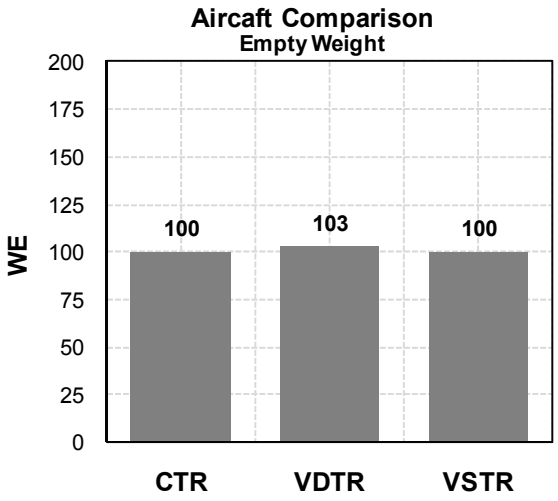

Figure 6. Weight empty (WE) comparison.

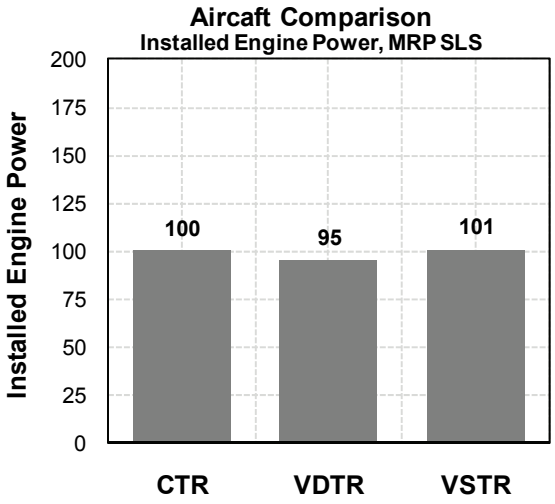

Figure 7. Installed maximum rated power (MRP) at sea-level standard (SLS) comparison.

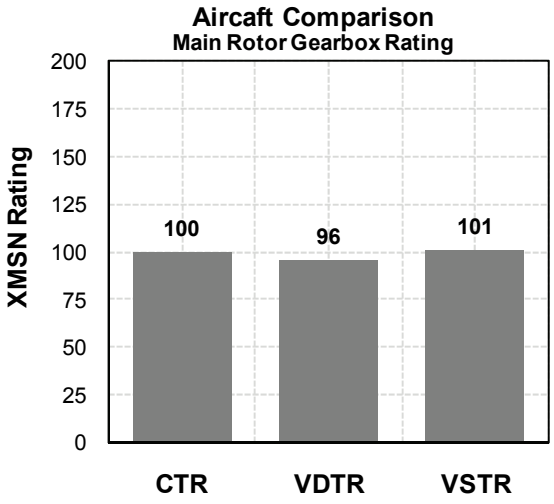

Figure 8. Transmission rating comparison.

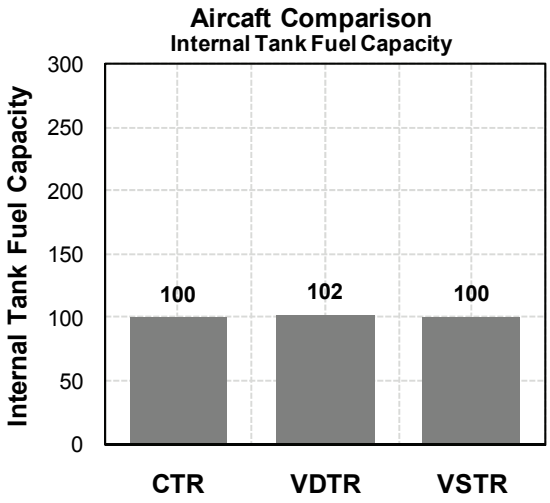

Figure 9. Internal-fuel-tank volume comparison.

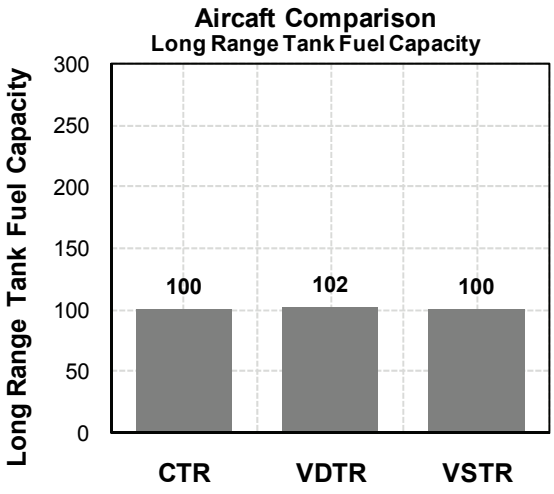

Figure 10. Long-range-tank volume comparison.

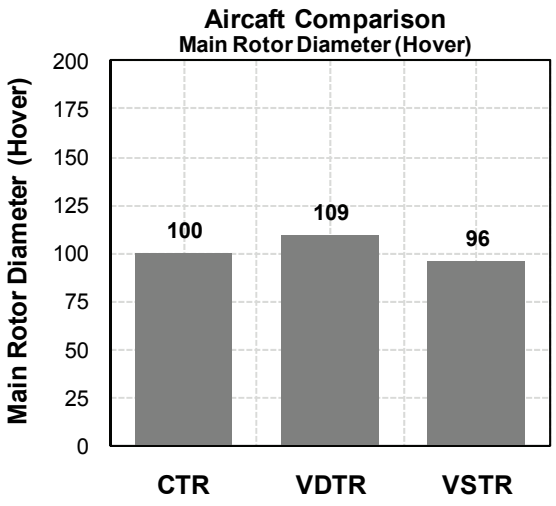

Figure 11. Rotor hover-diameter comparison.

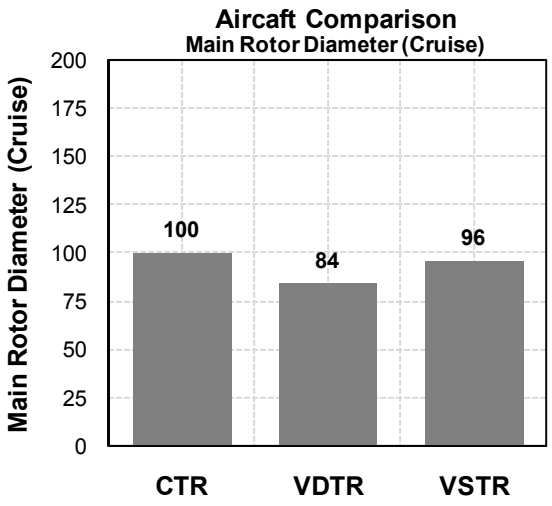

Figure 12. Rotor cruise-diameter comparison.

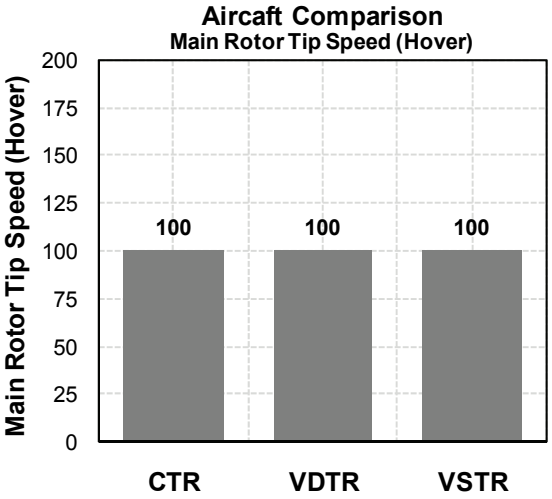

Figure 13. Rotor hover-tip-speed comparison.

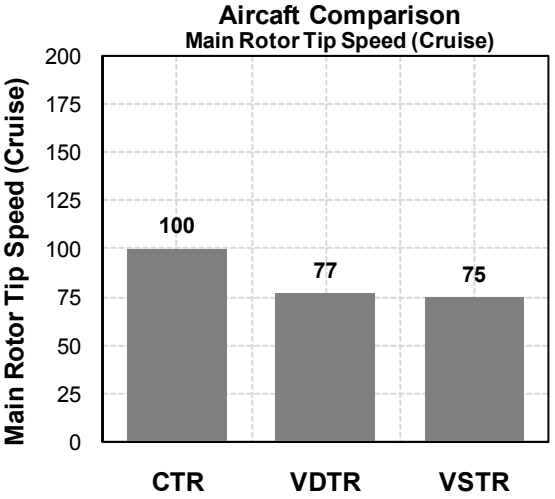

Figure 14. Rotor cruise-tip-speed comparison.

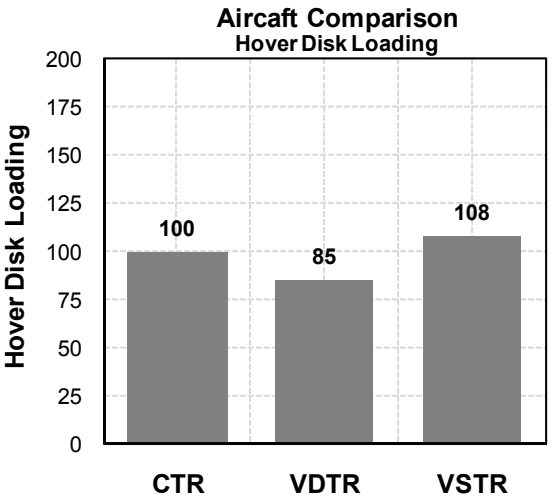

Figure 15. Hover disk-loading comparison.

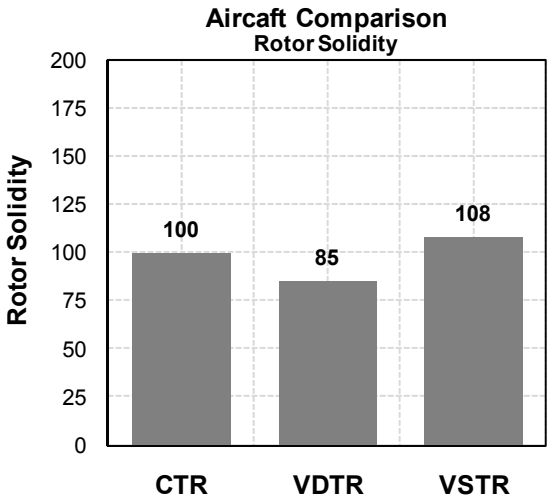

Figure 16. Rotor solidity comparison.

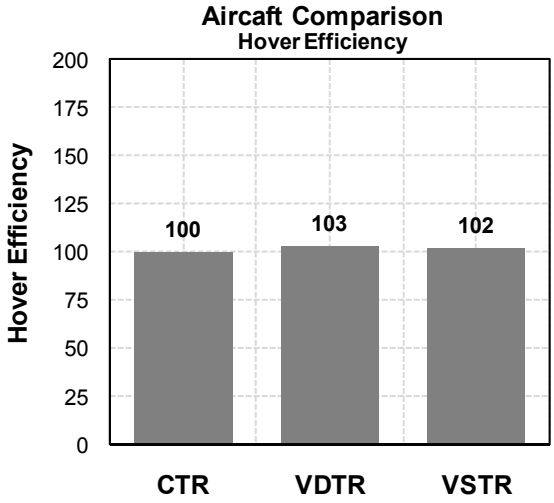

Figure 17. Hover-efficiency comparison.

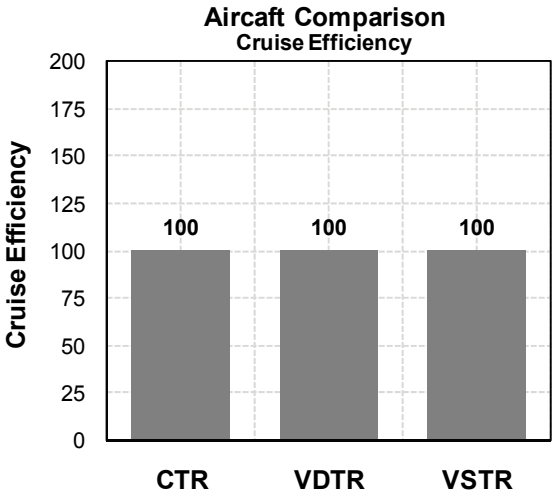

Figure 18. Cruise-efficiency comparison.

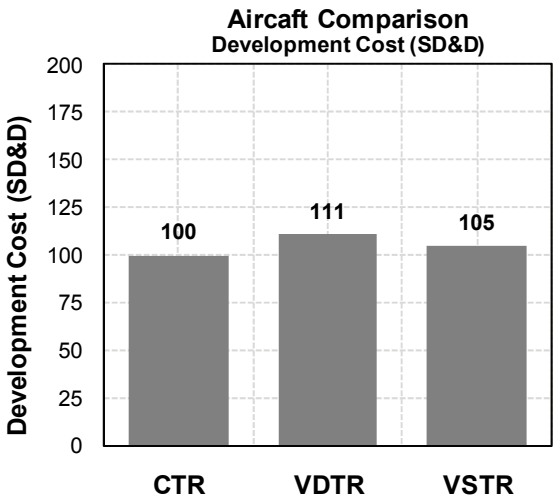

Figure 19. Development-cost comparison.

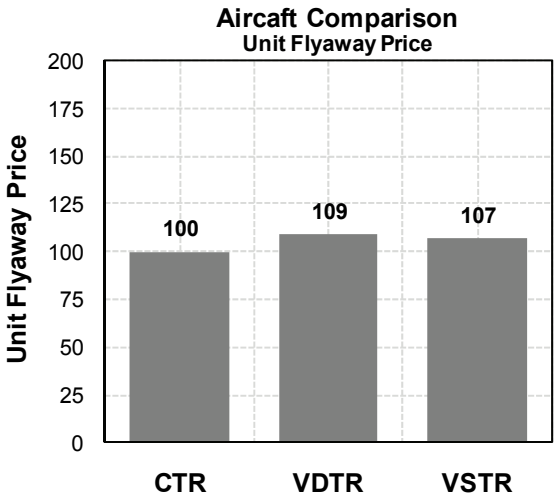

Figure 20. Unit-flyaway-price comparison.

The three LVLT aircraft configurations are similar in their overall architecture and are described in the following section collectively. Unique features of the configurations are noted and described. The LVLT aircraft all follow the lines of classic tiltrotor configurations. A large rotor is mounted on each wingtip, providing axial propeller thrust in the cruise configuration, and is rotated around a tilt axis to provide vertical-lift thrust in the hover configuration.

3.3.1 Main-Rotor System

All three aircraft employ a composite, flexbeam, nongimbaled rotor hub design as an alternative to a classic, gimbaled design. In concept, the composite flexbeam is mated with a pitch-bearing pair and allows for flapping motion while maintaining a stiff-in-plane rotor, an advantageous arrangement for mitigating propeller-whirl-flutter instability. The pitch-bearing pair isolates the flexbeam from the extreme collective pitch-range requirements required for high-speed tiltrotors.

The VDTR retraction mechanism is separated from the physical hub geometry, allowing for a simpler rotor hub, improved retraction-system life, and blade fold. The VSTR rotor design mirrors the work for the other configurations. During cruise the rotor rpm and centrifugal forces (CF) are significantly reduced. Maintaining rotor stability at these low rpms and reduced CF is a challenge for the VSTR rotor design, requiring the rotor of the VSTR to be designed with significantly increased hub and blade stiffness to maintain blade stability. The variable-speed aspect of the VSTR also affects the rotor design in more subtle ways such as blade-twist geometry and rotor-blade dynamics and tuning for the large-rpm variation.

The CTR and VSTR blades are traditional composite blades utilizing a graphite-blade spar, fiberglass skins, and titanium/nickel abrasion strip. Cross-sections were developed in Computer Aided Three-Dimensional Interactive Application (CATIA) and then iterated through ANSYS and Rotorcraft Comprehensive Analysis System (RCAS) to develop a Southwell plot that met dynamic stability requirements and resulted in a rotor with acceptable aerodynamic performance and strain levels.

The VDTR blade-design effort had two primary focuses: developing and refining a retraction system to govern the reduction in rotor diameter and then integrating that system into an acceptable rotor design. The retraction-drive research and development was assisted by the large-scale testing of VDTR systems completed by Sikorsky in the late 1990s, and the resulting LVLT VDTR system is believed to be an improvement over those efforts.

A trade study was conducted to select a blade retraction and extension system. While leaning heavily on past Sikorsky efforts, new configurations not previously studied were also considered. Previous Sikorsky efforts concentrated on two broad concepts: a ball screw embedded in the blade to serve as a linear actuator, and a fibrous strap that retains the blade and is wound around a retraction drive in the hub. Each concept was considered in detail and traded against one another. The strap-driven concepts studied react the blade centrifugal force with a woven strap or cable and then retract the blade by winding the strap around a drum at or near the center of the rotor. A primary advantage of these concepts is reduced weight. A second advantage is increased ballistic tolerance. A woven strap would be several inches wide, and the likelihood of a round of ammunition cutting through a critical cross-section is lower than through a ball screw of smaller diameter. Furthermore, a damaged strap can still be wound onto a drum, while the precise tolerance nut and ball bearings are unlikely to travel over a damaged section of a ball screw. Given the advantages of the strap and reel retraction mechanism compared to ball-screw actuators, a strap was selected as the primary candidate for design of the retraction system.

Several power sources are compatible with each of these ideas, including electrical, hydraulic, or direct drive from the transmission. The final selection of a concept and power source was a balance between weight, reliability, ease of integration, and redundancy, along with the requirement to maintain synchronous retraction and extension of the four rotor blades to maintain the rotor balance.

3.3.2 Drive System

The drive systems for the three aircraft configurations (CTR, VDTR, and VSTR) were developed around a fixed-engine configuration baseline that allows the rotor and primary gearbox to rotate for hover, but keeps the engines horizontal. This configuration eliminates hot exhaust-gas impingement on tarmac and ship-deck surfaces, but requires a unique gearbox and engine arrangement.

The drive systems of the three LVLT configurations are similar in that each has two turboshaft engines that lie horizontally, aft of the gearboxes in the nacelle. The engines are spaced to provide an adequate mounting footprint for the main gearbox, which must rotate with the rotor. Each engine feeds into a stationary nose gearbox, the redirected output of which feeds into the main module section of the main-rotor gearbox (MGB) and supplies power to the rotor though a collector face-gear mesh and conventional planetary assembly. Structurally, in addition to containing the drive gears, the gearbox must support all of the flight loads from the rotor and distribute them to the airframe. This support is achieved with a titanium main-rotor shaft, or mast, and an advanced aluminum housings and bearing system.

All three LVLT configurations employ a cross-shaft system to synchronize the proprotors and to provide protection against an engine failure. The VSTR gearbox requires an additional gearbox to provide the shifting mechanism to enable low rotor speeds for high-speed flight. The shifting gearbox is a two-speed mechanism using a low-power locking clutch (ref. 5).

3.3.3 Flight-Control System

The flight-control systems (FCSs) for the LVLT aircraft are digital, dual-triple-redundant fly-by-wire (FBW) flight-control systems incorporating advanced control laws and autopilot capability. The LVLT aircraft employ FBW in the FCS to capitalize on significant savings in system weight, complexity, and maintenance cost, as well as improvements in safety and capability over traditional mechanical flight-control systems. The FBW FCS enables tailored handling qualities and precision approach modes using the coupled flight director.

With FBW, the maintenance burden is significantly reduced because of the elimination of various components (e.g., trim servos, mixer assemblies, etc.) that require servicing, rigging checks, and other maintenance actions. The FBW electronic components are highly reliable and redundant.

3.3.4 Propulsion System

The propulsion systems of the three LVLT aircraft are based on four engines mounted in pairs in each wingtip nacelle. The engines are mounted in the fixed frame, as opposed to the tilting frame like the V-22 and XV-15 configurations. By not rotating the engines with the rotors, some weight savings was realized in the engines themselves as the engine bearings and lubrication systems were not required to operate over such a large variation in orientation. Operational considerations, however, favored the fixed-engine arrangement.

The engines selected for the aircraft are high-efficiency turboshaft engines designed to operate as efficiently as possible over a large range of rpms. These engines extract the maximum amount of energy from the exhaust but also have very high exhaust temperatures. Without cooling air mixing and significant infrared (IR) suppression efforts, these temperatures could pose a significant threat to the deck surfaces of ships and the asphalt surfaces of tarmacs, and could make operations from unprepared surfaces impossible. By keeping the engines fixed in the wing frame, the exhaust is ejected horizontally into the rotor downwash, providing ambient air mixing and preventing the direct impingement of exhaust gases on any ground surfaces or personnel below the rotors.

3.3.4.1 Inlets and Exhaust

To maximize the forward-flight performance cruise efficiency, the minimal inlets required for cruise flight face forward on the lower edges of the nacelle below the wing. The inlets were designed for minimal losses in the high-speed airflow environment.

On the lower surfaces of the nacelles, there is one larger hover inlet for each engine. The air passing through the hover inlets is “filtered” using an inlet particle separator (IPS) with no moving parts and very high separation efficiency. During hover and low-speed flight, the cruise inlets are blocked off, forcing all of the inlet flow through the IPS. During cruise flight, the positive pressure in the inlet duct prevents additional flow from coming through the IPS.

The exhaust systems of the aircraft employ a simple IR suppressor system. Since the engines are fixed horizontally during all flight regimes, the IR suppressor is not required to mix all of the exhaust flow down to safe operating temperatures for ground operations, but simply needs to provide the best line-of-sight (LOS) blockage to the engines while minimizing the performance impact on the engines.

3.3.4.2 Fuel System

The fuel system of the LVLT aircraft is similar to other fixed-wing transport aircraft. The primary fuel cells are located between the spars of the main wing in typical "wet-wing" fashion. The fuel cells in the wings are capable of carrying the fuel required for all the LVLT missions, allowing the cabin to be clear of auxiliary fuel systems for these missions. For longer-range missions, auxiliary tanks could be mounted in the cabin and plumbed into the aircraft fuel system, allowing for the vehicle management system to manage the appropriate fuel distribution for the given mission and cruise condition. There are no center wing tanks, but wing box tanks could be added if required. All tanks are cross-linked, allowing the vehicle management system to manage the fuel distribution for balance and mission requirements. As the aerodynamic and structural requirements for the wing drove the minimum wing thickness ratio, there is ample fuel volume available within the wings for each of the configurations.

3.3.5 Wings and Winglets

The wings of the LVLT aircraft are key components in the LVLT system design. The wing design completed a full iteration, including the design of a customized, supercritical airfoil, optimized wing planform, and a finite-element-method (FEM) analysis of the wing structure. As in other tilt-rotor configurations such as the V-22 and XV-15, the LVLT wing is thicker than large fixed-wing transport designs. The wings of the V-22 and XV-15 aircraft are 23% thick, whereas the wings of the LVLT aircraft are more aggressive. The thinner LVLT wing sections improve cruise efficiency but complicate the aeroelastic concerns of the design.

The structure of the LVLT wings is very similar to that of typical fixed-wing designs with a main spar forward and a secondary spar aft. The spars are joined by structural wing skins that carry the wing torsion moments created by the sweep and nacelle position.

The wings are equipped with both flaps and ailerons for flight control in hover and forward-flight modes. The sizing efforts for all three configurations have assumed simple flap and aileron geometries with the flaps and ailerons sized for 25% of wing chord. This assumption provided a good balance between reducing download and the remaining structural effectiveness of the wing spar and torque tube.

3.3.5.1 Wing-Planform Optimization

The LVLT aircraft sizing optimization was completed with the wing-planform variables allowed to float. The optimizer was allowed to adjust aspect ratio, incidence, and wing loading. For the CTR and VSTR, the inboard wing (between the rotors) is determined by the rotor radius and fuselage width. The space between the rotors was set at 25 ft, which includes space for the fuselage and additional clearance between the rotor tips and the fuselage. For the VDTR in hover, the rotors were allowed to overlap the fuselage but not intermesh. As a result, VDTR rotors with a 77%

reduction ratio allow the inboard wing to be smaller than the other configurations while still allowing adequate clearance between the rotor tips and the fuselage in the cruise configuration. As RDM manipulates the sizing variables (such as disk loading and wing loading), the weight effects were calculated and allowed to influence the overall design.

The overall wing planform (wing plus wing tips) was determined by wing loading and total aspect ratio. Wing loading was one of the independent optimization variables but was subject to the constraint that the C_L at the midpoint of the heaviest cruise segment of the LVLT mission be set to be at least 20% less than the maximum C_L of the airfoil at the cruise speed of the segment. This constraint prevented the optimizer from progressively increasing the wing loading, limiting wing size and weight.

3.3.5.2 Winglet Design

Articulated winglets proved to be the optimal solution to balancing weight and performance across the entire flight envelope. The wingtip configuration is also ideal for short takeoff performance optimization as the wingtips can be tailored for the desired flight performance. The final planform of the winglets for each configuration was determined by the wing planform optimization, and the span of the winglet was determined by the difference between the overall wingspan and the inboard wingspan. Because there is no significant mass outboard of the winglet, the airfoil of the winglet is much thinner than the inboard-wing airfoil.

The winglets are actuated to operate in the range of approximately +10° to –90° independently of the nacelle position. During hover operations the winglets are vertical, and during transition the winglets are actuated so that the winglet operates in a low-drag lifting position. During high-speed cruise flight, the winglets are fixed for efficient cruise.

4 Attributes and Aircraft Performance

The baseline CTR, VDTR, and VSTR LVLT aircraft performance was modeled using Sikorsky's Rotorcraft Design Model (RDM) using rotor aerodynamic performance data generated by the EPHIC (Evaluation of Hover Performance using Influence Coefficients) program.

As illustrated in Figure **4**, the LVLT hover requirement sized the rotor diameter, solidity, engine power, and gearbox power and torque limits. The inboard span of the wing was dictated by the rotor diameter to provide adequate fuselage clearance in cruise for CTR and VSTR and to provide adequate rotor-to-rotor clearance for the VDTR in hover. Wing area was set to provide reasonable cruise C_L for the aircraft based on the fallout cruise speed capability and LVLT cruise-mission weights. This area was added to both the outboard wingtips, and chord length was added over the inboard wingspan. The sensitivity of the design based on aspect ratio, wing loading, and disk loading was considered; the final geometry offering minimum empty weight was ultimately chosen.

4.1 Attributes Summary

4.1.1 Air Vehicle Aerodynamics

The total equivalent flat-plate drag areas at zero-degrees angle of attack of the CTR, VDTR, and VSTR were estimated using a methodology based upon wind tunnel drag measurements, empirical drag data, and computational fluid dynamics (CFD)-based analytical tools. Figure 21 illustrates the CTR, VDTR, and VSTR equivalent flat-plate drag area versus structural-design gross weight with historical aircraft for comparison. The constant lines represent levels of skin-friction coefficient, C_f, which is the constant of proportionality between the equivalent flat-plate drag area, f_e, and gross weight $(GW)^{2/3}$.

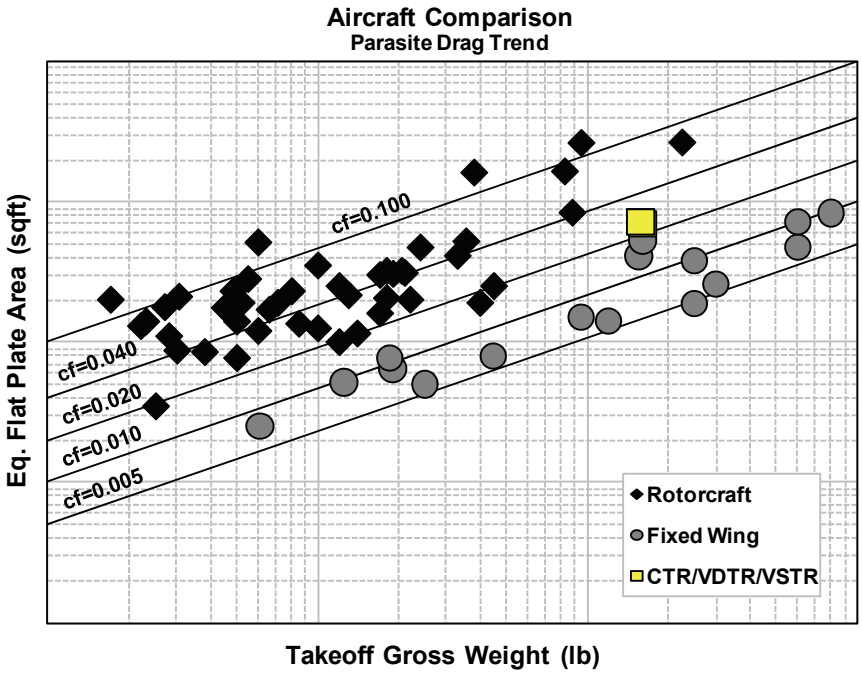

Figure 21. Equivalent flat-plate drag comparison.

The vertical drag of the LVLT aircraft was calculated using a Circulation Coupled Hover Analysis Program (CCHAP) file created with aircraft design parameters based on the CTR configuration, including fuselage and rotor-blade properties (planform and airfoil data). The CCHAP input file represented one-half of the fuselage, including one wing and one rotor. A symmetry plane was assumed at butt-line 0.0. Rotor thrust was assumed to be one-half the total thrust in hover. Assuming a rotor thrust and wing C_D, the vertical drag for the CTR wing under the rotor was calculated, resulting in a vertical drag similar to that of existing tiltrotor aircraft. A vertical-drag increment was applied to represent the rotor-wake-fountain contribution to download, based on V-22 data.

4.1.2 Rotor Aerodynamics

This study employed a method to quickly identify optimized blade geometries for any specified tiltrotor mission. A modified version of the Evaluation of Hover Performance using Influence Coefficients/Helicopter Rotor Optimization (EHPIC/HERO) analysis was developed by Continuum Dynamics Incorporated (CDI), as discussed in reference 11. A unique aspect of the approach is the ability to address highly nonlinear distributions of blade chord, twist, and sweep. The EHPIC/HERO analysis combines a highly efficient and accurate free-wake performance-prediction model with a comprehensive design-optimization algorithm to create an effective tool for design optimization of rotorcraft in hover and axial flight. Furthermore, this study incorporated Sikorsky proprietary code for optimizing blade geometry to simultaneously meet two separate design conditions. For proprotors, these conditions are the hover and cruise design points.

The development of this analysis was rooted in the study of "open-loop" performance prediction for hovering rotors. Early efforts to develop free-wake hover models using time-domain calculations were hampered by long computation time and poor (or nonexistent) convergence due to the inherent instability of the wake beneath a hovering rotor. Reference 12 describes the development of the baseline EHPIC free-wake relaxation scheme using influence coefficients that avoid these convergence problems. An initial guess for the blade loads and wake geometry is adjusted in a succession of solution steps using influence coefficients until the physically correct, self-preserving wake geometry is obtained. The unsteady wake beneath a hovering rotor is unstable about this solution, but average performance characteristics can be obtained using this wake geometry. This fact has been substantiated through numerous correlation studies with hover-performance measurements, some of which are cited in references 12 and 13. In EHPIC, rotor-performance characteristics are obtained by coupling the free-wake analysis to a vortex lattice treatment of the blade similar to that described in reference 14. This analysis can be extended to axial flight (i.e., helicopters in vertical climb or tiltrotors in cruise flight) simply through the addition of an appropriate uniform free-stream velocity.

The single-point optimization found in the general release of EHPIC/HERO optimizes blade geometry for hover or cruise, but not both simultaneously. Single-point optimization is valuable for understanding blade-geometry traits that improve performance in hover or in axial flight, but cannot be used to address the design compromises necessary for rotors that need to operate efficiently in several different flight conditions. With dual-point optimization, blade geometries are found that meet any prescribed weighting combination of the hover and cruise design points. Further, sweeping the design-goal weighting factor quickly produces a family of optimized blade

geometries that extend from pure hover to pure cruise. Reference 11 provides correlation comparisons of the EHPIC/HERO results with V-22 test data.

The desire to obtain the minimum possible rotor diameter during cruise was found to limit the combined hover/cruise performance of the VDTR. Although reducing blade diameter to limit excessive cruise-blade-profile power is fundamental to the VDTR concept, excessive diameter reduction actually decreased blade efficiency. This phenomenon occurred because excessive retraction overly constrained other important rotor design variables. Specifically, maximizing blade retraction constrains blade twist across 85% of the hover radius and 74% of the cruise radius. Because the large region of linear twist required for the retractable portion of the blade inhibited the nonlinear twist needed to approximate desirable distributions, overall blade efficiency was penalized rather than improved.

The solution to this conflict was to limit the cruise-blade retraction to 77% of the hover radius. This limitation was used with an N_R reduction to further increase the cruise-blade loading and decrease the cruise-tip Mach number. A secondary VDTR efficiency improvement was obtained by thinning the blade outer airfoil sections. Previous 66% radius cruise-retraction designs required a larger over-sliding region than the current 77% scheme. Relieving the need for thicker airfoils on a portion of the outer radius was beneficial in both hover and cruise.

The rotor-blade twist distribution for each aircraft was selected from a FM-η_P boundary that progressed from an ideal hover twist to an ideal propeller twist. Twist distributions for boundary points between the two extremes were then interpolated from the two end-point patterns. Figure 22 shows the relative FM-η_P boundaries for all three aircraft, normalized to the peak CTR FM and the peak CTR η_P. Figure 23 and Figure 24 show the relative design FM and η_P of the three aircraft. Note that the VDTR achieves 4% greater propulsive efficiency than the CTR, while losing only 3% FM.

Estimated rotor efficiencies were judged against similar projections using codes other than EHPIC. These calculations added confidence when the checks align, and served as a flag for more in-depth scrutiny when not aligned. To that end, limited cruise- and hover-efficiency comparisons were made between EHPIC predictions and those calculated with two additional rotor aerodynamic codes. Specifically the CDI CHARM code was exercised to estimate comparative hover FM and cruise η_P values for the CTR configuration, and both CHARM and LSAF were used to check the VDTR calculations. These additional evaluation codes were selected as having mature evaluation capabilities.

Figure 25 shows good EHPIC η_P validation against both CHARM and LSAF for the VDTR and between EHPIC and CHARM for the CTR. The high degree of agreement was not unexpected, since accurate propulsive-efficiency estimation for most tiltrotor designs is not difficult because of the relatively low importance of induced power loading for propellers operating at high advance ratios. Similarly, η_P prediction requires only that the codes properly resolve spanwise angle-of-attack and Mach number distributions, while referencing common 2-D airfoil tables.

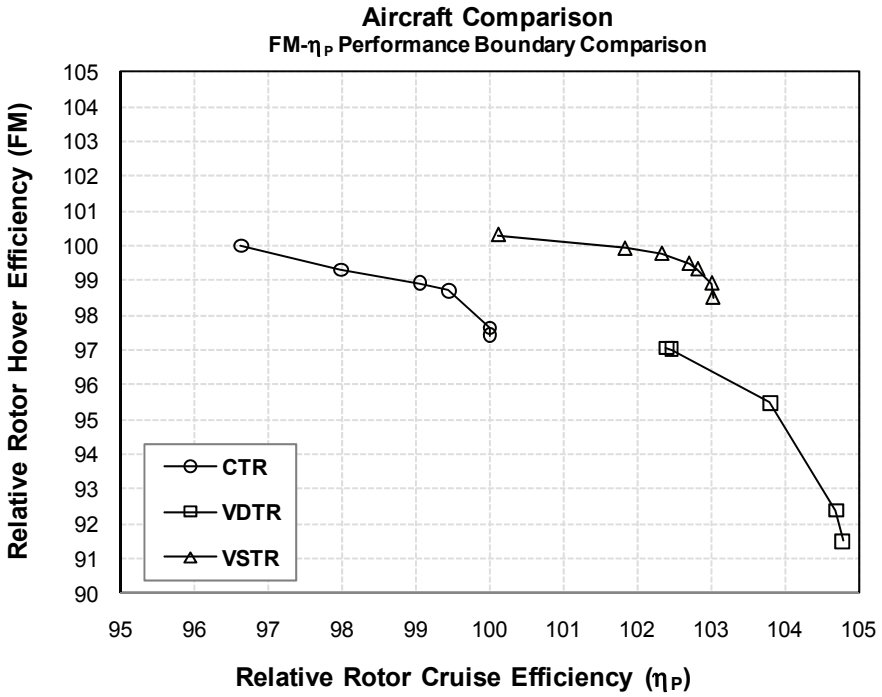

Figure 22. Hover-cruise-efficiency design trends.

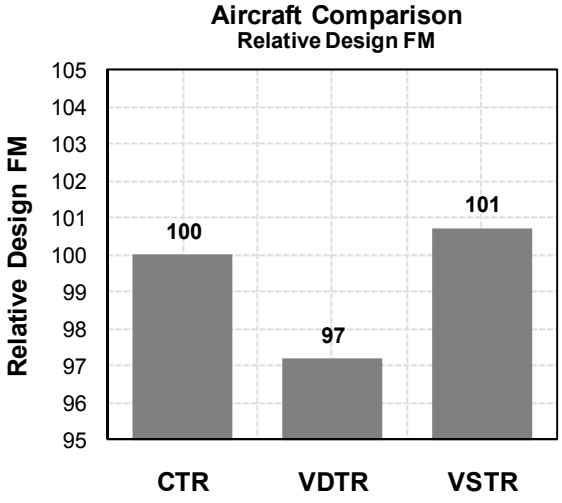

Figure 23. Design FM comparison.

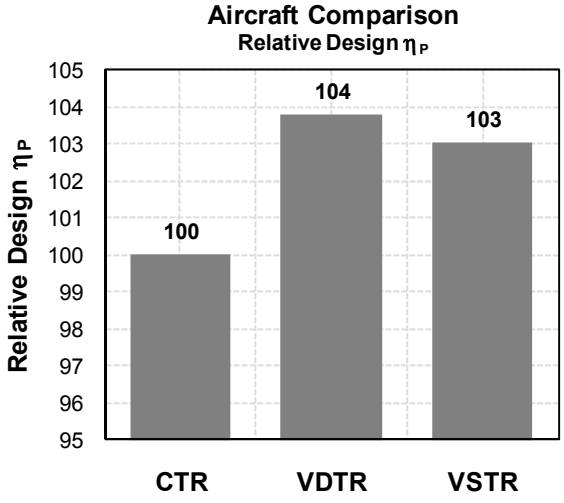

Figure 24. Design η_P comparison.

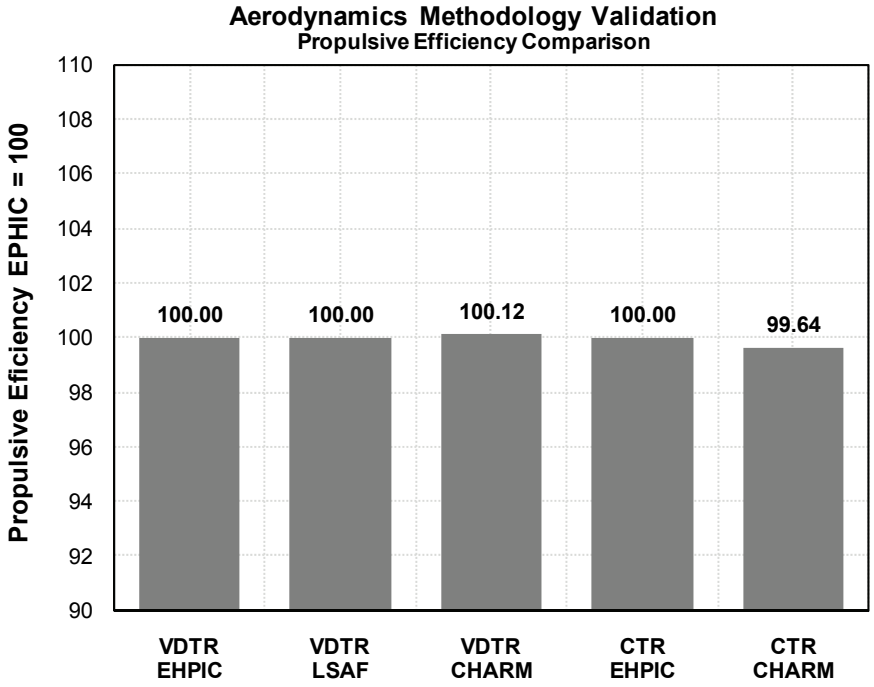

Figure 25. Cruise-efficiency-performance checks.

Figure 26 presents the corresponding hover-efficiency comparisons. In this case the agreement for the VDTR was again good. However, significant hover discrepancies were shown for the CTR rotor geometry. This result was unexpected since the VDTR case was deemed more challenging because of unavoidable twist and airfoil t/c constraints on the over-sliding portion. Based on the observed VDTR FM prediction consistency**,** only the CTR EHPIC and CHARM cases were further examined.

The figure shows predicted EHPIC and CHARM FM values for the Sikorsky CTR blade design. Again, both calculations were carried out at the CTR design C_T/σ and a common tip Mach number. It is noted that the large FM drop predicted with CHARM was limited to calculations at high blade loadings. For these conditions, CHARM predicted large tip angles of attack with local drag divergence, caused by released CHARM CTR tip-vortex filaments that stayed in the rotor plane and impacted the following blade.

The red bar in Figure 26 shows that the adverse CHARM CTR response to the calculated tip environment can be lessened. Substituting a 10% thick SC36210 tip airfoil for the base CTR 7% tip airfoil increases the drag divergence boundary, removing about half of the FM penalty. Additionally, a modest change to the CHARM sweep model, bringing it into alignment with the EHPIC formulation, moves the CHARM FM up to 0.80 at the CTR design condition. Further CHARM FM improvements are not likely, given the high tip angles of attack seen by the code.

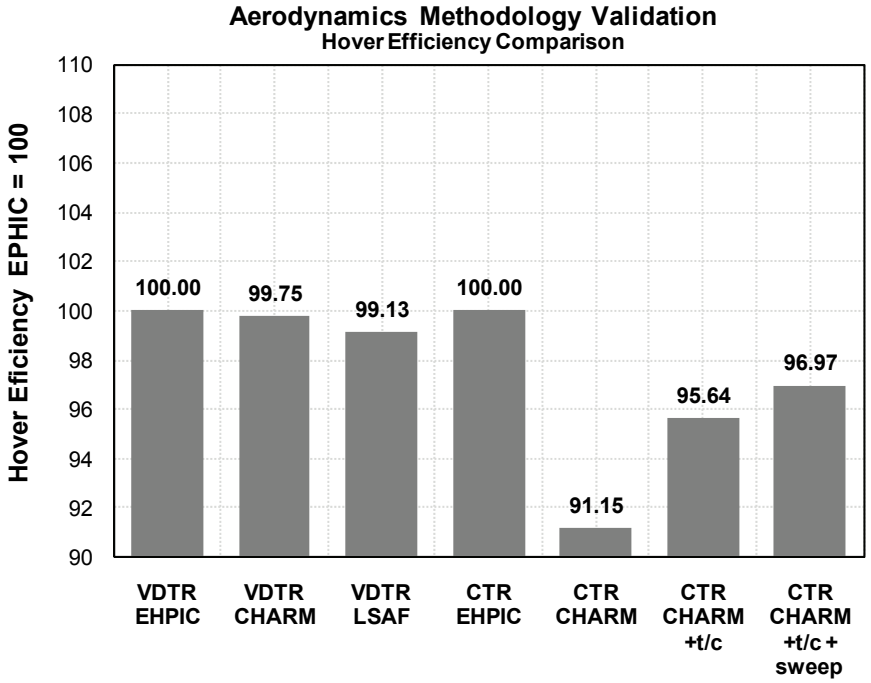

Figure 26. Hover-performance checks.

4.1.3 Wing Aerodynamics

Wing planform selection was based on the need to meet specified mission performance while minimizing vehicle empty weight. Because of the interplay between wing structural weight and wing aerodynamic performance, precise wing planform closure required several individual structural and aerodynamic optimization loops. Wing structural optimization preceded the equivalent wing aerodynamic optimization. This approach was undertaken since wing geometric pitch washout, as well as wing airfoil shape, offered practical knobs for fine tuning aerodynamic performance for a given wing planform.

Wing-performance tables were constructed for the isolated wing-prop geometry. These tables included separate induced and profile power terms for a variety of off-design wing flight conditions. After correction for wing-body and wing-nacelle installation, the tabular data were then used to produce an Oswald efficiency model for the installed wing-body–nacelle combination. The Oswald efficiency model was incorporated into RDM for the aircraft synthesis.

Wing-airfoil-section aerodynamic design was performed using the MSES CFD program. Initially, an airfoil section was generated by scaling a NASA 18% thick supercritical airfoil to the root thickness required by the wing structural analysis. At the airfoil section design condition, a supersonic region and shock formed on the upper surface. The initial airfoil was then modified using the MSES mixed (viscous) inverse procedure with the objectives of eliminating wave drag at the design condition and improving the airfoil-section drag at lift coefficients greater than the design target by delaying the onset of supersonic flow on the upper surface. A shock-free chordwise pressure distribution was prescribed on the airfoil upper surface, and the inverse method was allowed to modify the mean camber line while maintaining the initial design thickness

distribution. This modification produced the desired pressures on the upper surface while allowing the pressures on the lower surface to change. The Mach contours of the scaled airfoil and the designed airfoil are shown in Figure 27 and Figure 28, respectively.

At the design condition, the resulting designed airfoil had the same drag as the initial airfoil because the reduction in wave drag had been offset by an increase in viscous drag. At higher lift coefficients, the designed airfoil had lower drag because the development of supersonic flow was delayed relative to the initial airfoil. The improved performance of the designed airfoil for higher lift coefficients, however, was the result of increased camber, which caused more negative (unfavorable) values of pitching moment.

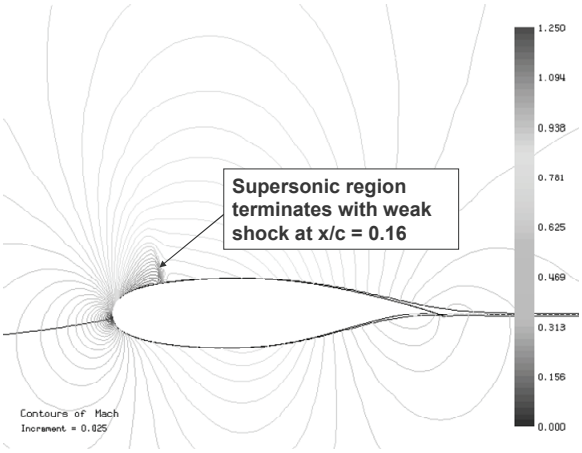

Figure 27. Scaled airfoil Mach contours.

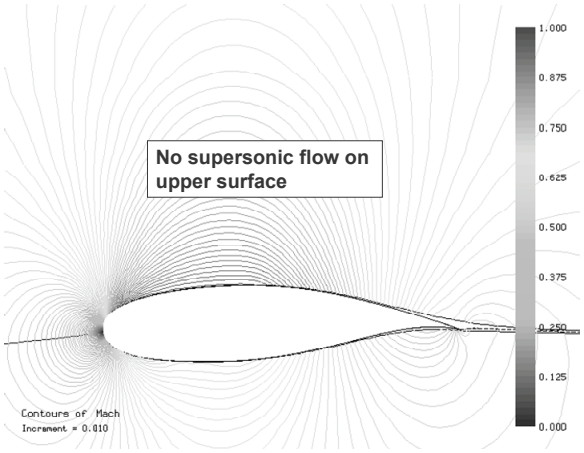

Figure 28. Designed airfoil Mach contours.

4.1.4 Aeroelastic-Stability Analysis

A literature review was conducted on the state-of-the-art analytical methods and tools available for aeroelastic stability predictions of tiltrotor aircraft. Theoretical and experimental studies of proprotor and tiltrotor whirl flutter were surveyed (refs. 5 and 15 through 18). The influence of design variables such as wing design (refs. 5 and 18), active stability augmentation (ref. 19), and variable geometry rotors (refs. 13, 20, and 21) on whirl-flutter stability was reviewed. Tiltrotor aeroelastic stability modeling methods and capabilities of aeroelastic analysis codes such as RCAS, Comprehensive Analytical Model of Rotorcraft Aerodynamics & Dynamics (CAMRAD), DYMORE, University of Maryland Advanced Rotorcraft Code (UMARC), and Proprotor Aeroelastic Stability Analysis (PASTA) were investigated (refs. 8, 9, 14, 20, 22, and 23). Based on the literature review and Sikorsky experience, RCAS was selected as the primary aeroelastic analysis tool.

RCAS validation was twofold. First, RCAS was validated for accuracy of whirl-flutter stability predictions though correlation with test data from the Wing and Rotor Aeroelastic Testing System (WRATS) and the corresponding DYMORE model data (Test 543 of the V-22 1/5 scale model conducted in the NASA Langley Transonic Dynamics Tunnel (TDT) in 2000). Second, the process

of modeling a detailed tiltrotor in RCAS was validated by comparing V-22 model results to analytical results from tools that were used to design the V-22 rotor.

A NASA Structural Analysis Program (NASTRAN) model of the WRATS Ground Vibration Test (GVT) configuration was developed based on the DYMORE GVT model received from the Army Research Lab (ARL) at NASA Langley. The geometry, element meshes, material, and section properties were translated from the DYMORE model into the NASTRAN model. The NASTRAN-predicted modal frequencies and mode shapes at the rotor hub correlated well with the DYMORE and GVT measurements. A comparison of the NASTRAN, RCAS, and DYMORE analytically predicted frequencies with the GVT measured frequencies for both the off- and on-downstop configurations is shown in Table 1. The validated NASTRAN model was converted to the RCAS model for whirl-flutter analysis.

TABLE 1. MEASURED AND PREDICTED WING-NACELLE FREQUENCIES

Mode	Prediction / Test Source	Frequency (Hz)	
		Off-downstop	On-downstop
Wing Beam	GVT Test	5.43	5.83
	DYMORE	5.16	N/A
	NASTRAN	5.14	5.59
	RCAS	5.28	5.68
Wing Chord	GVT Test	8.11	8.67
	DYMORE	8.28	N/A
	NASTRAN	8.33	8.33
	RCAS	8.30	8.31
Wing Torsion	GVT Test	10.54	12.02
	DYMORE	10.54	N/A
	NASTRAN	10.47	11.92
	RCAS	10.48	11.89

RCAS predicted natural frequencies of an isolated, clamped WRATS blade were validated with test results. RCAS natural frequencies predictions for the clamped, nonrotating blade in a vacuum are compared with test results and DYMORE predictions in Table 2.

TABLE 2. COMPARISON OF FREQUENCIES OF THE CLAMPED WRATS BLADE

Mode	Experiment (Hz) *	DYMORE (Hz) *	RCAS (Hz)
1st Flap	12.29	12.08	12.02
1st Chordwise	34.11	34.30	36.68
2nd Flap	52.44	56.25	53.34
1st Torsion	113.35	115.18	113.79

* Data from ref. 9

Validation of the isolated full rotor model was also been performed with a locked gimbal. The purpose of running the model with locked gimbal was to obtain blade frequencies with proper modeling of the flexbeam and control systems. The RCAS prediction of nonrotating frequencies for a single blade with flexbeam and control system is compared to experimental and DYMORE results in Table 3. The nonrotating blade natural frequencies correspond to a case with a 10-degree collective angle and locked gimbal.

TABLE 3. NONROTATING ROTOR FREQUENCIES WITH FLEXBEAM AND ROTOR CONTROL | GIMBAL LOCKED

Mode	Experiment (Hz) *	DYMORE (Hz) *	RCAS (Hz)
1st Flap	6.60	6.83	6.91
1st Lag	20.6	18.83	17.78
2nd Flap	25.2	26.78	26.04
3rd Flap	69.3	71.78	72.14
1st Torsion	112.6	110.57	107.71

* Data from ref. 9

After the isolated rotor model with locked gimbal was validated, the full rotor model with unlocked gimbal was analyzed. The validation of RCAS-predicted frequencies with experimental data and DYMORE results is given in Table 4.

TABLE 4. NONROTATING ROTOR FREQUENCIES WITH FLEXBEAM AND ROTOR CONTROL | FREE GIMBAL

Mode	Experiment (Hz) *	DYMORE (Hz) *	RCAS (Hz)
Gimbal	2.0	2.33	2.02
Cone	6.8	6.80	7.20
1st lag	19.7	18.74	18.50
2nd Flap	25.0	26.69	25.64
1st Torsion	112.1	110.57	106.14

* Data from ref. 9

The complete semispan WRATS model, created by combining the GVT model and the rotor model, was used to predict the whirl-flutter stability boundary of the wind tunnel test configuration in airplane mode. Whirl-flutter stability analysis was performed for the off-downstop configuration, which has pitch-flap coupling (delta-3) of –15 degrees and a rotor speed of 742 rpm. The airspeed was increased from 50 knots until the whirl-flutter speed was reached. The variations of the predicted and measured wing-beam-mode frequency and damping with airspeed are shown in Figure 29 and Figure 30.

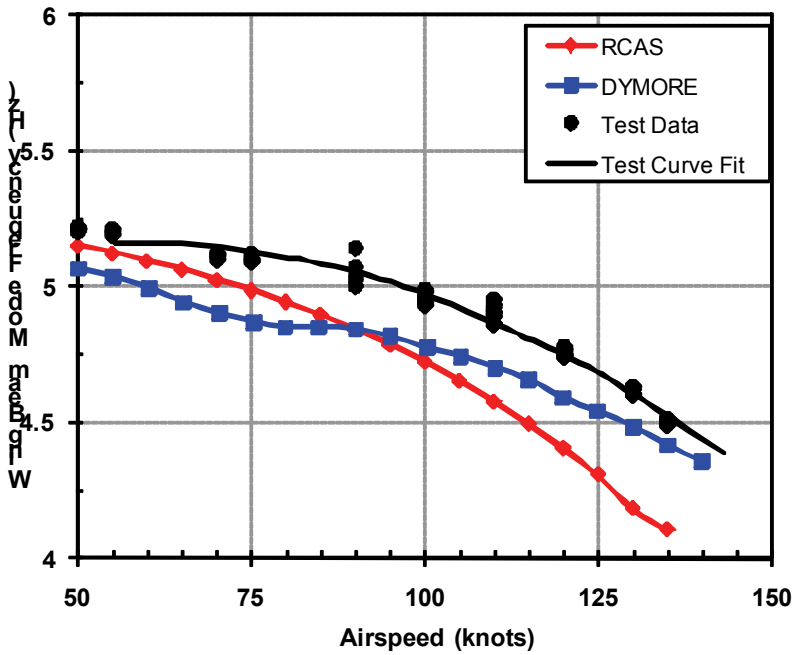

Figure 29. Wing-beam-mode frequency correlation.

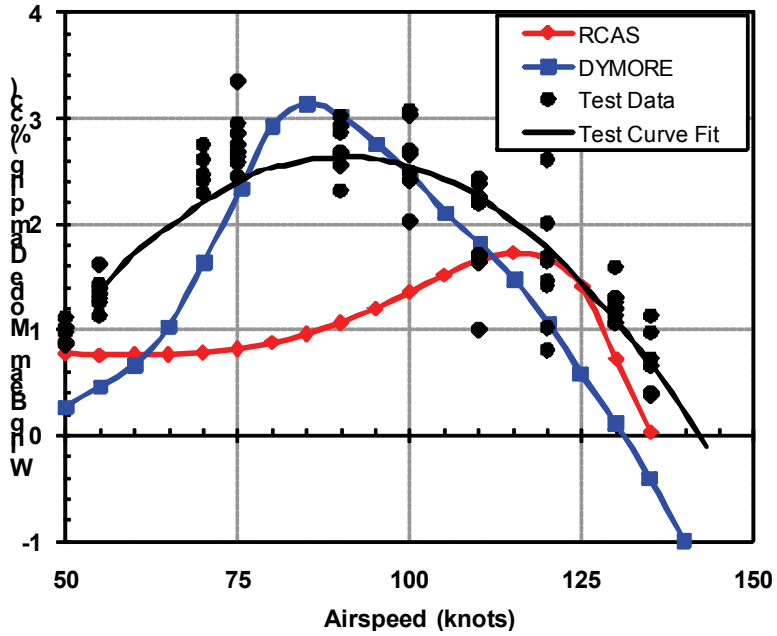

Figure 30. Wing-beam-mode damping correlation.

The black solid circles represent the measured data points obtained from the WRATS wind tunnel test database. The solid black line is the curve fit of the test results, similar to the data published in reference 18. The blue solid line with square symbols is the DYMORE prediction (ref. 9), while the red solid line with diamond symbols is the RCAS prediction. The measured and predicted whirl-flutter speeds are 142 knots from the test, 130 knots from DYMORE, and 135 knots from RCAS.

An isolated V-22 rotor model was created in RCAS, complete with representation of the yoke, grip, pitch bearings, control-system stiffness, and blade. The frequencies and mode shapes (both collective and cyclic) were calculated for a low-thrust case of 38° root collective and compared to those in the Bell/Boeing EMD flutter report. A root collective of 38° corresponds to about 12° of pitch at r/R = 0.75. Note that the elastomeric pitch bearing stiffnesses were not known, so a stiff spring ($1x10^8$ lb/ft) was used for the transverse flexibility in both axes of the pitch bearing. Also, the drive-system stiffness was not known, so the stiffness of the lag hinge was varied until the rigid collective lag-mode frequency matched that found in the report. A tabulated comparison of the normalized frequencies is shown in Table 5 and Table 6. The frequency results show reasonable correlation.

TABLE 5. V-22 COLLECTIVE FREQUENCIES | RCAS MODEL VS. EMD REPORT

Mode #	Mode Description	EMD Report	RCAS Model
1	Edgewise 1	0.34P	0.34P
2	Flap 1	1.17P	1.22P
3	Flap 2	2.74P	2.81P
4	Edgewise 2	4.37P	4.50P
5	Torsion 1	5.33P	5.36P
6	Flap 3	6.17P	6.42P
7	Torsion 2	9.26P	9.36P

TABLE 6. V-22 CYCLIC FREQUENCIES | RCAS MODEL VS. EMD REPORT

Mode #	Mode Description	EMD Report	RCAS Model
1	Flap 1	1.002P	1.004P
2	Edgewise 1	1.53P	1.47P
3	Flap 2	2.40P	2.57P
4	Torsion 1	4.49P	4.47P
5	Flap 3	5.36P	5.21P
6	Edgewise 2	7.06P	6.97P
7	Torsion 2 / Flap 4	8.67P	9.00P
8	Flap 4 / Torsion 2	9.60P	9.31P

The stability criteria consisted of a 20% margin from the maximum level cruise speed (VH) to account for dive speed (VDIVE) and a 15% margin from the dive speed as a stability margin. The final result was a stability margin of about 40% over the cruise speed.

The modeling approach for whirl flutter was common to all three aircraft. The fully coupled RCAS model consisted of a 4-bladed rotor model (including blades, torque tubes, and flexbeams) coupled to a modal representation of the wing, which consisted of frequencies and mode shapes at the hub as derived from a wing NASTRAN model. A detailed kinematic control-system model, pre-cone, and the dual-load-path torque tube were all included in the model. The detailed control system modeled the full translation of swashplate motion into blade pitch, accounting for geometric kinematic coupling. The swashplate and pitch horn were assumed to be rigid, and a dynamically stiff scaled V-22 stiffness was applied. The push rod was positioned (radially offset from the effective flapping hinge) to provide a design negative delta-3 when the top of the push rod is in the plane of the rotor.

Several assumptions were made in the whirl-flutter analysis. Specifically, a semispan NASTRAN wing model was used, so only symmetric wing modes (the first five elastic modes) were considered, as the symmetric modes are typically most important for whirl flutter. The same wing model was used for all the aircraft to allow for a fair comparison. Also, no wing aerodynamic effects were modeled; this assumption is conservative since aerodynamic damping was not accounted for. However, this assumption removed the potential to analytically predict wing divergence or fixed surface flutter. A conservative critical damping was applied to the wing modes based on the minimum elastic fuselage damping observed in shake test results of composite fuselage structures. To prevent the rotor polar moment of inertia from coupling with the wing and depressing the wing-mode frequencies, a torsional hinge was added between the rotor and the wing in lieu of modeling a separate, complex drive train. The rotor was trimmed to zero power.

As designed, all three aircraft satisfied the whirl-flutter stability requirements and were stable up to the required 140% V_H speed. Two sensitivity analyses were performed on all the aircraft to gain confidence in the models and to better understand the design space: rotor delta-3 and wing stiffness.

Rotor delta-3 coupling was controlled by offsetting the pushrod from the blade-flap axis. A negative value indicates flap up–pitch up coupling where –15° means 1° of flap induces 0.25° of blade pitch. For 3-bladed gimbaled rotors like the V-22, optimal delta-3 angle is near –15°, with an inherent trade-off between optimizing flap-lag stability, which wants more negative delta-3, and whirl-flutter stability, which wants less negative delta-3.

The sensitivity of whirl-flutter stability to delta-3 for all three aircraft plus an example gimbaled CTR is shown in Figure 31, where V_H is represented as 100, the required stability speed is represented as 140, and the delta-3 angle is normalized to a baseline value of 100. The gimbaled CTR sensitivity is consistent with the WRATS model delta-3 sensitivity (and other published results) and points to an optimal delta-3 between –10° and –7°. However, this optimal delta-3 still does not provide adequate stability to satisfy the requirements. The flexbeam-style rotors satisfied the whirl-flutter requirements within a reasonable band of delta-3 angles.

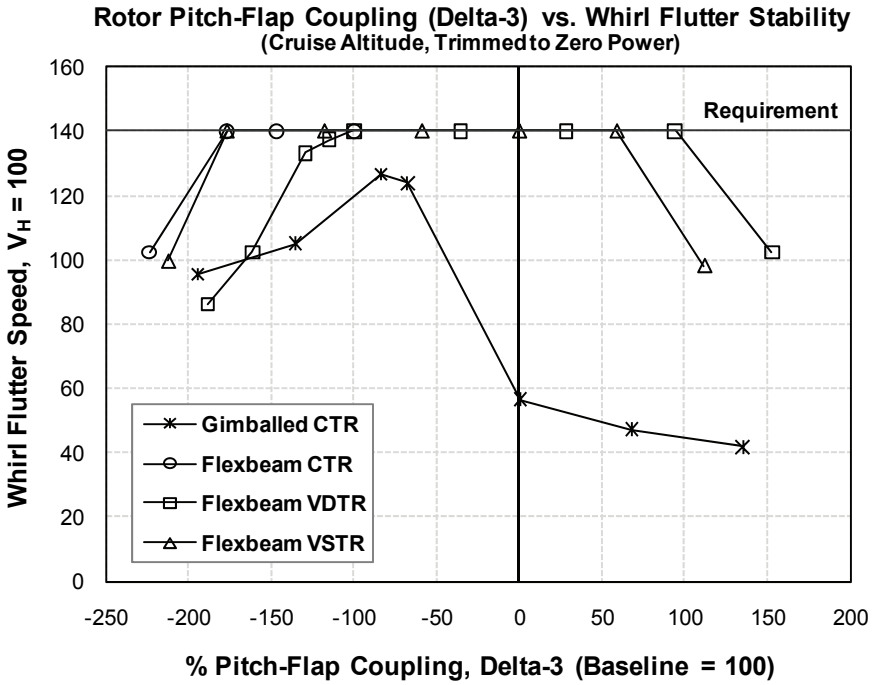

Figure 31. Whirl-flutter-stability sensitivity to delta-3 coupling.

A wing-stiffness-sensitivity study was performed to compare the aircraft and to quantify the effects of variable speed and variable diameter on whirl-flutter stability. The wing stiffness was artificially reduced by applying a uniform factor to the NASTRAN material properties, resulting in wing-mode-frequency reductions equal to the square root of the applied factor. The sensitivity of whirl-flutter stability to wing stiffness for the three aircraft plus the gimbaled CTR is shown in Figure 32. The same wing was used for all aircraft to allow for a fair comparison. The wing was initially designed for a gimbaled CTR with whirl-flutter requirements being the limiting factor in the design. This wing design is close to satisfying the requirements for a gimbaled CTR but falls about 50 knots short. Switching to the flexbeam-style rotors significantly improves stability. The fact that a wing stiffness that is 20% of the baseline is required to induce instability with the flexbeam rotors indicates that whirl flutter is most likely not the design driver for the wing anymore. Instead wing loads, wing divergence, or fixed surface flutter will govern the wing design and could result in a wing that weighs less than the current wing after detailed design iterations.

Reducing wing frequency introduces classical whirl-flutter instability involving coalescence of the rotor regressive flap mode, rotor regressive lag mode, and wing-beam bending mode. Zooming in on the case where the wing frequencies have been reduced by 70% (10% wing stiffness) allows for comparison of the different technologies (variable speed and variable diameter) relative to the conventional tiltrotor.

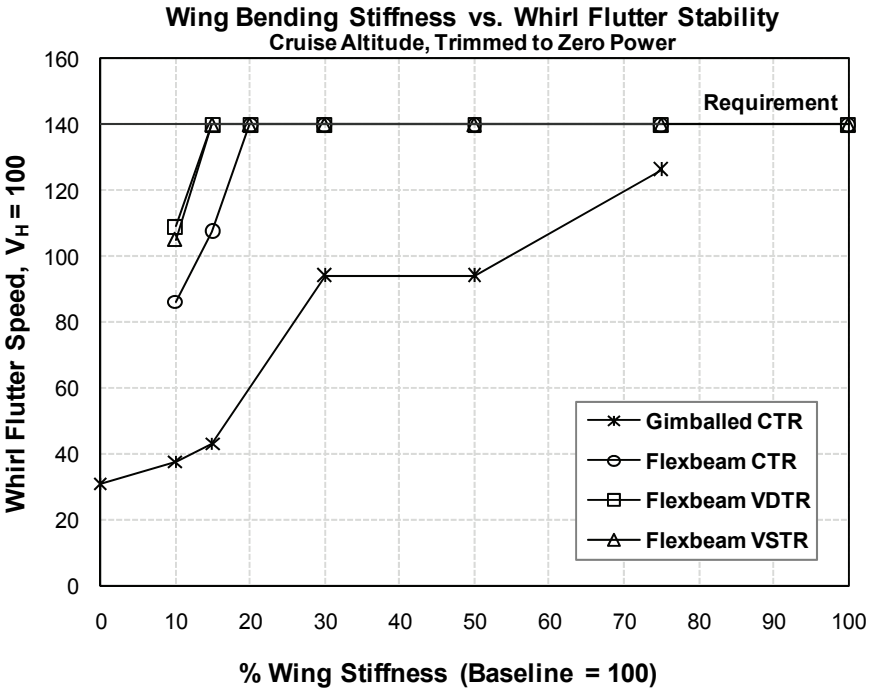

Figure 32. Whirl-flutter-stability sensitivity to wing stiffness.

The wing-beam-mode damping versus airspeed is plotted in Figure 33 for the three flexbeam rotors and example gimbaled CTR rotor. The gimbaled CTR is unstable at a very low speed (as would be expected since the frequencies have been reduced by 70% from the design point). The VSTR and VDTR show a respective 22% and 28% stability improvement over the flexbeam CTR. Most of the improvement for the VSTR, however, comes from the fact that the flexbeam is 2x stiffer than the CTR and the VDTR. The same stiffened flexbeam could be used on either of those rotors at the expense of increased loads.

The whirl-flutter speeds for the four aircraft including the 1x and 2x stiffness flexbeam for the VSTR are summarized in Table 7 for the case where the wing frequencies have been reduced by 70%.

The aeroelastic-stability-analysis results indicated that the flexbeam-style hub configuration offers significant stability advantages compared to the gimbaled hub configuration. The flexbeam-style rotor changes the way the blades are constrained to each other so that a perturbation of one blade does not strongly affect the others because the blades are not hard mounted to a gimbaled structure. This design reduces rotor yaw deflections which in turn reduce the destabilizing gyroscopic moments applied to the wing, thus improving whirl-flutter stability. Furthermore, the flexbeam hub design and delta-3 schedule allow for better frequency separation between rotor flap modes, rotor lag modes, and wing modes throughout the airspeed range because the first rotor flap mode is relatively constant with airspeed.

The variable-speed design (VSTR) offers a slight whirl-flutter stability improvement over a conventional tiltrotor (CTR) due to reduced rotor gyroscopic loads resulting from a decrease in rotor speed. The variable-diameter design (VDTR) offers a greater stability improvement over a conventional tiltrotor (CTR) due to reduced rotor gyroscopic loads resulting from decreased rotor speed and decreased diameter.

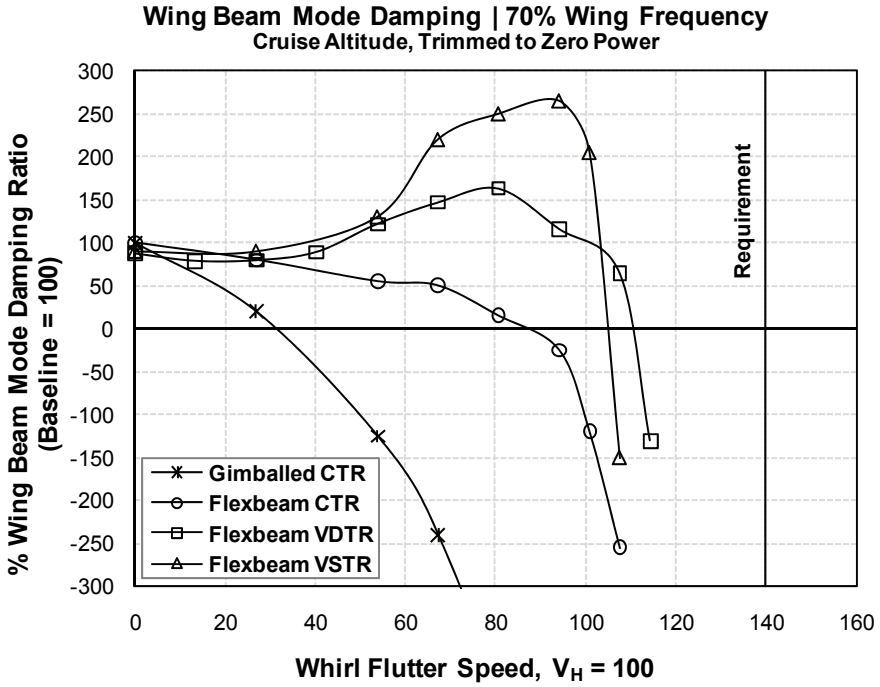

Figure 33. Wing-beam-mode damping vs. airspeed | 70% reduction in wing frequencies.

TABLE 7. WHIRL-FLUTTER SPEEDS FOR A 70% REDUCTION IN WING FREQUENCIES

Aircraft	Whirl Flutter Speed (V_{PWF}=100)
Gimbaled CTR	22
CTR (1x flexbeam stiffness)	62
VSTR (1x flexbeam stiffness)	63
VSTR (2x flexbeam stiffness)	75
VDTR (1x flexbeam stiffness)	79

4.1.5 Handling Qualities

Simulations of the XV-15, CTR, VDTR, and VSTR were developed from information in references 13 and 24, and trim and flight dynamics were analyzed with both simulations. The GenHel XV-15 simulation was used to evaluate longitudinal trim, trim in turns, and dynamic responses to control inputs, and to correlate with information in references 1, 13, and 24. A generic tiltrotor simulation was used to calculate trim solutions for CTR, VDTR, and VSTR in straight and level flight and to derive a nominal mast-angle schedule vs. flight speed.

The simulations were constructed using the Sikorsky General Helicopter (GenHel) Flight Dynamics Simulation program. GenHel is a generalized, modular analytical representation of a total helicopter system. The basic model is a total-force, nonlinear, large-angle representation in six rigid-body degrees of freedom. In addition to typical GenHel helicopter methodology, a software module was developed to calculate wing-pylon aerodynamic forces and moments, including wing download due to the rotors and downwash at the horizontal tail. A nacelle module was written to calculate the effect of mast tilt on the location of applied rotor forces and aircraft mass properties.

The GenHel simulations utilized two sets of longitudinal trimmers, one for helicopter mode and another for airplane mode. In helicopter mode with the rotor lifting the aircraft, pitch attitude was varied to trim longitudinal acceleration and collective pitch was varied to trim normal acceleration. In airplane mode with the wing lifting the aircraft and the rotors tilted forward, rotor collective pitch was varied to trim longitudinal acceleration and pitch attitude was varied to trim normal acceleration.

Flight dynamic responses to longitudinal control-stick inputs were calculated using GenHel to examine the simulation behavior and compare it with XV-15 flight-test data. The simulation was initially run in airplane mode at constant blade pitch and rotational speed, but small airspeed variations in response to stick inputs caused large changes in rotor thrust and torque. Therefore, a rotor-blade pitch controller was implemented and evaluated.

Flight dynamic responses to lateral-control-stick and pedal inputs were calculated with GenHel to examine the simulation behavior and compare it with XV-15 flight-test data. The analysis included a comparison between simulation results and flight-test data for a lateral-stick pulse in airplane mode in addition to calculated responses to lateral-stick and pedal inputs in hover.

Longitudinal trim analysis of CTR, VDTR, and VSTR was conducted by calculating the required power, pitch attitude, and wing lift coefficient vs. airspeed on curves of constant mast angle, flap deflection, and wingtip incidence. These constant curves were then examined and nominal schedules in level flight at constant airspeed (zero longitudinal acceleration) were defined, subject to constraints on power, wing lift coefficient, and pitch attitude in transition mode. The schedules were developed with the objectives of operating the aircraft near minimum power and near level pitch attitude without exceeding a wing lift coefficient of 80% $(C_L)_{MAX}$. Note that the maximum available wing lift coefficient varies with mast angle and flap deflection. Transition to airplane

mode was scheduled to occur just above an airspeed at which wing lift alone was sufficient for level flight, and flap retraction was also scheduled at a minimum safe airspeed. Table 8 shows a relative ranking of handling qualities for the three aircraft.

TABLE 8. HANDLING-QUALITIES SUMMARY

	CTR	VDTR	VSTR
Transition Power Required	◐	●	◐
Transition Power Margin	◐	●	○
Transition Complexity	●	◑	●
Banked Turn	◐	●	◐
Heading Change	●	○	◐
Combat Maneuvers (Time to Climb)	●	◑	○
Combat Maneuvers (Footprint)	◐	●	◐

● 1st ◐ 2nd ○ 3rd

4.1.6 Mass Properties

The weight-prediction methodology employed for the three tiltrotor concepts was based on a combination of statistical, semianalytical, and analytical methods. These methods were mathematically modeled in Sikorsky's Rotorcraft Design Model (RDM) computer program to permit weight trending as a function of primary aircraft design parameters, and to facilitate evaluation of the numerous point and variant designs and impact analyses required by the study. The parametric weight estimates were generally correlated to V-22 weight data, incorporating technology where appropriate. Additional factors were applied to the rotor system for the VDTR concept, and to the drive system for the VSTR concept to account for their unique design features. Figure 34 through Figure 41 show relative component weights; that is, the baseline CTR is set to the nominal value of 100.

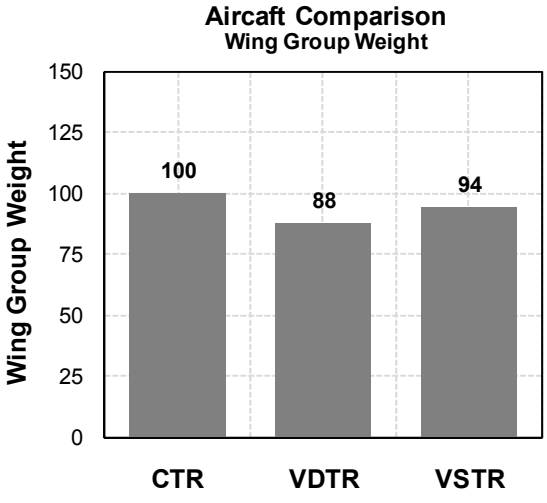

Figure 34. Wing-weight comparison.

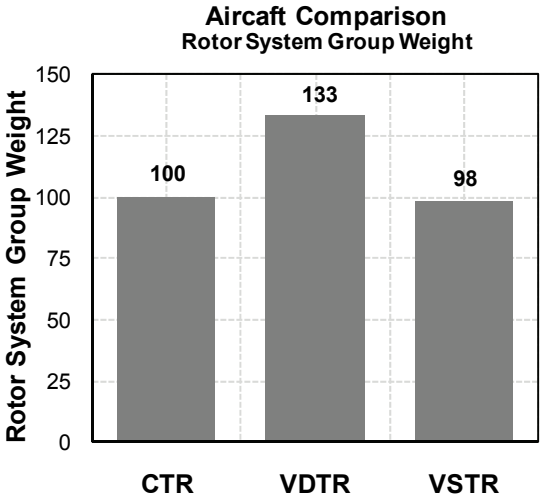

Figure 35. Rotor-weight comparison.

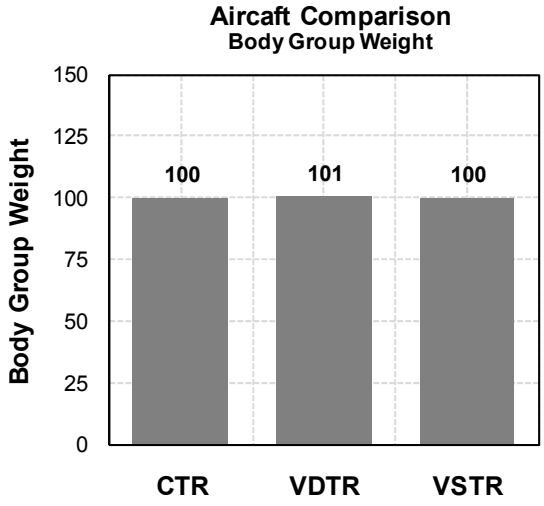

Figure 36. Body-weight comparison.

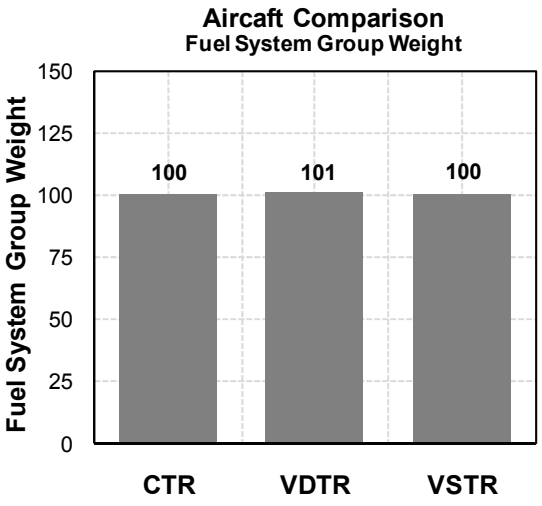

Figure 37. Fuel-system-weight comparison.

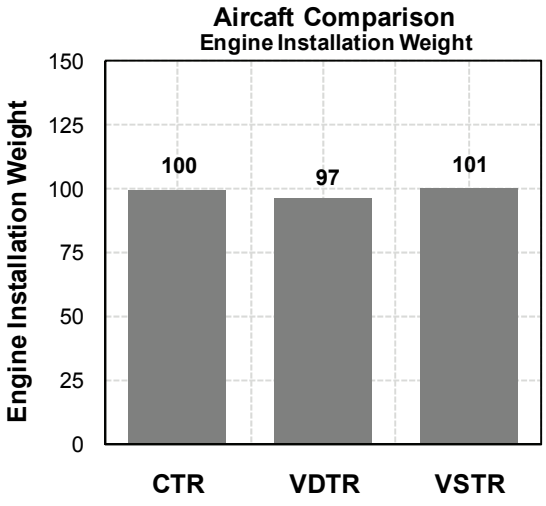

Figure 38. Engine-weight comparison.

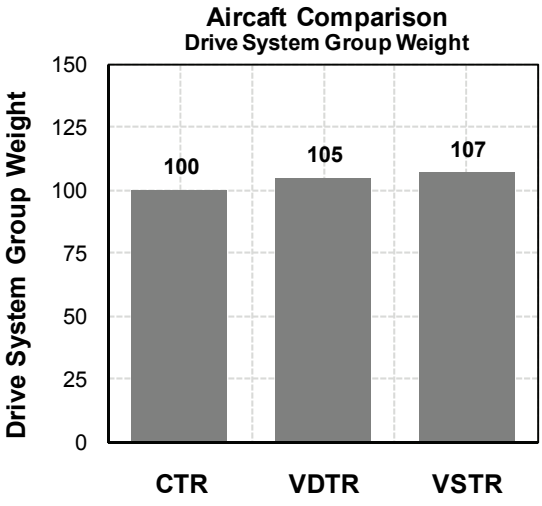

Figure 39. Transmission-weight comparison.

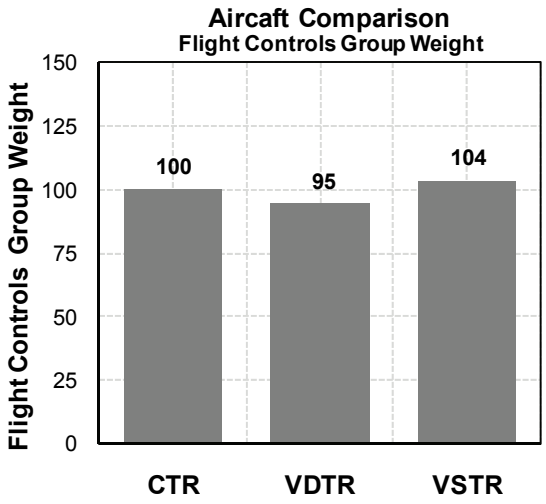

Figure 40. Flight-controls comparison.

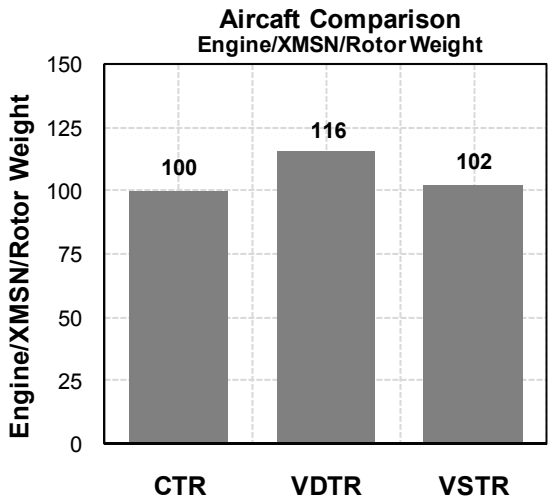

Figure 41. Engine/transmission (XMSN)/ rotor-weight comparison.

4.2 Aircraft Performance

Upon completion of the design synthesis for each aircraft, the performance of each aircraft was compared to the design requirements and to the relative performance of the other designs. The relative strengths and weaknesses of the designs were quantified as an indication of the merits of the underlying technology for each concept. The attributes that showed the greatest differences between the various technology systems are described in detail in the following sections.

4.2.1 Downwash/Outwash Characteristics

The expanded rotor diameter of the VDTR greatly benefits hover and low-speed operations. Increasing the hover diameter effectively reduces the power loading of the aircraft, allowing the hover-gross-weight capability of the VDTR to exceed the capabilities of the CTR and VSTR even though the VDTR has close to 5% less power installed on the aircraft. The large rotor diameter decreases the VDTR disk loading in hover, thereby decreasing the outwash velocity experienced by personnel and structures that are in the near vicinity of the hovering aircraft. Figure 42 provides a comparison of the outwash velocity for the VDTR, CTR, and VSTR. Figure 43 and Figure 44 show the relative maximum outwash force and overturning moment exerted on a standing person.

4.2.2 Hover Performance

Figure 45 and Figure 46 show the International Standard Atmosphere (ISA) and constant 95°F weight-altitude-temperature (WAT) capabilities of the three tiltrotor aircraft. Note that while the VDTR has the lowest rotor figure of merit (because of its exposed inboard spar section), it has the greatest hover efficiency, evident in its expanded WAT envelope, because while rotor figure of merit is purely a measure of rotor efficiency, aircraft power loading (as manifested in disk loading) is a measure of overall hover efficiency. Hover efficiency is more strongly driven by disk loading than by rotor figure of merit. The higher disk loading of the VSTR is mitigated by its improved

rotor figure of merit mainly because VSTR benefits from the fact that the optimum rotor twist needed for efficient cruise performance at reduced rpm is closer to the optimum rotor twist in hover at 100% rpm.

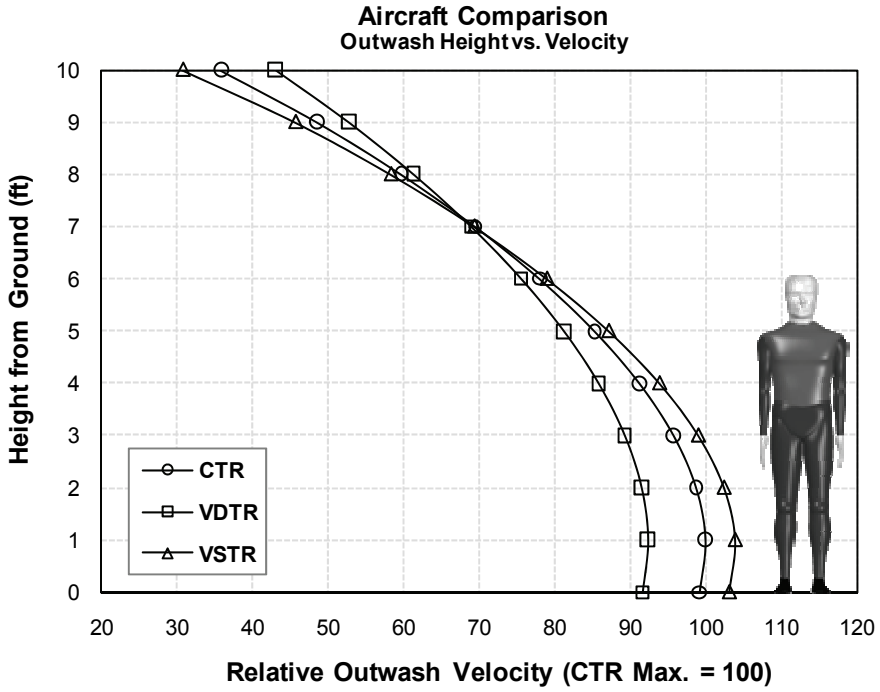

Figure 42. Tiltrotor-outwash comparison.

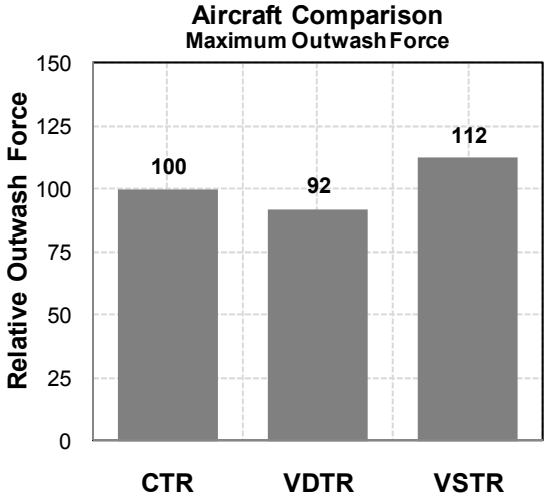

Figure 43. Outwash-force comparison.

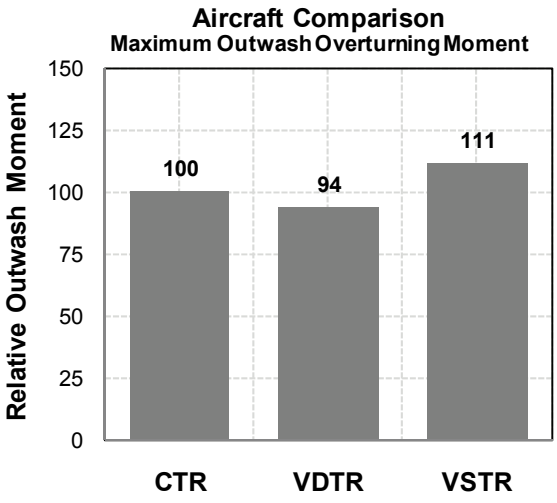

Figure 44. Outwash-moment comparison.

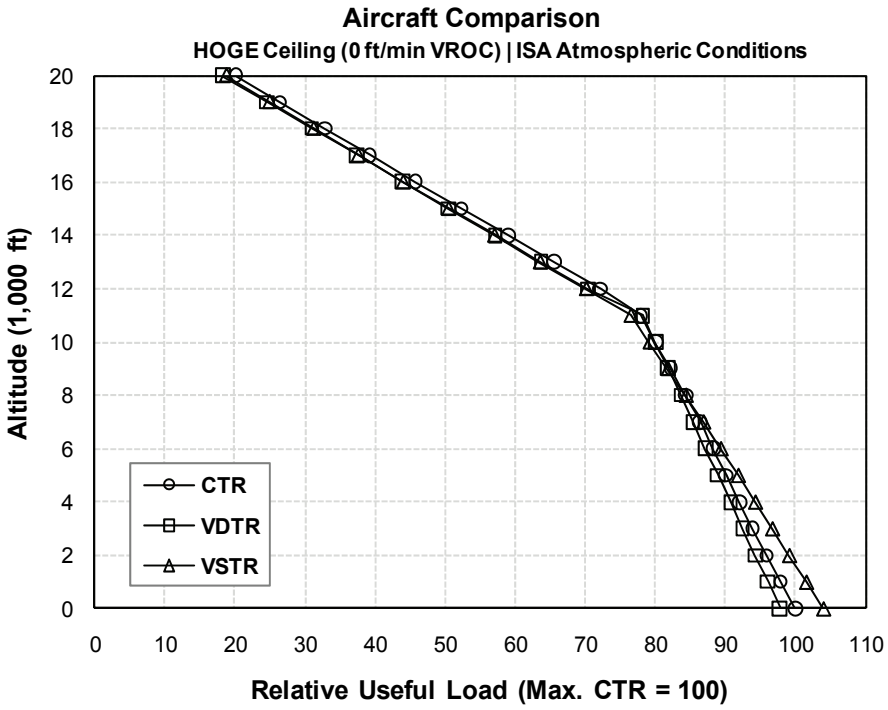

Figure 45. ISA WAT-capability comparison.

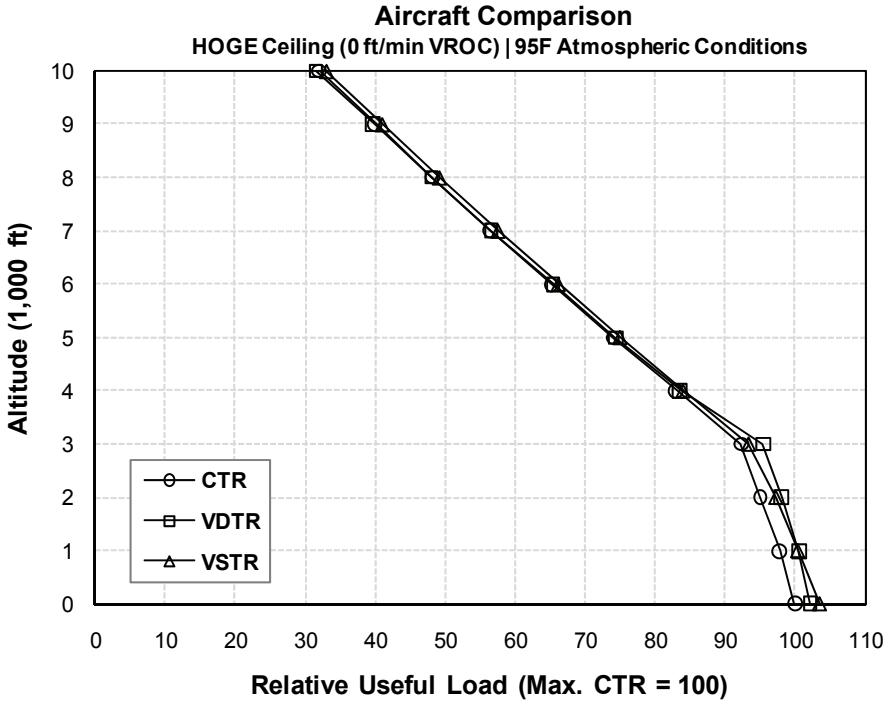

Figure 46. 95˚F WAT-capability comparison.

4.2.3 Short-Takeoff Capability

Figure 47 and Figure 48 show the short-takeoff (STO) ground-roll distance and total distance to clear an obstacle as a function of gross weight at SL/hot conditions. Figure 49 and Figure 50 show the STO ground-roll distance and total distance as a function of gross weight at high altitude/hot day (Hi/hot) conditions. The ordinates of Figure 47 through Figure 50 represent the aircraft weight at some nominal value. The maximum aircraft weight is 100. Lower weights are percentages of the maximum weight. For example, a nominal weight of 95 is a gross weight 5% less than the maximum weight. The abscissas of Figure 47 through Figure 50 represent the STO ground roll and distance and total distance to clear an obstacle, normalized to the CTR, respectively.

Figure 51 and Figure 52 show the STO ground-roll distance and total distance at maximum takeoff gross weight (MTOW) at SL/hot conditions, normalized to the CTR, respectively. Figure 53 and Figure 54 show the STO ground-roll distance and total distance at MTOW at Hi/hot conditions, normalized to the CTR, respectively.

Generally speaking, STO performance increases with larger wings and larger rotors. The CTR has the largest wing and a nominally large rotor. The VDTR has the largest rotor and nominally large wing. The VSTR has the smallest rotor and the smallest wing. Thus, the CTR performs nominally during STO operations, the VDTR has the greatest performance, and the VSTR performs worst. This phenomenon is clearly illustrated in Figure 47 through Figure 50, where for a given weight the VDTR has significantly less ground roll and less distance required to clear an obstacle.

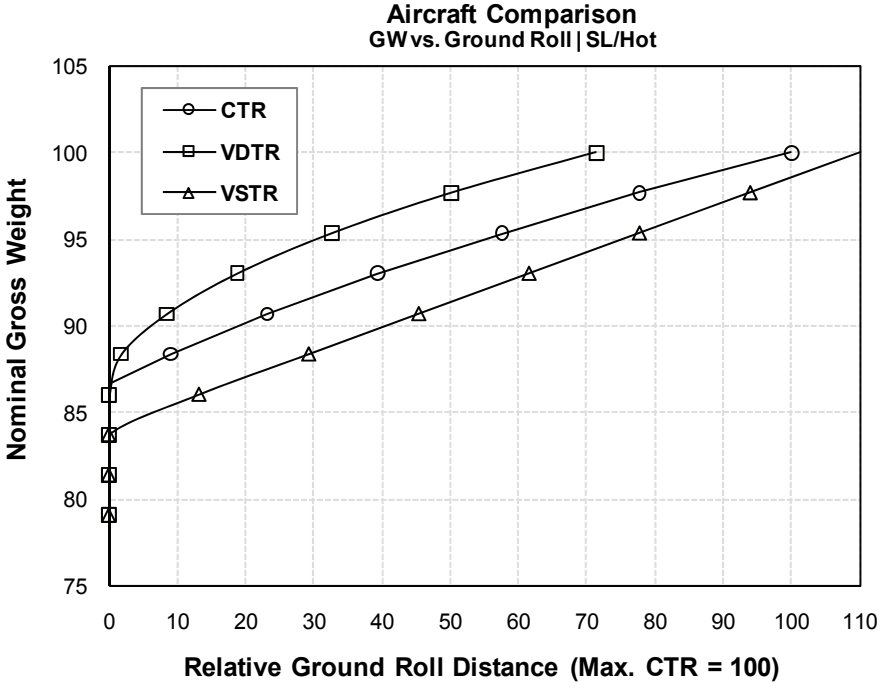

Figure 47. STO ground-roll-capability comparison | SL/hot.

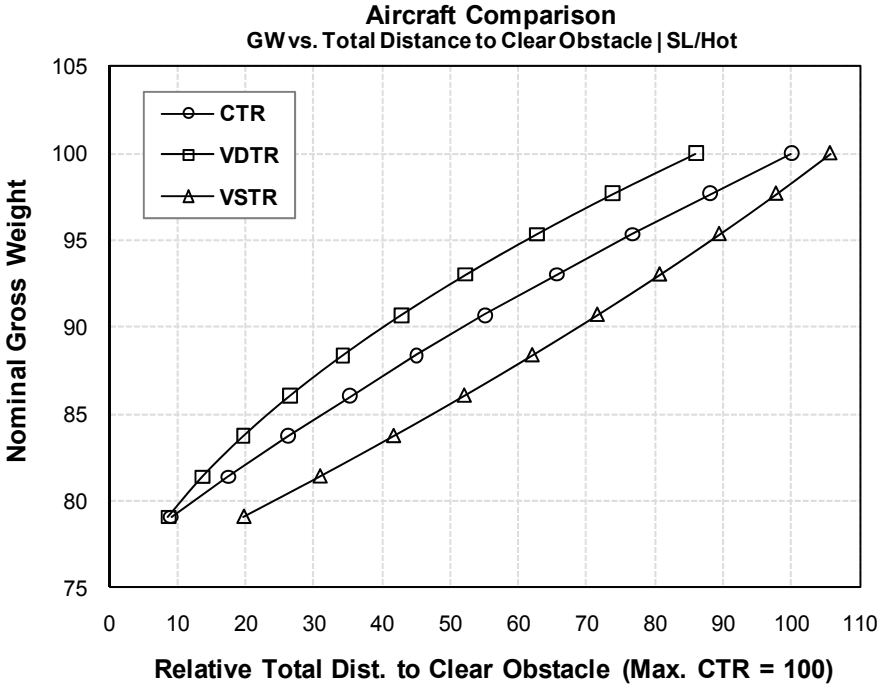

Figure 48. STO total-distance-capability comparison | SL/hot.

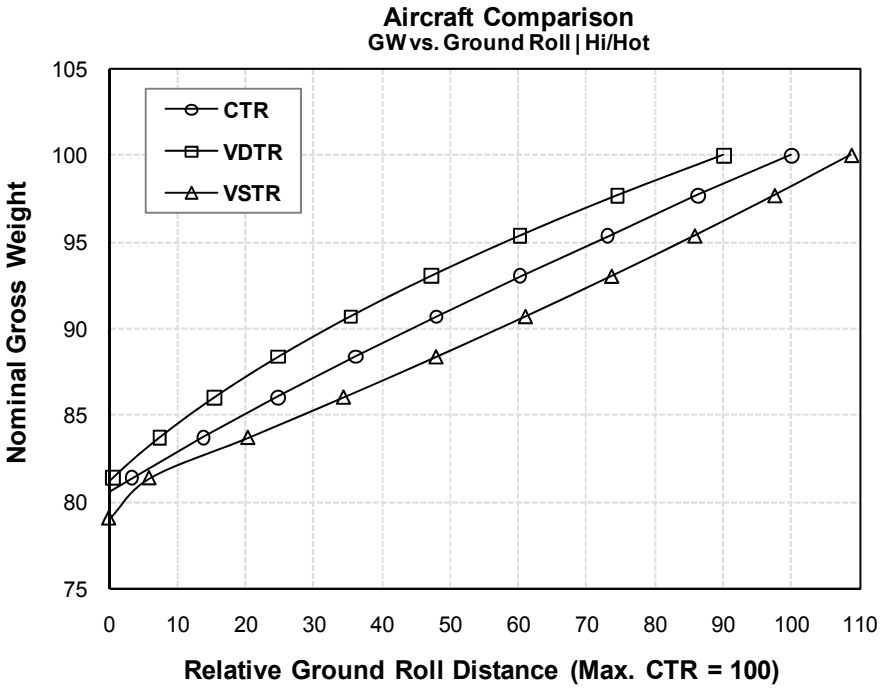

Figure 49. STO ground-roll-capability comparison | Hi/hot.

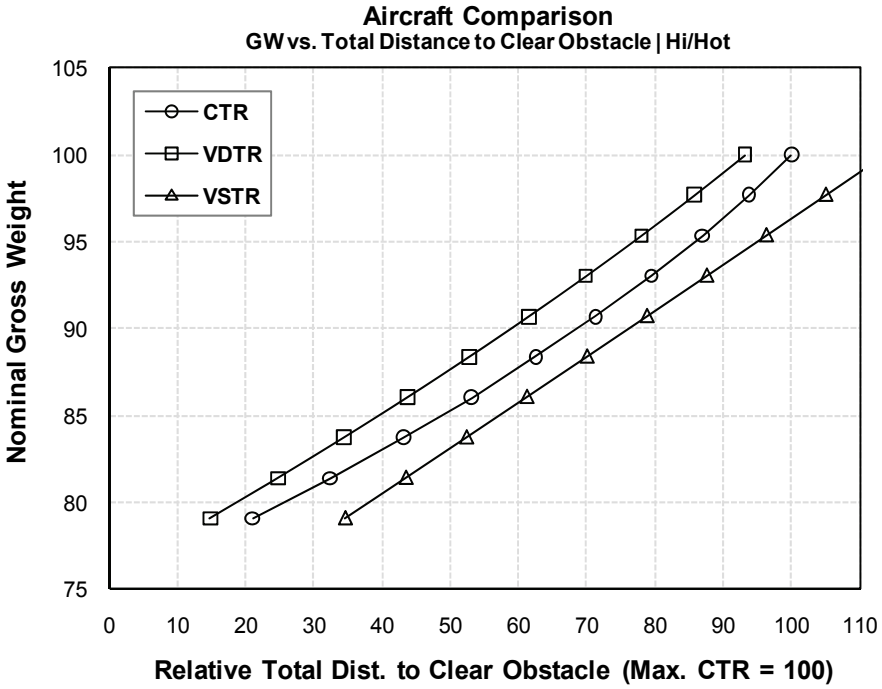

Figure 50. STO total-distance-capability comparison | Hi/hot.

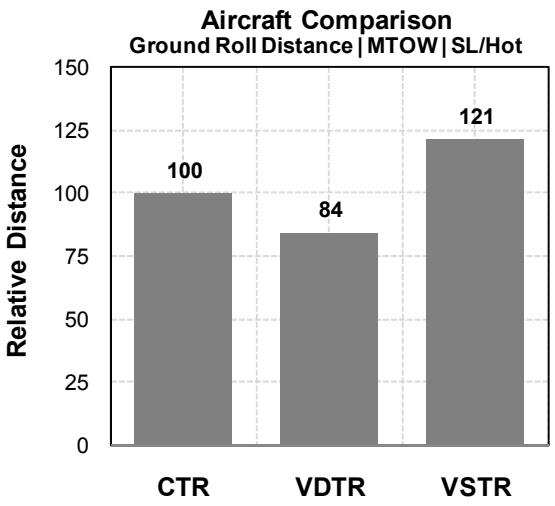

Figure 51. STO ground roll | MTOW | SL/hot.

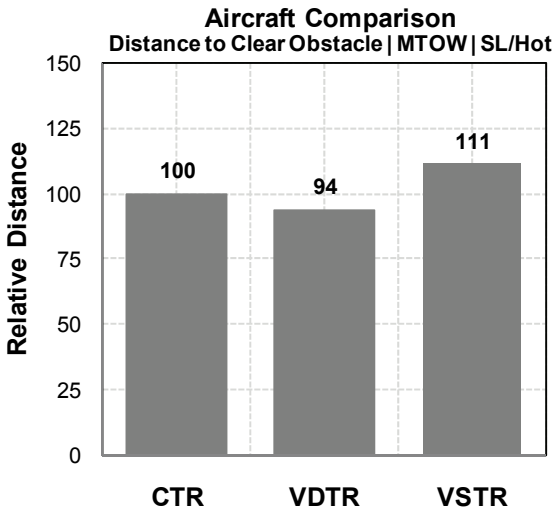

Figure 52. STO total distance | MTOW | SL/hot.

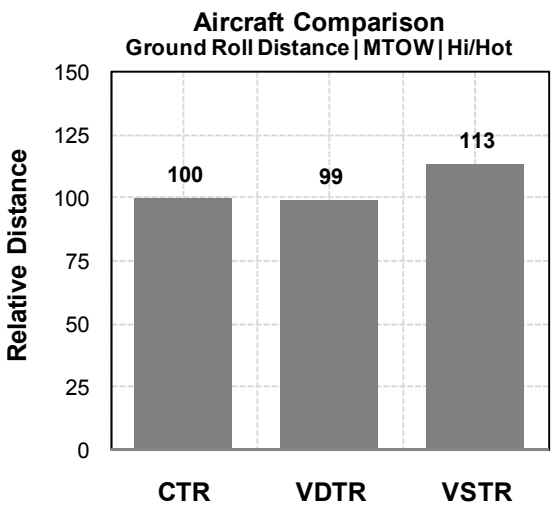

Figure 53. STO ground roll | MTOW | Hi/hot.

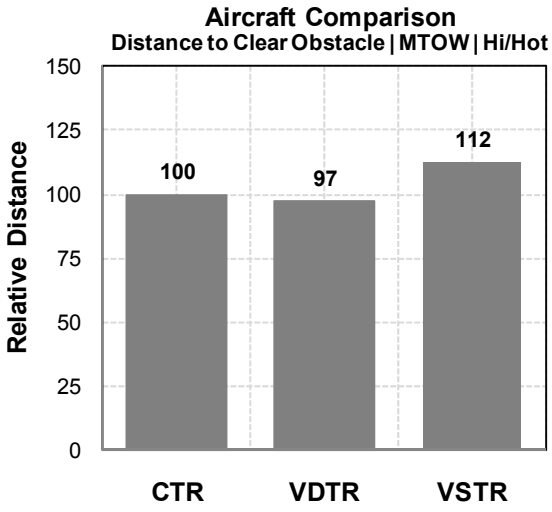

Figure 54. STO total distance | MTOW | Hi/hot.

4.2.4 Speed Capability

Figure 55 through Figure 60 show the velocity for best endurance (V_{BE}), velocity for 99% best specific range (V_{BR}), and velocity for engine maximum continuous power or transmission torque (V_{MCP}) speed comparison of the three tiltrotors, as a function of altitude under ISA and constant 95˚F conditions. Figures 61 through 66 show the V_{BE}, V_{BR}, and V_{MCP} speed capability of the three tiltrotor aircraft at 30k/ISA and 4k/95 conditions.

The VDTR offers a broader spectrum of speed performance compared to the CTR and VSTR. Its smaller cruise rotor diameter is more efficient for high-speed flight. The VDTR transmission torque capability is retained because its rotor rpm is not reduced as much as that for the VSTR. The VSTR has two modes in which it can operate: "efficiency mode," where the rotor is slowed via gearbox reduction and the engine operates at reduced rpm; and "performance mode," where the rotor is slowed via engine rpm reduction only, equivalent to the rpm reduction used on the CTR and VDTR. In "efficiency mode," the VSTR operates at high rotor propulsive efficiency, but because its transmission power available is significantly reduced by the rpm reduction, its speed performance is limited. In "performance mode," the VSTR speed capability improves beyond that of the CTR, yet is still less than the VDTR. The performance gain of the VSTR in "performance mode" is at the expense of a significant propulsive efficiency penalty, as its rotor is not optimized for both high-speed and -rotor rpm. The VDTR, being designed for both high-speed and higher-rotor rpm, enables simultaneous high-speed and high-efficiency cruise flight.

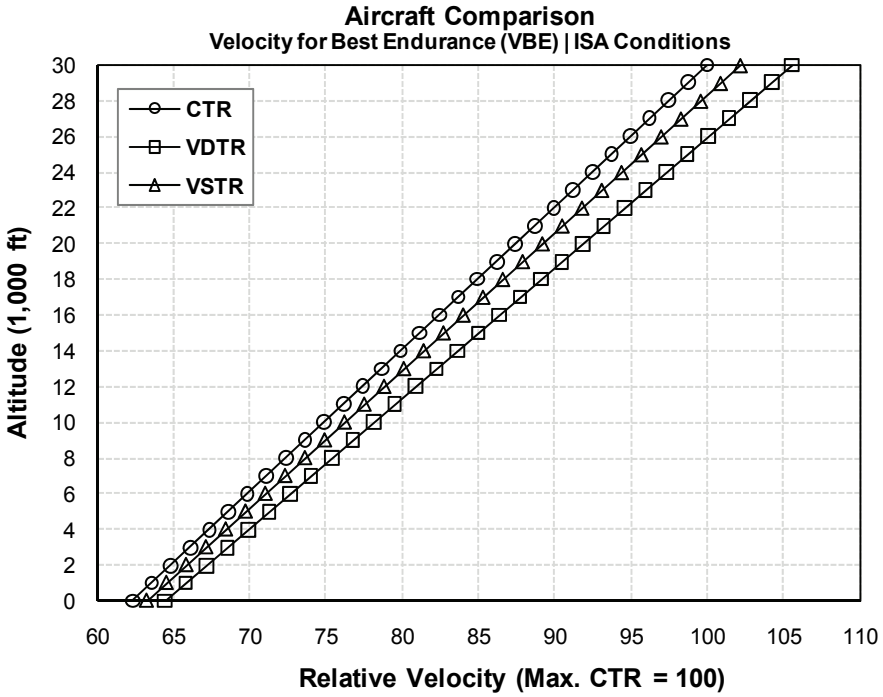

Figure 55. V_{BE} capability comparison | ISA.

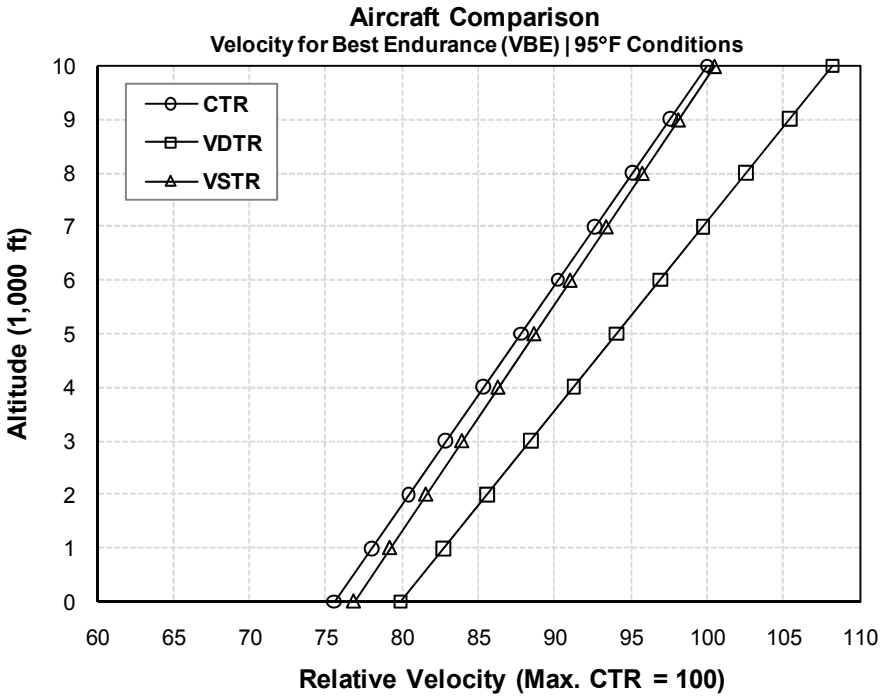

Figure 56. V_{BE} capability comparison | 95°F.

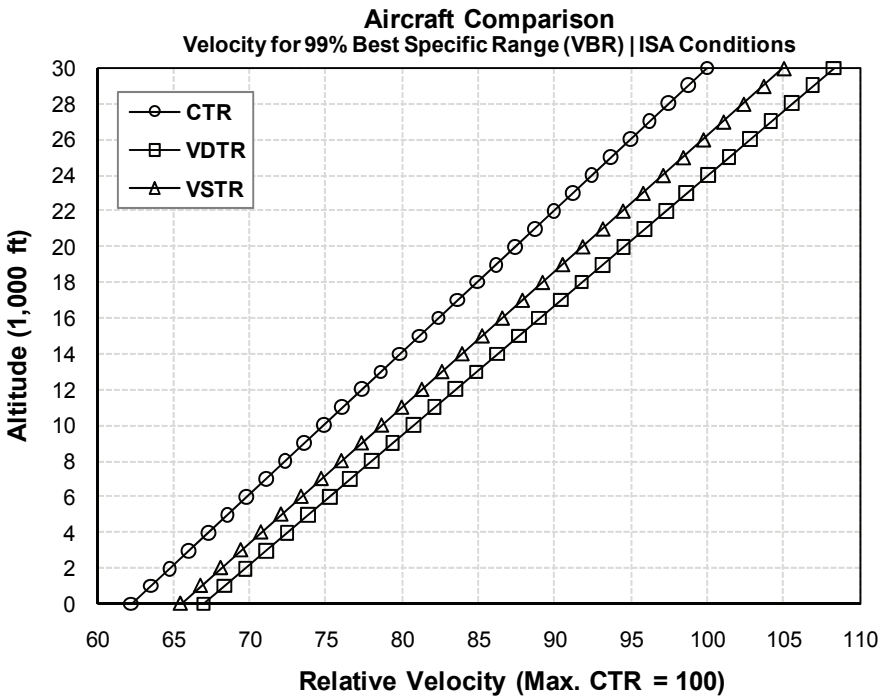

Figure 57. V_{BR} capability comparison | ISA.

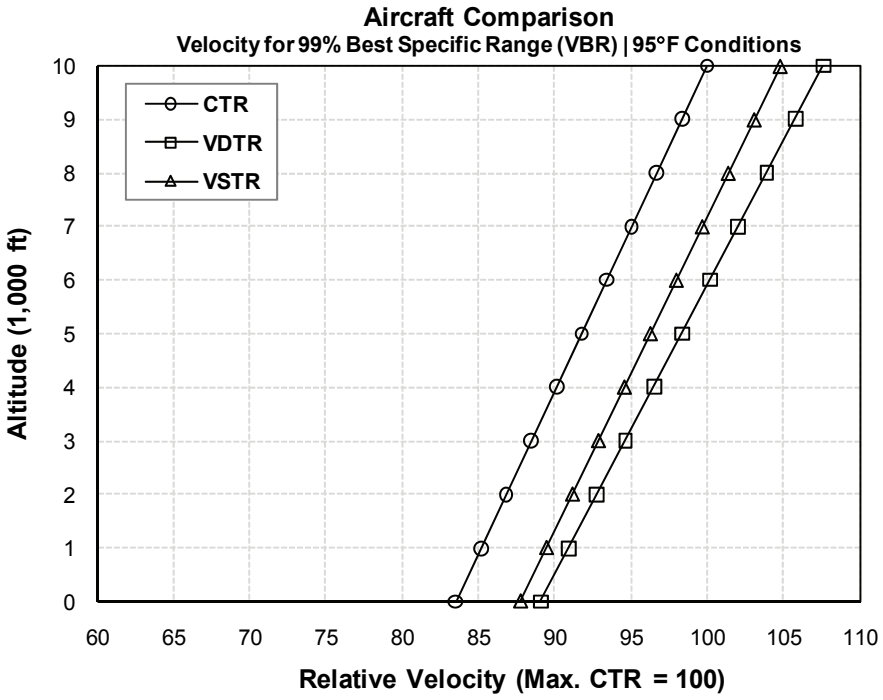

Figure 58. V_{BR} capability comparison | 95°F.

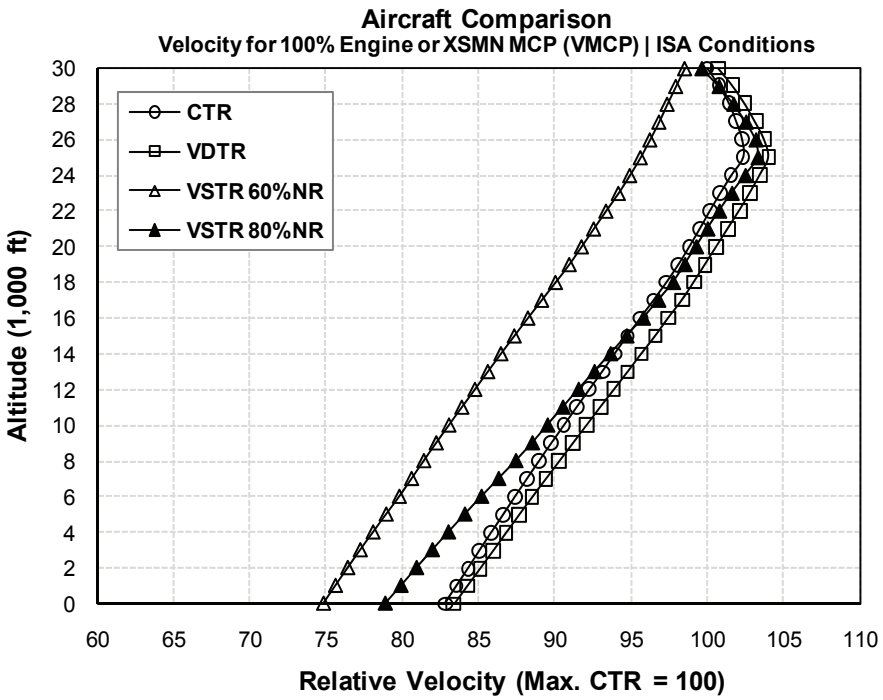

Figure 59. V_{MCP} capability comparison | ISA.

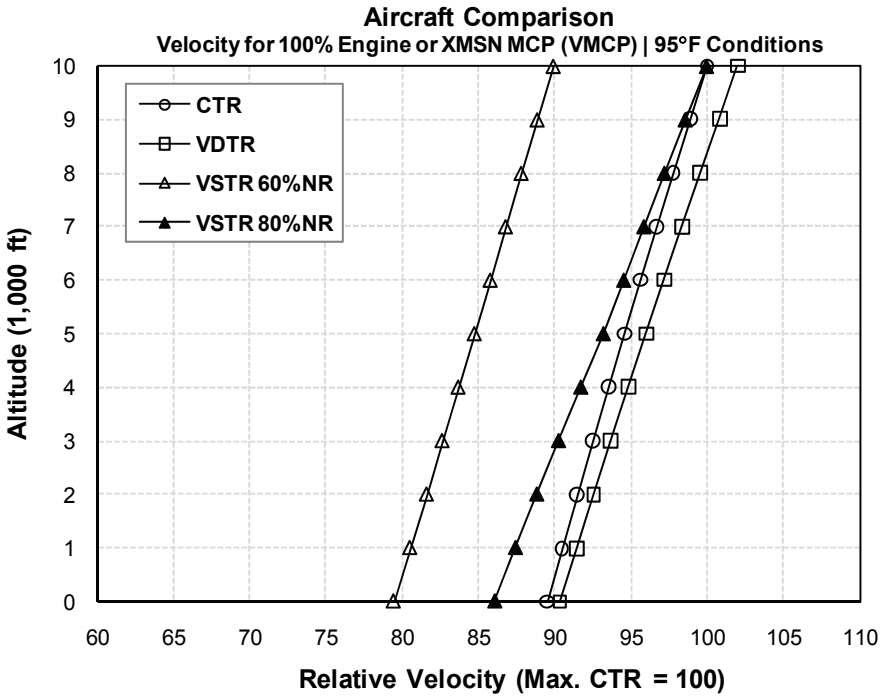

Figure 60. V_{MCP} capability comparison | 95°F.

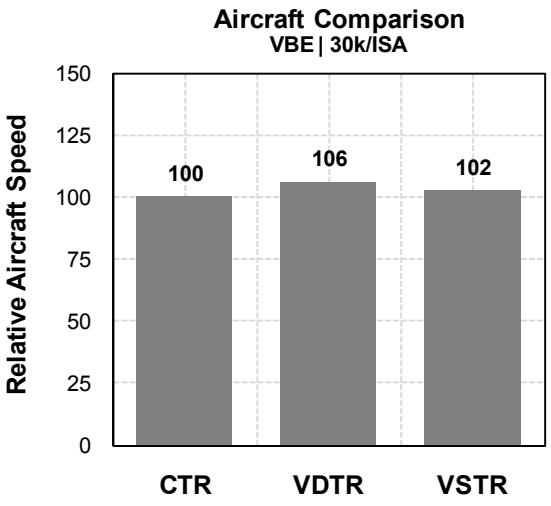

Figure 61. V_{BE} | 30k/ISA | capability comparison.

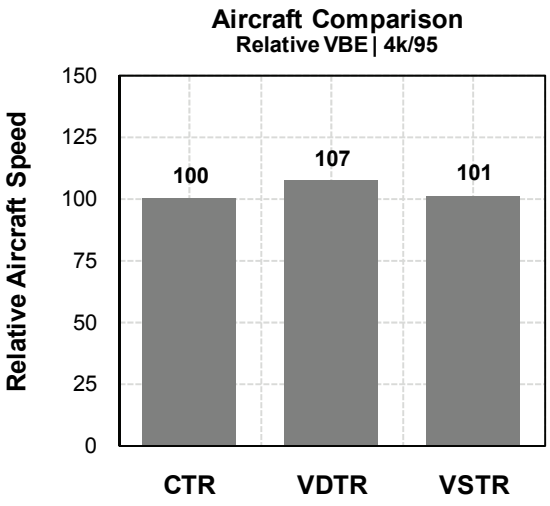

Figure 62. V_{BE} | 4k/95 | capability comparison.

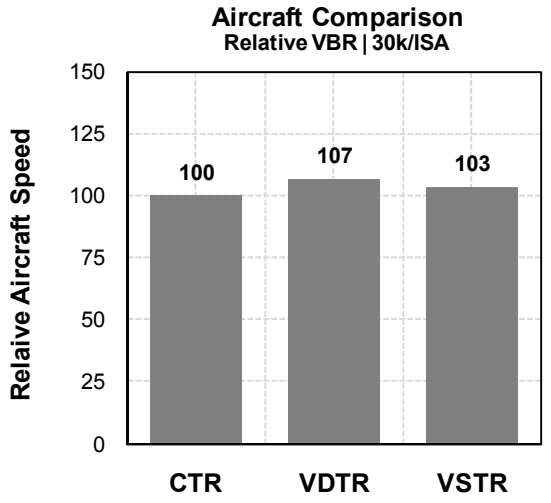

Figure 63. V_{BR} | 30k/ISA | capability comparison.

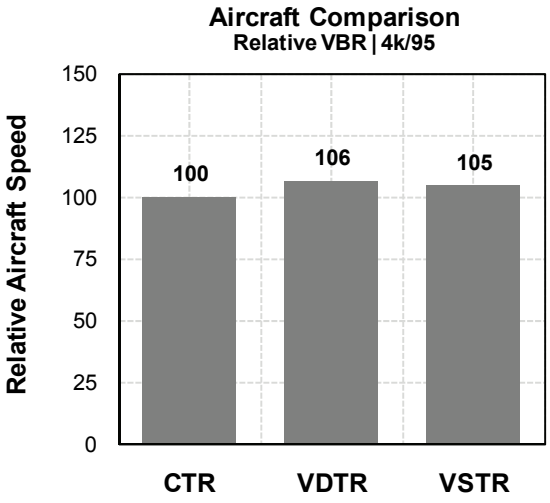

Figure 64. V_{BR} | 4k/95 | capability comparison.

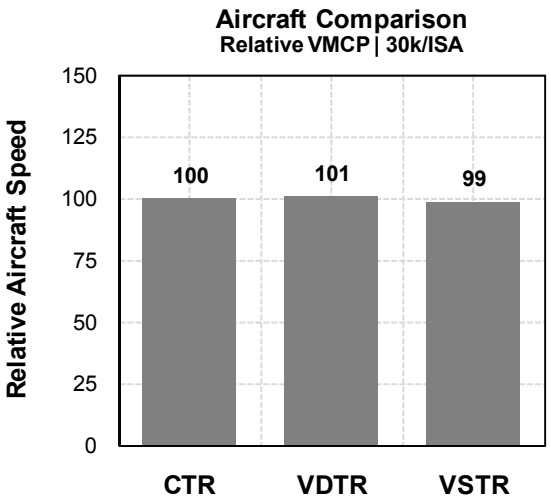

Figure 65. V_{MCP} | 30k/ISA | capability comparison.

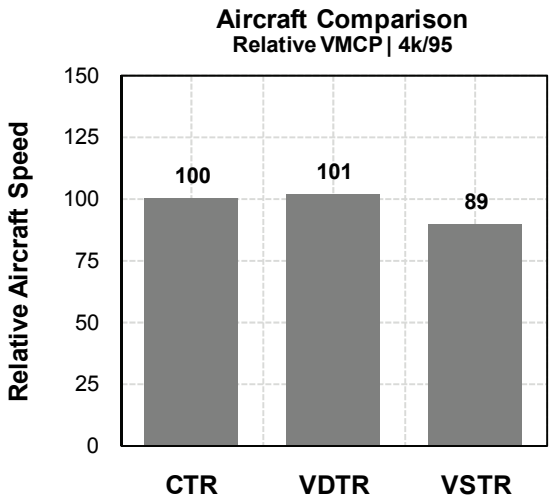

Figure 66. V_{MCP} | 4k/95 | capability comparison.

4.2.5 Mission-Performance Capability

All three aircraft are capable of executing heavy-lift, long-range transport missions required of the LVLT mission set. While the VDTR is the heaviest of the three solutions, it also offers the potential for the highest cruise speed with improved efficiency over the CTR. During high-speed transport missions, the VDTR and VSTR have improved range capability beyond the CTR due to their improved cruise efficiency. During low-speed external load or rotary-wing air-to-air refueling missions, the VDTR and VSTR (which have smaller wings) suffer reduced range capability with respect to the CTR. Figure 67 through Figure 73 show several representative mission profiles for the LVLT mission set. In the figures, the payload-range/radius performance of the three aircraft is presented relative to the mission required payload and range/radius (which are normalized to 100).

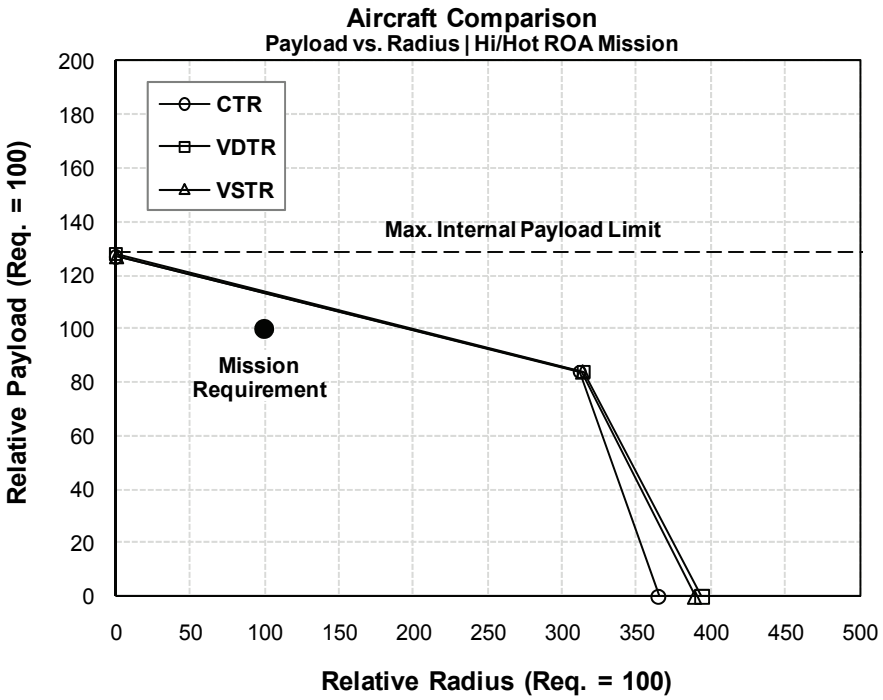

Figure 67. Hi/hot ROA mission | payload-radius comparison.

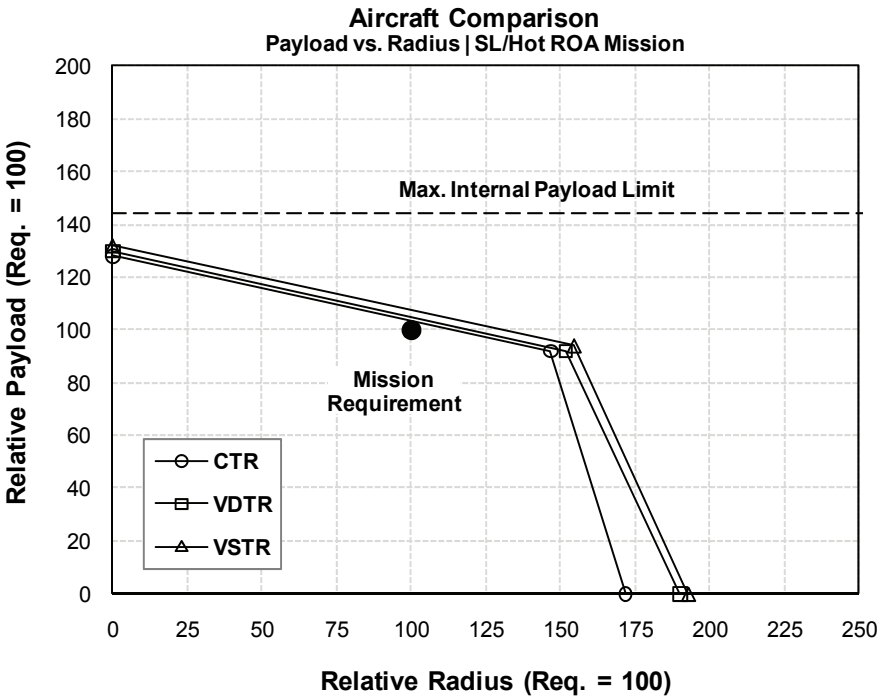

Figure 68. SL/hot ROA mission | payload-radius comparison.

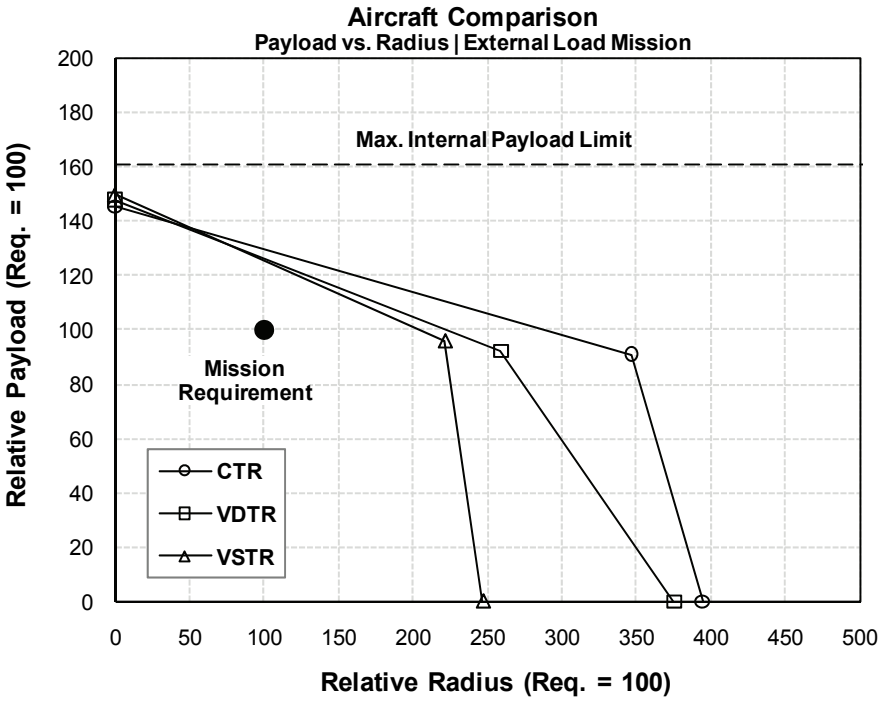

Figure 69. External-load mission | payload-radius comparison.

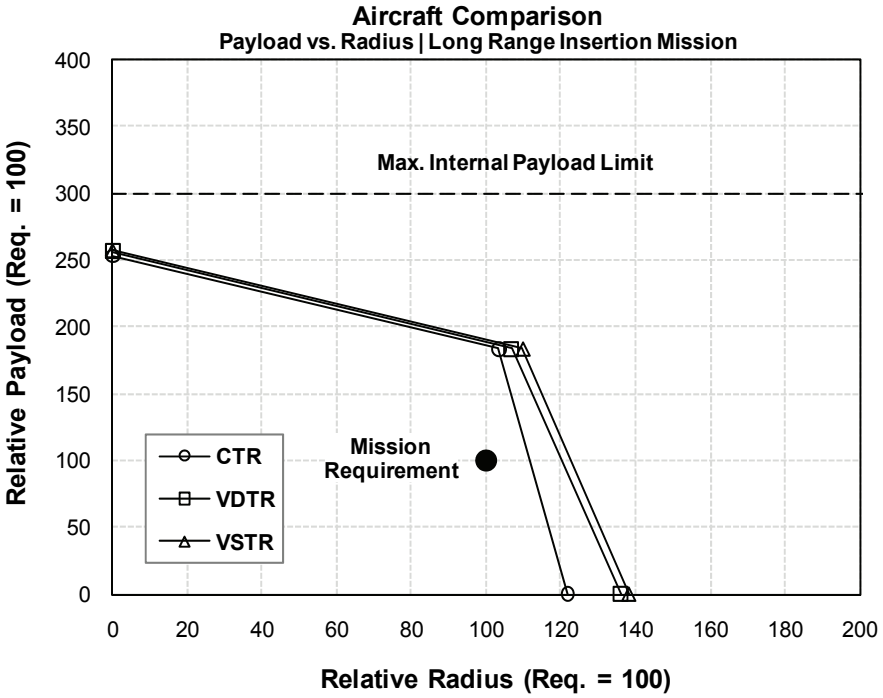

Figure 70. Long-range insertion mission | payload-radius comparison.

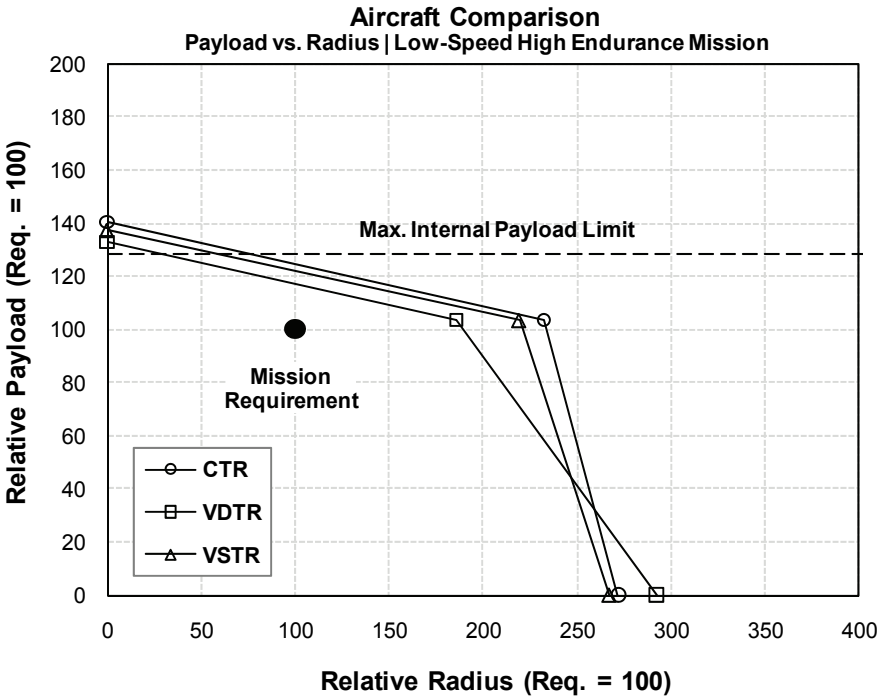

Figure 71. Low-speed high-endurance mission | payload-radius comparison.

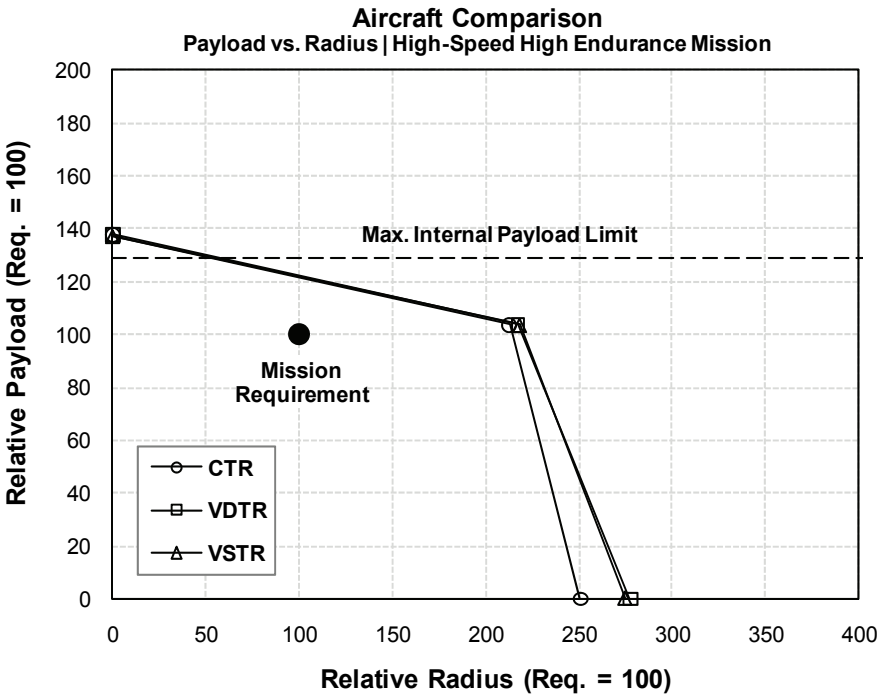

Figure 72. High-speed high-endurance mission | payload-radius comparison.

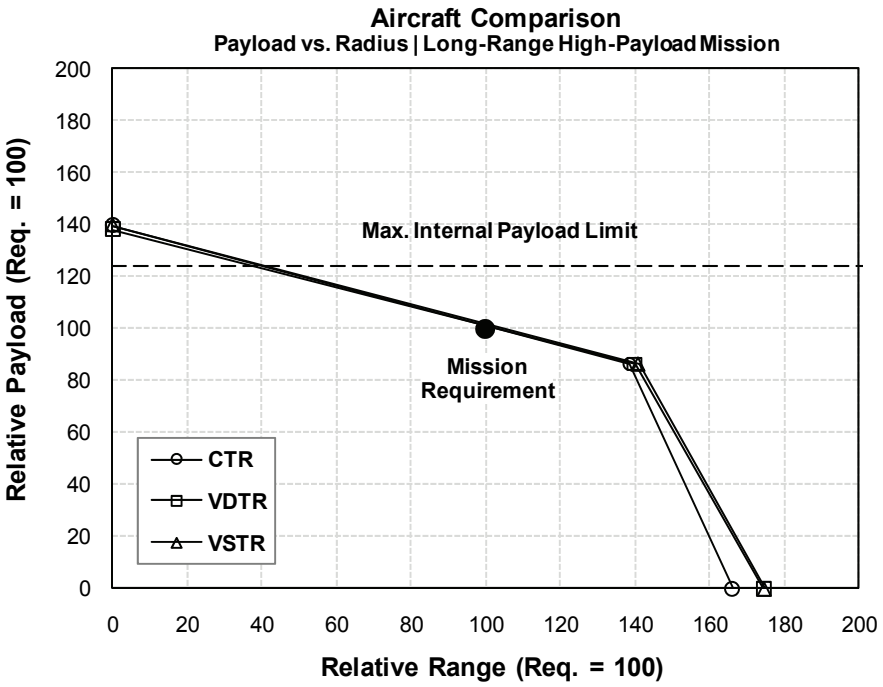

Figure 73. Long-range high-payload mission | payload-range comparison.

4.3 Configuration Evaluation

Ten disparate attributes were chosen to evaluate the three aircraft, presented in terms of a pure 1st, 2nd, or 3rd place ranking in Table 9. This evaluation, however, does not consider the value weighting associated with each attribute. Using requirements-driven weightings representative for the LVLT mission and usage spectrum, a resultant score can be obtained that depicts the relative ranking of the three concepts based on the operator's needs.

TABLE 9. ATTRIBUTE RANKING

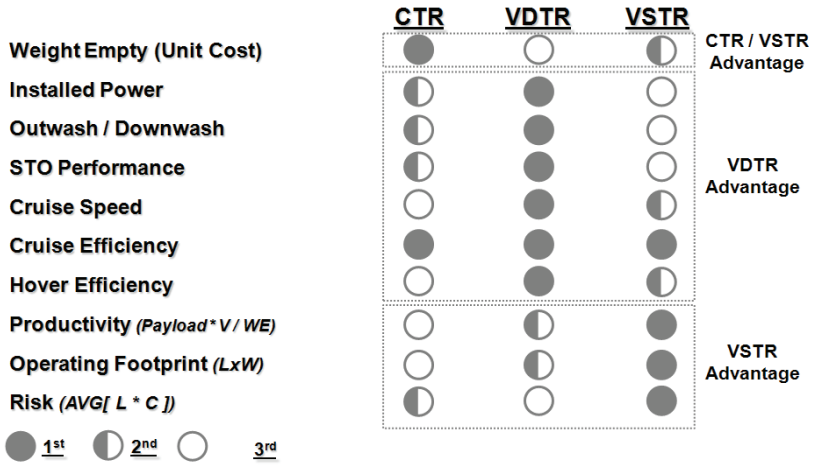

The ultimate measure of the relative value of an aircraft was provided by the United Technologies Corporation (UTC)-proprietary Value-Based Gage (VBG) methodology (ref. 25). The VBG process was used to develop an objective and auditable metric or scale, which was used to compare the aircraft. The VBG process is based upon Quality Function Deployment (QFD) or "House of Quality" analysis to provide a link between the engineering characteristics (e.g., weight or speed) of a concept and the overall needs of the decision makers. A key feature of the gauge is that soft metrics (e.g., risk) can be included with hard metrics, such as weight, power consumption, and drag. A response-surface-approximation methodology was used to express the VBG score for each concept as a function of the attribute weighting factors, as depicted in Figure 74.

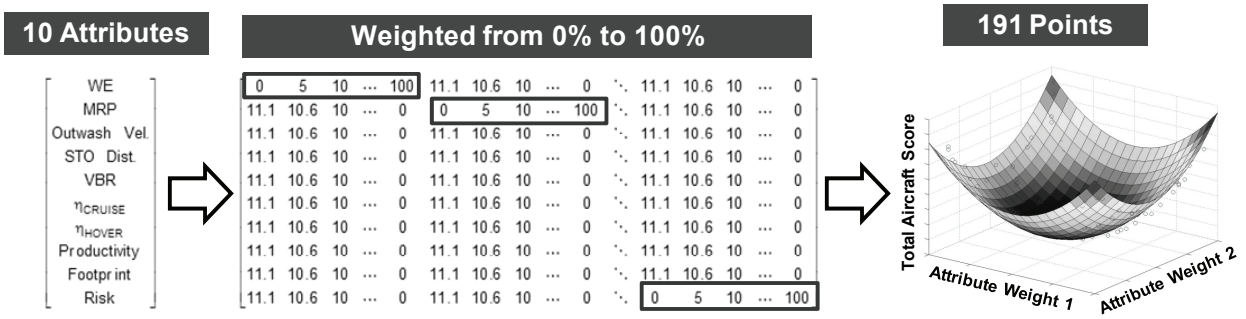

Figure 74. Response-surface methodology used for configuration evaluation.

The weighting factors for each attribute were systematically varied to attain a matrix of VBG sets valid for a variety of weighting schemes. The weighting factors were permeated to yield 191 VBG ranked sets. The sets included: a) all attributes weighted equally; and, b) each attribute weighted from 5% to 100% in steps of 5% with the other attributes equally ranked (for example, if WE was weighted at 10%, then all other attributes would be weighted at 9%; and, if WE was weighted at 70%, then all other attributes would be weighted at 3%). A linear multivariate regression, shown in equation (1), was found to give the closest correlation to the dataset. The regression coefficients are given in Table 10.

$$VBG = \alpha + \beta_1 x_1 + \beta_2 x_2 + \beta_3 x_3 + \beta_4 x_4 + \beta_5 x_5 + \beta_6 x_6 + \beta_7 x_7 + \beta_8 x_8 + \beta_9 x_9 + \beta_{10} x_{10} \quad (1)$$

TABLE 10. VBG RESPONSE SURFACE LINEAR MULTIVARIATE REGRESSION COEFFICIENTS

Coefficient	Attribute		CTR	VDTR	VSTR
α	---		0.8507442427	-0.8769132653	2.2755102041
$\beta 1$	WE	x_1	0.0014925576	0.0087691327	-0.0129595119
$\beta 2$	MRP	x_2	-0.0070355404	0.0187691327	-0.0227551020
$\beta 3$	$V_{OUTWASH}$	x_3	-0.0051196304	0.0187691327	-0.0227551020
$\beta 4$	x_{STO}	x_4	-0.0003488022	0.0187691327	-0.0227551020
$\beta 5$	V_{BR}	x_5	-0.0085074424	0.0187691327	-0.0166834356
$\beta 6$	η_{CRUISE}	x_6	-0.0085074424	0.0087691327	-0.0227551020
$\beta 7$	η_{HOVER}	x_7	-0.0085074424	0.0187691327	-0.0164734857
$\beta 8$	Productivity	x_8	-0.0085074424	0.0130143890	-0.0127551020
$\beta 9$	Footprint	x_9	-0.0085074424	0.0173538275	-0.0127551020
$\beta 10$	Risk	x_{10}	-0.0025510204	0.0087691327	-0.0127551020

Figure 75 shows the average value of each aircraft (relative to the CTR) for the 191 scenarios of VBG weighting schemes, equivalent to weighting all attributes equally. As shown in Figure 75, if the CTR has a baseline value of 100, then the VDTR is 26% more valuable and the VSTR is 18% more valuable. Figure 76 through 78 show the likelihood of an aircraft ranking 1st, 2nd, or 3rd, respectively, for any of the 191 VBG weighting scenarios.

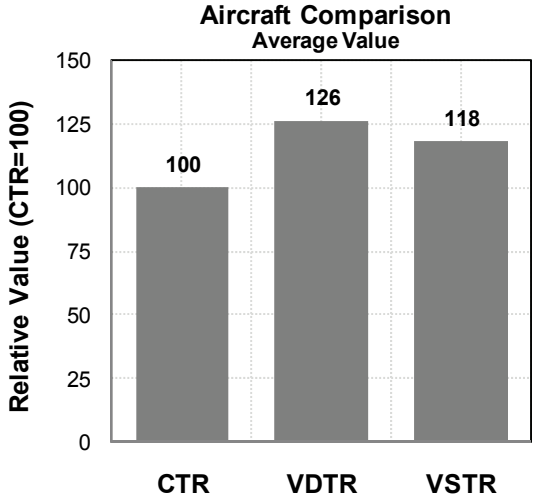

Figure 75. VBG results | average value.

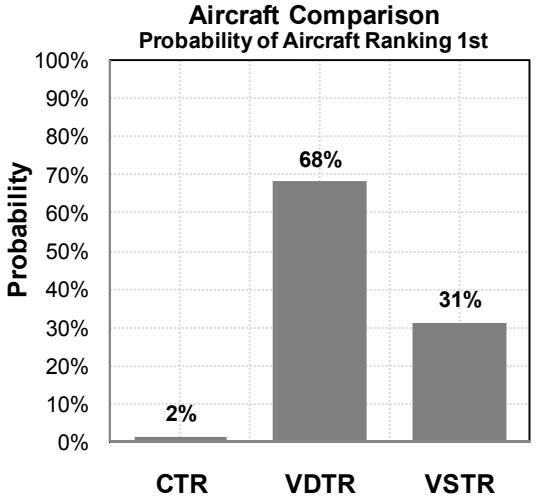

Figure 76. VBG results | 1st place likelihood.

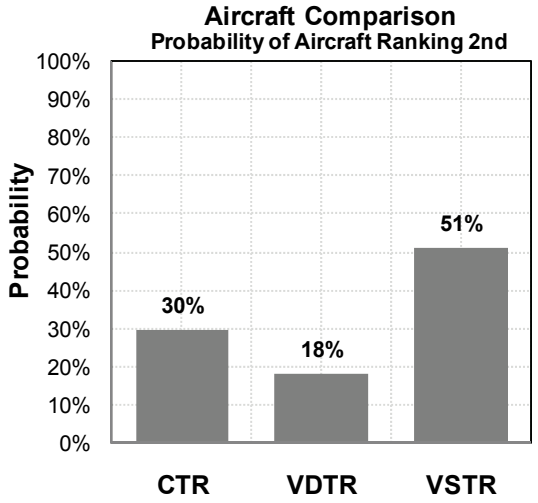

Figure 77. VBG results | 2nd place likelihood.

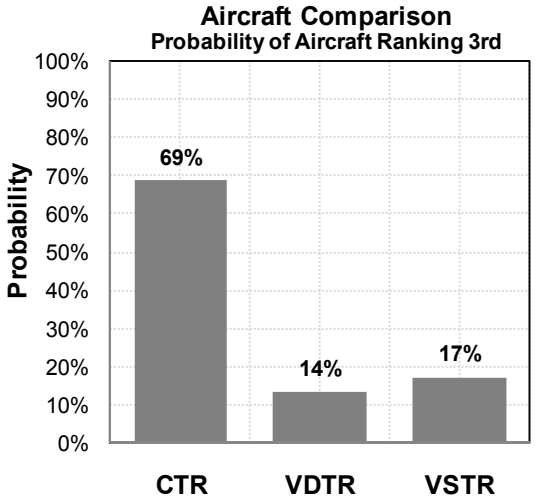

Figure 78. VBG results | 3rd place likelihood.

5 Alternate Designs

In addition to the three "clean-sheet" tiltrotor aircraft, two alternate-configuration aircraft were synthesized: a shipboard-suitable VDTR concept, arranged in a canard configuration with shortened fuselage and tandem cockpit, and a fixed-wing variant. These aircraft offer increased shipboard capability and potential cost savings, respectively, through their novel design characteristics.

5.1 Fixed-Wing Variant Description

The LVLT Fixed-Wing Variant (FWV) was synthesized using the CTR as a launching point. As the missions extend to the longer ranges typical of fixed-wing aircraft, the question arises as to the viability of the LVLT aircraft solely as a VTOL aircraft. The design team examined the paradigm of a mixed fleet of aircraft filling the LVLT role while simultaneously filling the role of the midsize fixed-wing transports. The hypothesis is that there would be a significant programmatic and financial benefit to producing a fixed-wing transport aircraft based on the VTOL LVLT fuselage.

The fuselage of the fixed-wing LVLT would be identical to that of the VTOL aircraft, built on the same production line. The landing gear would be common between the fixed-wing and VTOL configuration since it is capable of roll-on landings at high speeds. As a result, the LVLT-FWV would be capable of short-takeoff-and-landing (STOL) operations from unpaved airfields.

The fuselage-commonality concept is a key to achieving programmatic cost savings. An integrated production line could use common tooling and facilities for both the VTOL and fixed-wing LVLT variants. The cockpit and cabin systems could all be common, including environmental systems, cargo systems, wiring, and plumbing. The pilot interface with the aircraft (side stick versus cyclic stick) and some panel layout may be unique. The hydraulic arrangement of the VTOL LVLT, with the hydraulics contained only in the nacelle areas, could allow the fixed-wing variant to use a unique hydraulic system, contained only in the wing system that is independent of the fuselage. Electro-hydraulic and electro-mechanical actuators are used throughout the fuselage systems, further enhancing the production commonality.

The wing of the fixed-wing aircraft would be completely unique but would be mounted using the same structure as that for the VTOL wing, requiring that only the nonstructural wing fairings be custom for the fuselage. The wing of the fixed-wing aircraft would be much thinner than the thick wing required for the VTOL aircraft and would support four wing-mounted turboprop nacelles. The thin wing would allow for efficient high-speed cruise flight, at speeds greater than those that a VTOL aircraft can achieve.

One aspect of the wing for the fixed-wing variant that will require further study is the weight and balance of the fixed-wing aircraft. The VTOL configuration has its own unique balance constraints because the center of gravity (cg) moves during transition. In the cruise mode, the cg is well forward, but as the nacelles rotate during transition the cg moves aft, eventually lining up near the tilt axis and allowing the aircraft to hover in equilibrium without any rotor head moment or

excessive flapping. The fixed-wing variant would only be constrained by typical fixed-wing weight and balance limits, but would ideally be aft-swept with forward-mounted, under-slung, turboprop nacelles. This arrangement creates a unique balance situation and would have to be investigated fully to allow for the optimal positioning of the wing and engines.

One of the greatest advantages of the fixed-wing variant is the use of engines that are common to the VTOL platform. History has shown that common cores can be used for turbo-shaft and turboprop engines. The VTOL LVLT will require new turboshaft engines, and it is foreseeable that these engines could be designed early in the design process for commonality or even complete interchangeability of the large engine sections. Prop reduction gearboxes would be required, but could likely be incorporated in the engine development with no detrimental performance or weight impact.

The engine development will be one of the largest single-cost drivers for the LVLT program, and distributing this development cost across additional aircraft would appreciably reduce the cost per aircraft. A first-order cost analysis for the LVLT aircraft shows a cost reduction per aircraft of 4% to 5% for the VTOL aircraft if an equal number of additional fixed-wing fuselages and engine ship sets are included. This analysis is a simplified approximation, but it shows the potential benefit of commonality between the VTOL and fixed-wing variants.

5.2 Shipboard-Suitable VDTR Description

The baseline LVLT aircraft does not incorporate folding, so a shipboard suitability trade study was conducted. The focus of this effort was to maximize shipboard suitability, and to study the shipboard operation requirements, while providing an aircraft design that accentuates the strengths of the design with the nuances of the requirements and unique operating environment. The shipboard-suitable aircraft is based on VDTR and is denoted VDTR-S.

The VDTR-S aircraft minimizes the overall aircraft length by eliminating the conventional empennage and replacing it with a canard for pitch control. The aerodynamics of the canard configuration allow the aircraft mean aerodynamic center to be much further forward than on a traditional wing and tail configuration. This setup enables the tilt axis to be positioned more favorably at the wing tips, reducing the complexity of the cross-shaft gear meshes and shortening the overall gearbox drive system.

To improve the pilot visibility during shipboard operations, the cockpit system has been reconfigured to a tandem arrangement. This tandem fighter aircraft style of canopy allows the pilot to see the entire aircraft behind him, including the nacelles and rotors. The pilot also has better visibility around the front of the aircraft and improved downward visibility. However, this canopy arrangement is likely not the optimal weight solution. Another drawback of this cockpit configuration is that the crew cannot get out of their seats and move around during long missions. While early 1950's large aircraft such as the B47 had tandem cockpits, modern transport-pilot crews have grown accustomed to working in a side-by-side collaborative environment. Fighter-pilot crews, however, have mastered the tandem cockpit arrangement. The pilot protocol for each arrangement

is unique, and transport-pilot crews would have to adapt to the fighter-pilot style for this cockpit to work effectively.

The cockpit arrangement, although unconventional, also enables the aircraft to be loaded and unloaded using cargo-ramp doors at both ends of the aircraft, even with the rotors turning and the engines running. For tight shipboard operations where space is at a premium, the aircraft can be positioned for ease of loading using either ramp, opening up the loading possibilities for the ship crew and load master.

The wings of the VDTR-S fold for stowage on the ships; they fold along the sides of the fuselage and rest vertically nestled under the nacelles with the engines in front of the cockpit.

6 Conclusions

The technical community has identified rotor efficiency as a critical enabling technology for large vertical-lift transport (LVLT) rotorcraft. The size and performance of LVLT aircraft will be far beyond current aircraft capabilities, enabling a transformational change in cargo transport effectiveness. Several viable alternatives were identified as candidate technologies capable of meeting the rotor performance requirements of the LVLT mission, including rotors with widely variable tip speeds and rotors with variable diameters. This study quantified the capabilities and efficiencies of these technologies compared to a conventional tiltrotor reference design. Ultimately, three aircraft concepts were synthesized and the attributes of these aircraft were compared as a measurement of the effectiveness of the underlying rotor technology.

Sikorsky was selected to conduct this analysis largely because of the company's previous variable-diameter-tiltrotor (VDTR) development efforts. These efforts spanned approximately 10 years during the 1990s. The VDTR development efforts included preliminary and detailed design of both the aircraft and rotor-system components as well as proof-of-concept testing of the system-level benefits and risk-reduction testing of the critical sub-system components. A summary of this previous work was discussed along with the relevance of these efforts to the current LVLT aircraft designs.

The three aircraft were optimized and designed around a common set of requirements with the intent of exposing the nuances that differentiate the configurations. Where common designs could be applied to all of the configurations, a single design was applied to all three configurations. Subsystems such as the rotor, drive system, and wing were designed in greater detail because these areas had the greatest potential to affect the capabilities of the three designs. Each of these systems was tailored to the specific needs of the rotor system applied to a given design, affecting the overall size and weight of the sub-system and the overall aircraft.

The design of the VDTR rotor was noteworthy in that the analysis brought forth an interesting nuance related to the VDTR synthesis for the LVLT requirements. Previous VDTR work emphasized the maximum rotor retraction possible relative to hover, with most designs employing a 34%-diameter retraction. Such large retractions, however, penalize hover performance two-fold: the hover twist is not optimal because of the requirement of linear twist on the retractable portion of the blade; and the exposed area of the elliptical inboard blade spar is greater, lowering figure of merit (FM). Because the LVLT mission required austere hover conditions at high mission weights, cruise performance was balanced by hover performance, leading to lower disk loading and a lower retraction ratio of 23%.

The resulting designs for the conventional tiltrotor (CTR), VDTR, and variable-speed tiltrotor (VSTR) were all relatively similar in size, weight, and installed power—not necessarily a surprising result given that the aircraft were optimized using the same ground rules and requirements set. Generally, the VDTR was the heaviest of the three concepts and had the least installed power. The VSTR was lighter than the VDTR but had the most installed power. The CTR was the lightest aircraft of the three, and had more power installed than the VDTR but less power installed than the VSTR.

The similar size, weight, and power of the three aircraft concepts lead to similar performance and handling-qualities capabilities, as well as similar levels of risk and cost. Several critical performance attributes were evaluated. These attributes were chosen because they showed the greatest differentiation between the three aircraft designs. The downwash, hover, and short-takeoff (STO) capability analyses favored the aircraft with the largest rotor, the VDTR, since these attributes are heavily influenced by the power loading of the aircraft.

The VDTR offered a broader spectrum of speed performance compared to the CTR and VSTR. Its smaller cruise-rotor diameter is more efficient for high-speed flight. The transmission torque capability of the VDTR is retained because its rotor revolutions per minute (rpm) is not reduced as much as with the VSTR. The VSTR has two modes in which it can operate: "efficiency mode," where the rotor is slowed via gearbox reduction and the engine operates at reduced rpm; and "performance mode," where the rotor is slowed via engine rpm reduction only, equivalent to the rpm reduction used on the CTR and VDTR. In "efficiency mode," the VSTR operates at high rotor-propulsive efficiency, but because its available transmission power is significantly reduced by the rpm reduction, its speed performance is severely limited. In "performance mode," the speed capability of the VSTR improves beyond that of the CTR, yet is still less than that of the VDTR. The performance gain of the VSTR in "performance mode" is at the expense of a significant propulsive-efficiency penalty, as its rotor is not optimized for both high-speed and high-rotor rpm. The VDTR, being designed for both high-speed and higher-rotor rpm, enables simultaneous high-speed and high-efficiency cruise flight.

Similar trends were observed in the payload-range performance of the aircraft. Missions involving arduous hover or low-speed conditions, including external lift, favored the VDTR because of the large rotor-disk area. Missions that favored high cruise efficiency also favored the VDTR because of its small, efficient propellers. The VSTR also performed the long-range cruise missions well because of its high efficiency, but it required greater installed power to perform the hover and low-speed missions.

Analysis of the aircraft-handling qualities again yielded similar results. Maneuvers that were similar to those executed by a helicopter, i.e., low-speed banked turns, heading changes in hover, and low-speed climbs, all favored either the VDTR because of its larger rotor or the CTR because of its larger wing area. Finally, additional analysis was conducted to quantify the risk and cost of these aircraft configurations, though this part of the study is not discussed in the report. These analyses indicate that the VDTR faces the largest development risk, followed by the VSTR. Development and life-cycle costs for these aircraft are also similar.

The comparison of the three aircraft, CTR, VDTR, and VSTR, indicates that the VDTR and VSTR are enabling technologies for the LVLT mission requirements, and that they can both be developed at reasonable levels of technical risk and development cost. Furthermore, the VDTR and VSTR developments are only incrementally more expensive than a similar CTR development, and add only incrementally greater risk. The performance benefits of the VDTR and VSTR make them worth the additional investment.

7 References

1. Fradenburgh, E.A.; and Matuska, D.G.: Advancing Tiltrotor State-of-the-Art with Variable Diameter Rotors. Am. Helicopter Soc. 48th Annual Forum, Washington, D.C., June 1992.
2. Fradenburgh, E.A.: Application of a Variable Diameter Rotor System to Advanced VTOL Aircraft. Am. Helicopter Soc. 31st Annual Forum, Washington, D.C., May 1975.
3. Fradenburgh, E.A.: Improving Tilt Rotor Aircraft Performance with Variable-Diameter Rotors. Fourteenth European Rotorcraft Forum, Milano, Italy, Sept. 1988.
4. Fradenburgh, E.A.: The Variable Diameter Rotor – A Key to High Performance Rotorcraft. Am. Helicopter Soc., VERTIFLITE Magazine, March/April 1990.
5. Nixon, M.W.; Piatak, D.J.; Corso, L.M.; Popelka, D.A.: Aeroelastic Tailoring for Stability Augmentation and Performance Enhancements of Tiltrotor Aircraft. Am. Helicopter Soc. 55th Annual Forum, Montréal, Quebec, Canada, May 1999.
6. Scott, M.W.: Technology Needs for High Speed Rotorcraft (2). NASA CR-177590, Aug. 1991.
7. Scott, M.W.: Summary of Technology Needs for High Speed Rotorcraft Study. AIAA Paper 91-2148, June 1991.
8. UMARC THEORETICAL MANUAL, University of Maryland, 1993.
9. Shen, J.; Masarati, P.; Roget, B.; Piatak, D.J.; Singleton, J.D.; and Nixon, M.W.: Modeling a Stiff-Inplane Tiltrotor Using Two Multibody Analyses: A Validation Study. AHS 64th Annual Forum, Montreal, Canada, 2008.
10. Studebaker Fletcher, K.; Decker, W.A.; Matuska, D.G.; Morris, P.; and Smith, M.T.: VMS Simulation of a Variable Diameter Tiltrotor. Am. Helicopter Soc. 53rd Annual Forum, Virginia Beach, Va., Apr. 1997.
11. Davis, S.J.; Moffitt, R.; Quackenbush, T.R.; and Wachspress, D.A.: Aerodynamic Design Optimization of a Variable Diameter Tilt Rotor. Am. Helicopter Soc. 51st Annual Forum, Ft. Worth, Tx., May 1995.
12. Brender, S.; Mark, H.; and Aguilera, F.: The Attributes of a Variable-Diameter Rotor System Applied to Civil Tiltrotor Aircraft. NASA CR-203092, Feb. 1997.
13. Acree, C.W., Jr., et al.: Rotor Design for Whirl Flutter: An Examination of Options for Improving Tiltrotor Aeroelastic Stability Margins. AHS 55th Annual Forum, Montreal, Quebec, Canada, May 25–27, 1999.
14. Bauchau, O.: DYMORE USER'S MANUAL, Georgia Institute of Technology, 2007.
15. Houbolt, J.C.; and Reed, W.H., III: Propeller-Nacelle Whirl Flutter. IAS 29th Annual Meeting, IAS Paper No. 61–34, New York, N.Y., 1961.
16. Reed, W.H., III: Review of Propeller-Rotor Whirl Flutter. NASA TR R-264, 1967.
17. Kvaternik, R.G.: Studies in Tiltrotor VTOL Aircraft Aeroelasticity. Ph.D. Dissertation, Case Western Reserve University, 1973.

18. Piatak, D.; Kvaternik, R.; Nixon, M.; Langston, C.; Singleton, J.; Bennett, R.; and Brown, R.: A Parametric Investigation of Whirl-Flutter Stability on the WRATS Tiltrotor Mode. J. Am. Helicopter Soc., vol. 47, no. 3, July 2002.

19. Kvaternik, R.G.; Piatak, D.J.; Nixon, M.W.; Langston, C.W.; Singleton, J.D.; Bennett, R.L.; and Brown, R.K.: An Experimental Evaluation of Generalized Predictive Control for Tiltrotor Aeroelastic Stability Augmentation in Airplane Mode of Flight. Am. Helicopter Soc. 57th Annual Forum, Washington, D.C., May 2001.

20. Acree, C.W., Jr.: Rotor Design Options for Improving V-22 Whirl-Mode Stability. AHS 58th Annual Forum, Montreal, Quebec, Canada, June 11–13, 2002.

21. Matuska, D.; Dale, A.; and Lorber, P.: Wind Tunnel Test of a Variable-Diameter Tiltrotor (VDTR) Model. NASA CR-177629, Jan. 1994.

22. Johnson, W.: Analytical Modeling Requirements for Tiltrotor Proprotor Aircraft Dynamics. NASA TN D-8013, July 1975.

23. RCAS THEORY MANUAL, U.S. Army Aviation and Missile Command, Moffett Field, Calif., 2003.

24. Ferguson, S.W.: A Mathematical Model for Real Time Flight Simulation of a Generic Tiltrotor Aircraft. NASA CR-166536, Sept. 1988.

25. Goodman, C.; and Zeidner, L.: Value-Based Gauge Process Overview. UTRC memorandum, Nov. 5, 2008.

8 Bibliography

Arrington, W., Kumpel, M., Marr, R., and McEntire, K.: XV-15 Tilt Rotor Research Aircraft Flight Test Data Report. NASA CR-177406, June 1985.

Bottasso, C.L.; and Bauchau, O.A.: Finite Element Multibody Modeling of Rotorcraft Systems. Twenty-Seventh European Rotorcraft Forum, Moscow, Russia, Sept. 2001.

Ferguson, S.W.: EMA Report 90-1-1, Rotor Induced Velocity and Induced Airframe Angle-of-Attack Improvements to the Generic Tilt Rotor Simulation Program. Oct. 1990.

Palcic, P.; Garcia, T.; and, Gmirya, Y.: Variable Speed Transmission for a Rotary Wing Aircraft. U.S. Patent 7,296,767.

Scott, M.W.: Mission Performance Comparison Between Tilt Rotor, Variable Diameter Tilt Rotor and Tilt Wing Aircraft. Am. Helicopter Soc. Vertical Lift Aircraft Design Conference, San Francisco, Calif., Jan. 1990.

Studebaker, K.; and Matuska, D.G.: Variable Diameter Tiltrotor Wind Tunnel Test Results. Am. Helicopter Soc. 49th Annual Forum, St. Louis, Mo., May 1993.

Visintainer, J.; O'Neill, J.; and Murty, H.: VDTR Measured Acoustic and Aerodynamic Data Compared with the V-22 at the NASA Langley Research Center 14- by 22-Foot Wind Tunnel Test. NASA CDCR 10028, Nov. 2002.

Wang, J.M.; Jones, C.T.; and Nixon, M.W.: A Variable Diameter Short Haul Civil Tiltrotor. Am. Helicopter Soc. 55th Annual Forum, Montreal, Canada, May 1999.